POLITECNICO DI TORINO

Collegio di Ingegneria Energetica e Nucleare

Corso di Laurea Magistrale in Ingegneria Energetica e Nucleare

Master's degree thesis

Improvement of the energy consumption of an internal combustion vehicle according to the 2021 EU emission limit

Relatore

Prof. Marco Carlo Masoero

Candidato

Antonino Leandro Petrone

Sessione di Laurea: Luglio 2018
Anno Accademico: 2017/2018

SUMMARY

LIST OF FIGURES

LIST OF TABLES

INTRODUCTION

The present thesis has been developed thanks to the collaboration with FCA Italy and C.R.F which have followed the work evolution in all its aspects, representing a strong reference point for each criticality.

The thesis has been edited largely thanks to the employment of the software LMS Imagine.Lab Amesim, produced by Siemens. The project work has been divided in many steps aimed to focus the attention on the energy consumption related to the operation of the air conditioning system of a passenger car.

It is appropriate to specify that accessory systems as the AC system are not generally switched on during homologation tests of vehicles; then this project is also aimed to highlight how driving cycles employed for homologation are not always coherent with the actual vehicle operation performed by users. Nevertheless, the assessment of the energy consumption of the AC system has been simulated taking into account the most important driving cycles which carmakers' homologation tests are based on: NEDC (European), WLTC (Worldwide) and SC03 (U.S. Federal). In particular, in order to obtain a driving mission profile warranting a certain operation regularity, the driving cycles listed above have been slightly modified omitting the time steps in which the engine was switched off and considering it at the minimum rotary speed. In this way it has been possible to make considerations on the consumption reduction deriving from a continue cooldown mission.

The first chapter contains a deep world energy study based on data published by the most important agencies: the International Energy Agency (IEA) and the U.S. Energy Information Administration (U.S. EIA). In particular, the study has been organized starting from the energy overview, proceeding with the study of environmental implications and then restricting the analysis focusing on the transportation sector and its impact with respect to the CO_2 emission. Furthermore, after having distinguished all the kinds of mean of transport, a most centred analysis has been performed on the LDV (Light Duty Vehicles), showing percentages on the fuels employed and studying their evolution in the last 15 years and in the next 20 years.

The second chapter is an introduction to the thermal comfort and to the tools adopted to reach it in occupied spaces according to legislations. An accurate description of the AHSRAE Standard 55 and of the main parameters involved in the definition of thermal comfort has been edited, characterizing the application according to the automotive field. Furthermore, an analysis of the main components of an HVAC system has been performed, describing firstly a general application and focusing thereafter the attention on automotive application.

The third chapter represents the real introduction to the project work. It contains the analysis of the choice of the vehicle (which will not be mentioned in this document according to the carmaker policies concerning privacy) and the characterization of engine and AC system, paying attention to report only public information.

The central part of the project work has been constructed by two structured parts.

The ***"PROJECT WORK. PART I"*** has been discussed in the fourth chapter; it has been divided in many steps to obtain an accurate validation of the Amesim model containing the car cabin and AC system with respect to the Cooldown test data provided by FCA Italy.

The ***"PROJECT WORK. PART II"*** has instead concerned: the description of the cabin improvements, the estimation of the end-soak temperature trends and the internal cabin temperature behaviour. In particular, an analysis on the differences between standard and improved application has been produced and during the soaking and during the operation of the AC system. In the end a short assessment of the fuel consumption and CO_2 emission has been performed, reporting the final results of the study and characterizing them with respect to the average distance travelled by a vehicle in one year.

CHAPTER I: ENERGY AND ENVIRONMENT

1.1 Energy consumption

Since industrial revolutions to today the energy production overview has radically changed, highlighting the important transition from the uncontrolled exploitation of fossil sources to the awareness of needing to find more clean ways to produce energy.

The Climate-Energy plan (also called 20-20-20 strategy) approved by the European Union in 2006, has replaced the Kyoto Protocol in 2009. The normative obligations established the achievement of three environmental and energetic goals within 2020:

- the reduction of greenhouse gases emission by 20%;
- the reduction of energy consumption by 20%, increasing the energy efficiency;
- to satisfy the 20% of the European energy demand with renewable sources.

In order to control the trend of the energy consumption and production, many agencies have been introduced; the aim is to report every year the energy World overview according to the data collected and to give a possible forecast for the following years according to the existing and announced countries' policies. In the group of the world energy agencies, the IEA and the EIA will be used as reference for the presentation of World energy trends.

The *International Energy Agency* (IEA) has been instituted in 1974 by the *Organization for Economic Co-operation and Development* (OECD) after the energy crisis of the previous year. The IEA monitors every year the development of World's strategies aimed at reaching these obligations and it reports the energy consumption trend and the consequent implications on the environment. Furthermore, it has two principal tasks: encourage the energetic safety involving all the members States in the block of the oil furniture and encourage authoritative researches and analysis to achieve clean and safe energy sources [1].

The *U.S. Energy Information Administration* (EIA) has been established by the Department of Energy Organization Act in 1977 and it is now part of the U.S. Department of Energy. It is a principal agency of the U.S. Federal Statistical System and it is responsible of analysing and collecting energy information in order to report energy World scenarios [2].

Since the World energy status has developed towards a more controlled and clean future, the agencies have started to redact World Energy Outlooks to draw the energy trends, analysing the most significant energy strategies and policies and evaluating the consequence on the global energy consumption evolution.

According to the World Energy Outlook 2017 (WEO-2017) [1] published by the IEA, the most important trend to be noticed is addicted to the continuous growing of the energy consumption, evaluated in almost all the World countries. As matter of the fact in the International Energy Outlook 2017 published by the U.S. EIA [2] everything is confirmed and clarified characterizing the World energy consumption with respect to countries and end-use sector and observing the current trend and the forecast for the future. In the following graph it is possible to observe how the World energy consumption has developed in the last twenty years and how it might develop from now to 2040 according to current and declared energy policies:

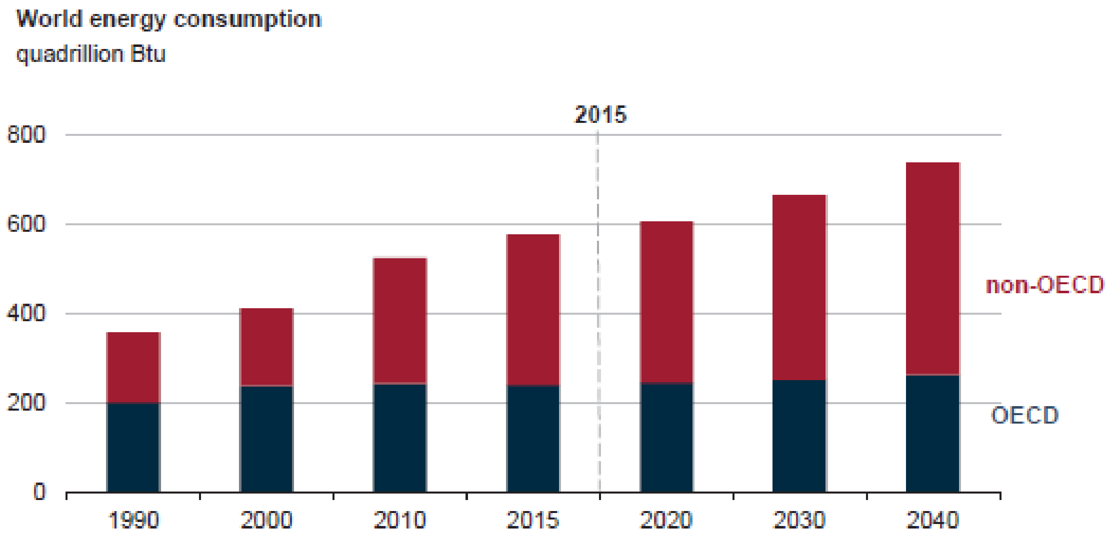

Figure 1. World energy consumption 1990 - 2040. [2]

It is clear how energy country development is already defined for OECD countries, while the non-OECD ones are continuously having more confidence with an always more energivorous life. The most significant energy sectors are: industrial, transportation and buildings. While the industrial energy trend is predicted as rising rapidly, transportation and buildings energy consumption will probably be subjected to a more slowly growth. The growth is due to the Energy Zero Building projects and the transition to electric vehicles, while the slowness is due to a complex combination between gains and amortization of the cost for the users. In the graph below it is showed how the energy consumption trend has developed in these years and how forecasts predict it will develop:

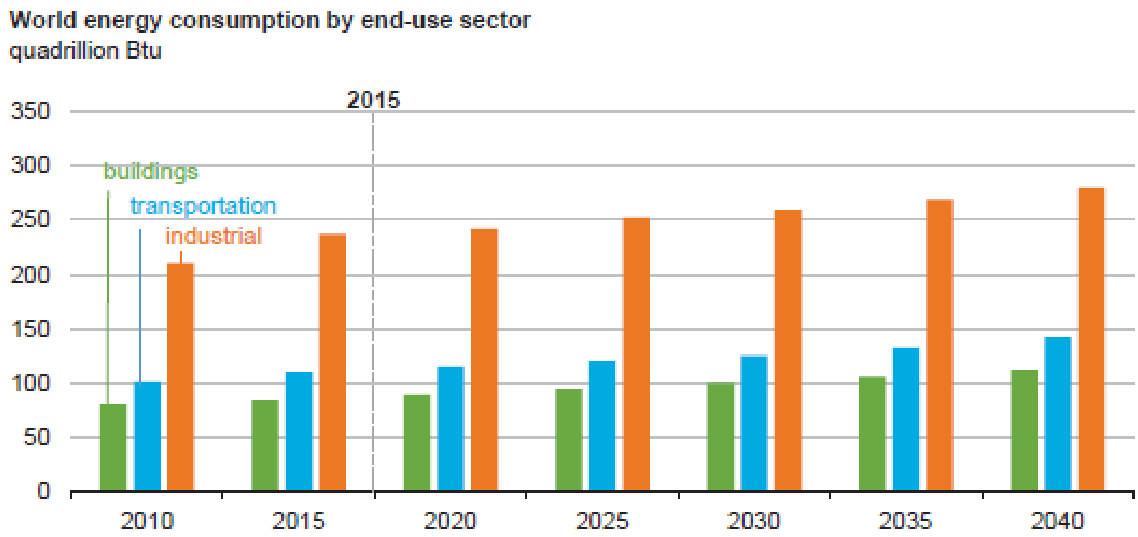

Figure 2. World energy consumption by end-use sector 2010 - 2040. [2]

According to the World Energy Outlook 2017 (WEO-2017) published by the International Energy Agency, four important trends have furthermore been noticed:

- fast diffusion and cost reduction of clean energy technologies;
- growing electrification of energetic final uses;
- transition toward a cleaner economy and energy mix in China;
- resilience of shale gas and tight oil in USA.

In the New Policies Scenario predicted by the IEA, global energy needs are now rising slowly but they will expand to 30% in the next 30 years due to the access to energy obtained by developing countries of Southeast Asia, Middle East, Africa and Latin America.

The continuous rising of world energy consumption is also justified by the growing electrification energy, due to a higher percentage of people accessing to the electricity and to the electrification of more final uses in the already developed countries.

According to the World Energy Outlook in fact, since 2012 to today 100 million people per year have gained access to electricity thanks particularly to the impressive progress whose Indonesia and India are principal characters. It has also been estimated that in 2016 *"spending by the world's consumers on electricity approached parity with their* *spending on oil product"* [1]; that's represent a clear signal that the World is moving to more clean and safe ways to produce energy.

As matter of the fact the figure below shows a graph representing the growth of the renewable energy sources is reported, going from today to 2040:

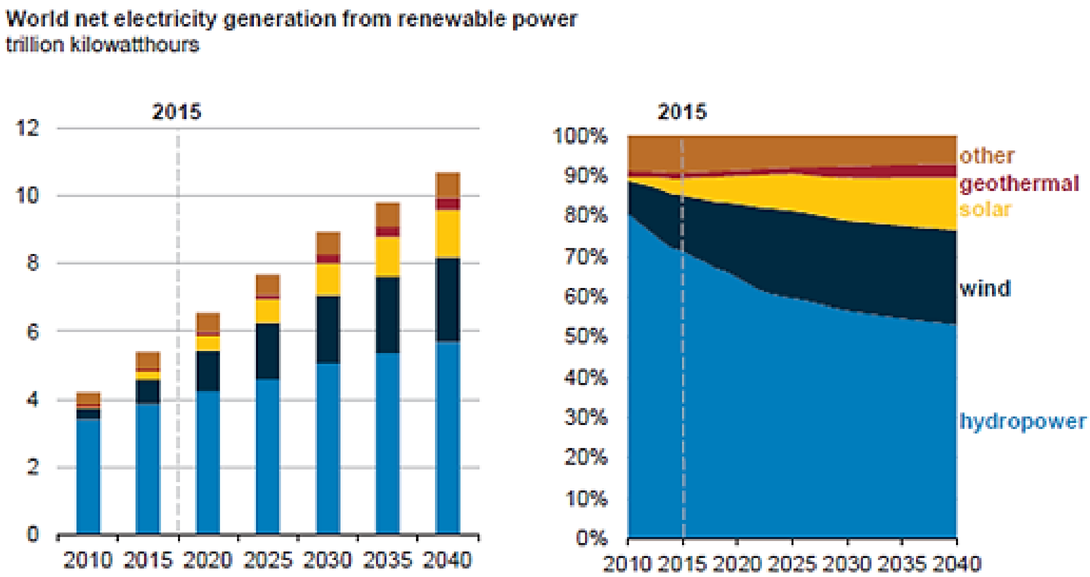

Figure 3. World net electricity generation from renewable power 2010 - 2040. [2]

Compared to 1990's the energy need of the World is satisfied in a total different way. As a matter of the fact, the global energy status is now characterized by natural gas, by a fast rise of renewable sources and by energy efficiency. In particular, in 2016 the solar photovoltaic and the wind capacity have increased thanks to the cost reduction by 70% for the solar PV and by 25% for the wind plants. The forecasts edited by the IEA predict a rapid deployment of solar photovoltaics, led by China and India that will help the renewable penetration in the global power generation to reach the 40% around in 2040.

At the same time, even if since 2000 the c oal-fired power generation capacity has increased to around 900 GW, the forecasts from today to 2040 are promising and show a capacity reduction by around 50%. This trend inversion is also confirmed by the International Energy Outlook published by the U.S. Energy Information Administration which links the reduction of power generation capacity (whose China owns almost the 70%) with the rising development of renewables. In the following graph the coal consumption and the coal imports in China are reported, showing the slow reduction in the last years and a strong reduction predicted for 2040 with respect to the energy sectors:

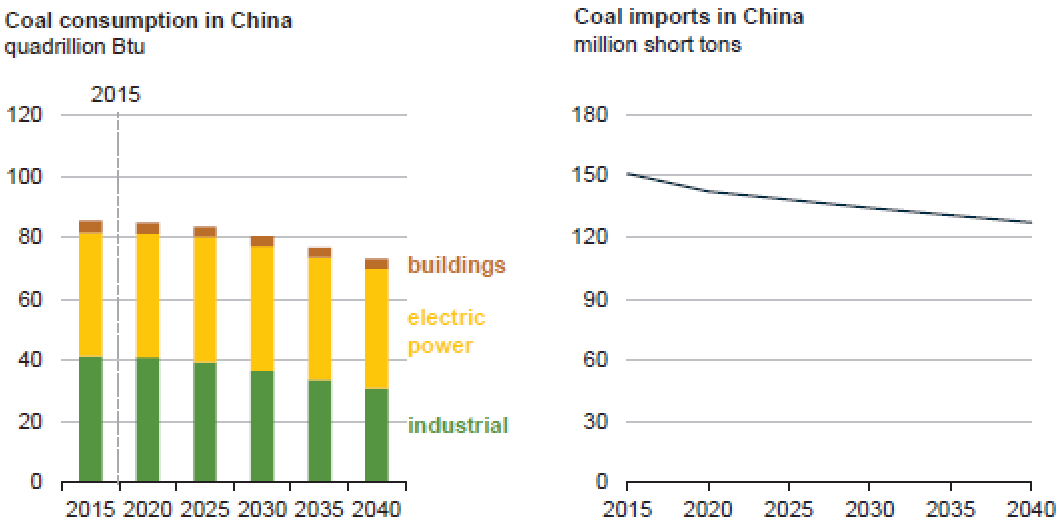

Figure 4. Coal consumption and imports in China 2015 - 2040. [2]

1.2 Energy and environment: greenhouse gases

Although the World Energy Outlook 2017 has registered an observance of the route by the U.S.A which count on the resilience of shale gas and tight oil, the other OECD countries have invested on green energy in almost all sectors. As already mentioned in the previous paragraph, the World energy strategy has in fact been directed toward a more clean and safe way to produce energy in order to reduce the environment impact due to the uncontrolled greenhouse emissions.

Two fundamental reasons made the base of this change of trend:

- the convergence to the exhaustion of fossil sources;
- the evolution to a catastrophic ruin of Earth.

The first aspect is the real starting point of the energy consumption evolution; fossil fuels are in fact very old and need thousands of years to born and become usable. For instance, North Sea oil deposits are around 150 million years old and British's coal deposits began their development 300 million years ago. Although humans have probably used fossil fuels in ancient times, the Industrial Revolution led to their wide-scale extraction. The uncontrolled deployment of fossil fuels has caused an increasing reduction of the stocks because the rate at which the world consumes is greater than the rate of regeneration of fuels. According to an estimation of all fuel reserve and consumption realized by the *U.S. Central Intelligence Agency* [3], the energy reserves derived from fossil fuels are going to exhaust within 2090. The graph below reports the evolution of coal, gas and oil reserves expressed in billion tonnes oil equivalent:

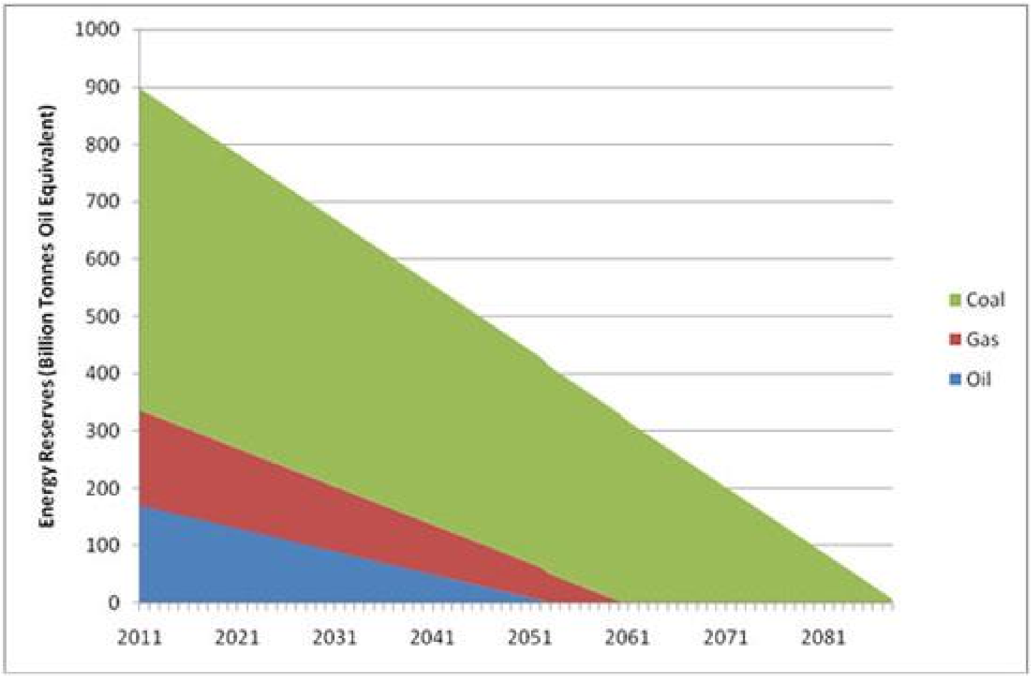

Figure 5. Energy reserves evolution 2011 - 2090. [3]

The need of finding an alternative kind of energy sources has been joined to a more attention to the environment impact; countries have paid specific attention to two phenomena:

- ozone depletion;
- anthropogenic global warming.

The former concerns the ozone layer present in the stratosphere which is fundamental for the interception of lethal ultraviolet radiations; the stratospheric ozone absorbs in fact almost totally the UV-C component and for the 90% the UV-B, responsible of melanomas and other types of cancer [4]. The ozone depletion is principally caused by chlorofluorocarbon (CFC), hydroclorofluorocarbon (HCFC), partially bromide chlorofluorocarbon (HALON). Chlorofluorocarbons are organic (saturated or unsaturated) compounds which derive from hydrocarbons; they come from the substitution of one or more hydrogen atoms with one or more halogen atoms. When chlorofluorocarbons are emitted in the atmosphere, thanks to their strong stability, they fly to the stratosphere without decaying and decomposing when arriving near the ozone layer. Basically, it is regulated by the equilibrium reactions which reign the stratosphere ozone:

$$3O_2 \rightarrow 2O_3 \qquad \textit{formation reaction}$$

$$2O_3 \rightarrow 3O_2 \qquad \textit{depletion reaction}$$

Naturally both reactions happen slowly and maintaining the conservation of reagents and products; nevertheless, when halogens keep in touch with the ozone, they become catalysts of the reaction, modifying it. The most representative ozone depletion is the catalytic depletion due to the chlorine, which modifies the reaction as reported below:

$$Cl + O_3 \rightarrow ClO + O_2$$

$$O + ClO \rightarrow 3Cl + O_2$$

and therefore, the balance of oxygen becomes:

$$O_3 + O \rightarrow O_2 + O_2$$

In this way the reactions give as products very stable halogen oxide, reducing the oxygen concentration and therefore the ozone concentration, causing the famous “ozone hole”.

In order to fight for the stratospheric ozone saving many countries have signed the Montréal Protocol, an international treaty established in 1987 which had as goal the ban of the most of polluting artificial gases.

In order to control and quantify the ozone depletion an index has been introduced to characterize every gas: the ODP or Ozone Depletion Potential. It is the depletion potential that a chemical mixture has in the stratospheric ozone and it is defined as the ratio between the ozone depletion due to a substance and the ozone depletion due to the same quantity of trichlorofluoromethane, also called Freon-11 or R-11. The standard chemical mixture is in fact R-11 which has an ODP equal to 1; other examples are the bromofluorocarbons with an ODP included in the interval 5 ÷ 15, the hydrofluorocarbons with an ODP included between 0.005 ÷ 0.2 [5].

The anthropogenic global warming (AGW) concerns the growth of the global temperature observed in the last 50 years. Although the opinions regarding the real reasons of the global warming are contrasting, many scientific experts consider the uncontrolled greenhouse gases emissions as the most significant contribute. In the group of greenhouse gases many fluids (also natural) are included: carbon dioxide CO_2, methane CH_4, water vapour H_2O, nitrous oxide N_2O, fluorinated gases. Carbon dioxide and nitrous oxide are directly related to the combustion of fossil fuels, methane is related to production and transport of coal, natural gas and oil. In the matter of fluorinated gases, they are sometimes used as substitutes of CFC, HCFC and HALONs; they are synthetic and represent the more powerful greenhouse gases produced by every industrial sector.

Similarly to the ozone depletion control, in order to evaluate the impact of greenhouse gases emitted with respect to the anthropogenic global warming, another index has been introduced: the GWP or Global Warming Potential. It is a coefficient useful to measure how much a greenhouse gas is involved in the heat trapping in the atmosphere; it is equal to the equivalent mass of CO_2 trapping the same heat of a gram of the gas considered with respect to a time interval spent in atmosphere equal to 100 years. The Global Warming Potential depends on three factors:

- the absorption of infrared radiation;
- the location of the absorbing wavelengths;
- the atmospheric lifetime of species.

For this reason, a gas with a large infrared absorption and a long lifetime has a high GWP. For example, the R134a (mostly used in air conditioning systems) has a very long lifetime and its GWP is equal to 1430, the methane CH_4 has a GWP equal to 21. The GWP for the standard gas CO_2 is instead equal to 1 [5].

According to the motivations which have led the countries to sign the Montréal Protocol, in 1997 the *United Nations Framework Convention on Climate Change* (UNFCCC) [6] has established the Kyoto Protocol to reduce the pollutant emissions peremptorily by the 8.65% with respect to the 1985. Although at first only 40 countries in the World have signed it, in 2009 almost the totality subscribed the agreement except the U.S.A.

It is possible to observe the agreement penetration thanks to the graph reported below:

- green: signed and ratified;
- yellow: signed, ratification pending;
- red: signed, ratification declined;
- grey: countries without position.

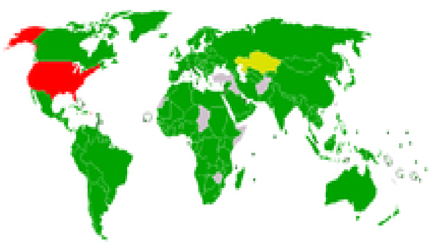

Figure 6. World Map – Countries position with respect to the Kyoto Protocol in 2015. [6]

As integration to the GWP, in order to evaluate all the contributes of a refrigerating system, it has been established another index named TEWI, or Total Equipment World Index. It is a coefficient that accounts the GWP contribute and the related-system CO_2 emitted. In particular:

$$TEWI = m * GWP + \alpha_{CO_2} * e * t \text{ [5]}$$

where m is the mass of the greenhouse gas in $[kg\ of\ gas]$, GWP is expressed as $\left[\frac{kg\ of\ CO_2}{kg\ of\ gas}\right]$, α_{CO2} is the carbon dioxide mass emitted in order to produce a $[kWh_{el}]$and it is therefore expressed as $\left[\frac{kg\ of\ CO_2}{kWh_{el}}\right]$ (it depends on the energy production system: a thermoelectric central uses fossil fuel to produce energy and so it has high values of α, a nuclear or hydroelectric central does not emit CO_2 and hence its α is equal to zero), e is the average power needed by machine to work and it is expressed in $[kW_{el}]$ and t is the life-time of the machine expressed in $[h]$. In this way the index TEWI expressed in $[kg\ of\ CO_2]$ is able to give a more correct information about the emission of a refrigerant machine [5].

Below a graph showing the global greenhouse gases percentages with respect to the total is reported, splitting twice the CO_2 contribution: the former and most significant concerns industrial processes and fossil fuel, the latter concerns agriculture, forestry and other land uses:

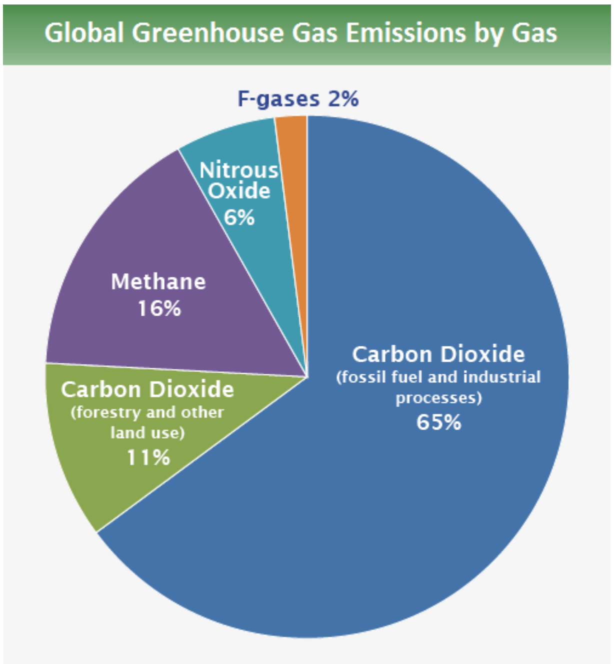

Figure 7.Global GHG Emissions by Gas - 2014. [8]

Carbon dioxide due to fossil fuel and industrial processes derives mostly from the hydrocarbon combustion and amount for about the 65% of the global greenhouse emissions. Let's now consider a typical combustion reaction, highlighting only the usual products:

$$C_nH_m + O_2 + 3.76N_2 \rightarrow CO_2 + H_2O + 3.76N_2$$

where *n* and *m* are the number of carbon and hydrogen atoms of the hydrocarbon.

The products of the reaction written above are carbon dioxide and water vapour and amount almost to the totality; nevertheless, in particular situations the right-side of the reaction can count: carbon monoxide CO, NO_x and SO_x. If the reaction occurs with a quantity of oxygen less than the stoichiometric one, the combustion become incomplete: the consequence is the production of carbon monoxide CO, an odourless and tasteless gas which is very toxic and therefore dangerous for human health. In order to reduce the production of this clinker, very noxious for concentrations greater than 100 ppm, it is useful to choose an air excess index significantly greater than the stoichiometric one. Usually it is equal almost to 1.3 ÷ 1.4, maintaining an excess of air equal to 30% ÷ 40% with respect to a stoichiometric balanced reaction.

Furthermore, since the combustion of hydrocarbons occurs with air and not with only oxygen, it is important to explain that the real composition of the combustive accounts the 21% of oxygen and 79% of nitrogen (in volume). With regard to the nitrogen, it is an inert gas and therefore it is not involved in any reaction usually. Nevertheless, in case of high combustion temperature, high air surplus and presence of nitrogen in the hydrocarbon, nitrogen can react with the oxygen and create nitrous oxides NO_x. They include: nitrogen oxide NO, nitrogen dioxide NO_2, nitrous oxide N_2O, nitrous trioxide N_2O_3, nitrous pentoxide N_2O_5. NO_x (in particular the nitrogen dioxide) are pollutant and can cause the beginning of respiratory problems in children, aggravate asthma problems and respiratory conditions of health-weak people. With regard to nitrous trioxide and nitrous pentoxide, they are soluble in water and can cause nitrous and nitric acids leading to the already known "acid rains", responsible of destruction of agricultural fields and consequently economic damage. In order to reduce the NO_x production, the combustion temperature must be kept sufficiently low and the air excess index must be convergent to a suitable balanced value in order to allow producing small quantities of carbon monoxide and also of NO_x. In the matter of the hydrocarbon composition, it is also possible to find in addition low percentage of sulphur; for example, the crude oil can contain around the 0.05% ÷ 4.5%, while the fossil coal is characterized by percentages around the 0.1% ÷ 6%. Although the emission of sulphur dioxide is mostly due to the natural emission deriving from volcanos activities, the combustion of hydrocarbons polluted by sulphur causes also the production of sulphur dioxide. This gas is colourless, inflammable, soluble in water and characterized by a strong odour; its density is greater than the water density, so it is mostly concentrated in atmosphere and therefore it represents the most diffuse and dangerous environmental pollutant. Thanks to its solubility in water, it is very noxious for human health; in fact, the sulphur dioxide is very irritating and can easily be absorbed by the mucous of the nose causing skin or eyes irritations and respiratory pathologies like asthma or bronchitis.

With regards to the environment, sulphur dioxide and sulphur trioxide are also responsible of "acid rains" and so they cause damage to animals and plants, destroying agriculture fields. After a preliminary analysis, results want the hydrocarbon combustion to be controlled and treated in order to avoid the emission in atmosphere of this pollutant, toxic and dangerous gases. The most part of plants is characterized by many solutions acted to the emission reduction.

In the end a short analysis is able to show how the direct dangerous consequences of combustion are mostly shielded by containment systems thanks to their low percentages. With regards to an anthropological problematic like the global warming, a more important attention needs to be focused on the most significant of the combustion products: the carbon dioxide. Climate scientists have indeed observed significant increases for the levels of CO_2, methane CH_4 and nitrous oxide N_2O. According to the "*CO_2 emissions from fuel combustion: highlights"* [7] published by the International Energy Agency in 2017, the 68% of the global anthropogenic GHG estimated in 2014 has been due to energy uses. In particular, a pie chart showing the estimated shares of global anthropogenic GHG is reported in the following page highlighting how the energy sectors are not only the most energivorous sectors but also the most emitters of greenhouse gases. The greater amount of energy-related emissions is in fact attributed to all the energy production systems. The 90% of the energy-related GHG emissions is represented by carbon dioxide emissions, while methane and nitrous oxide emissions amount respectively to around the 9% and 1%.

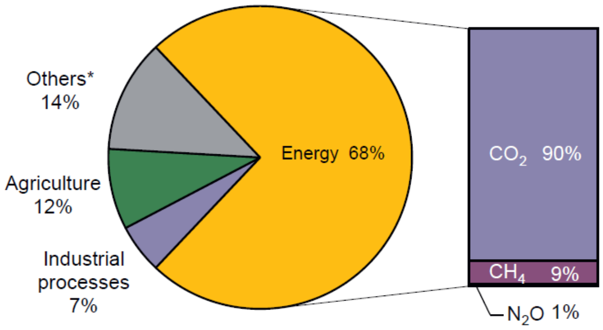

Figure 8. Estimated shares of global anthropogenic GHG, 2014. [7]

1.2.1 Carbon dioxide emissions

According to an estimation realized by the *Intergovernmental Panel on Climate Change* (IPCC) [8], member agency of the United Nations (UN), the greenhouse gases emissions have increased from 27 to 49 $\left[\frac{GtCO_2eq}{year}\right]$ between 1970 and 2010, recording a growth about 80% [7]. In particular, CO_2 emissions from fossil fuel combustion and industrial processes contributed about 78% on the total GHG emission increase, continuing his rise with a 3% between 2010 and 2011 and around 1-2% between 2011 and 2012. With respect to the "*CO_2 emissions from fuel combustion: highlights*" [7], thanks to the analysis accurately made by the *Carbon Dioxide Information Analysis Centre* of the *U.S. Department of Energy*, a graph reported the CO_2 emission trend from fossil fuels combustion is shown below:

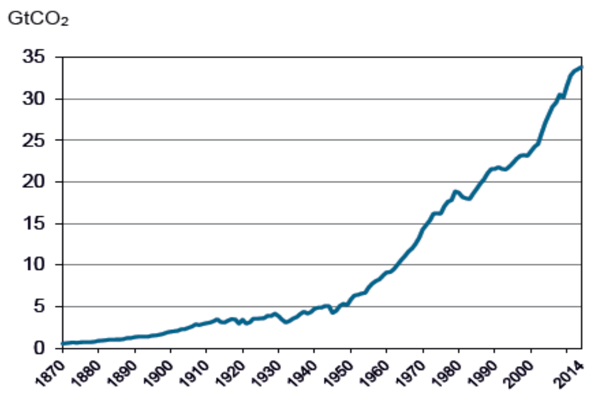

Figure 9. Trend in CO_2 emissions from fossil fuels combustion, 1870-2014. [7]

World carbon dioxide emissions are predicted to grow by 0.6% per year between 2015 and 2040, especially because of non-OECD countries. As a matter of the fact the *Energy Information Administration* has reported that in OECD countries energy-related CO2 emissions remain essentially flat through 2040 at 9% lower than the 2005 level, even though their economies gradually expand. On the other hand, non-OECD countries, after having been characterized by a growth rate around the 3% per year between 1990 and 2015, are projected to emit with a growth rate around the 1% per year between now and 2040. In the following figure a graph reporting the carbon dioxide emission due to energy is showed, highlighting non-OECD and OECD countries contributes:

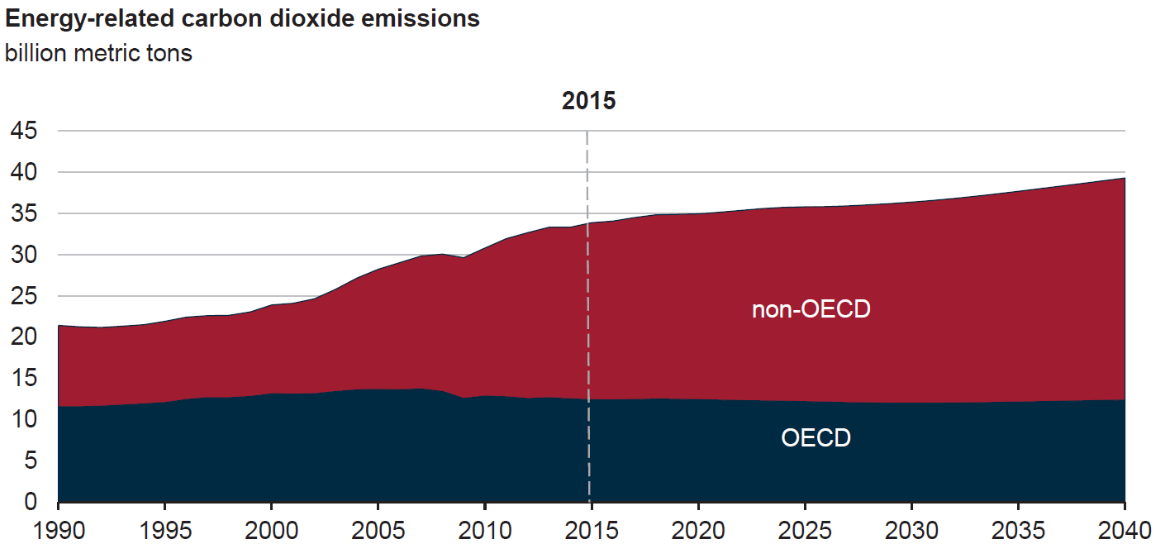

Figure 10. Energy-related carbon dioxide emissions. [2]

Even though coal have accounted for the 28% of the world total primary energy supply in 2015, the related emissions have represented the 45% of the global carbon dioxide emissions. In particular, because of its heavy carbon content per unit of energy released, coal has been responsible of almost twice the emissions compared to natural gas.

According to the decrease of the emission growing rate by non-OECD countries, an important feedback is given by China which is going to deal with the shift from first coal consumer to leader of the transition towards a major use of natural gas, nuclear power and renewables. The projections for the carbon dioxide in China are indeed promising: CO_2 emission due to liquid fuels grows at a decreasing rate while the coal-related one decreases strongly, obtaining a world coal-related emission growth about the 0.1% per year with respect to the rate of 2.3% per year recorded between 1990 and 2015.

In the figure reported below a carbon dioxide emission trend due to energy consumption has been drawn, splitting the graph in the situation observed before 2015 and in the predicted situation for the future. In particular, three trajectories are plotted in order to show how singularly coal, liquid fuels and natural gas affect and will affect the CO_2 emissions. The trends shown fit with the energy consumption evolution, highlighting a coal-related emission reduction and a GN-related emission increase, due to the transition from the coal to the natural gas for the energy production.

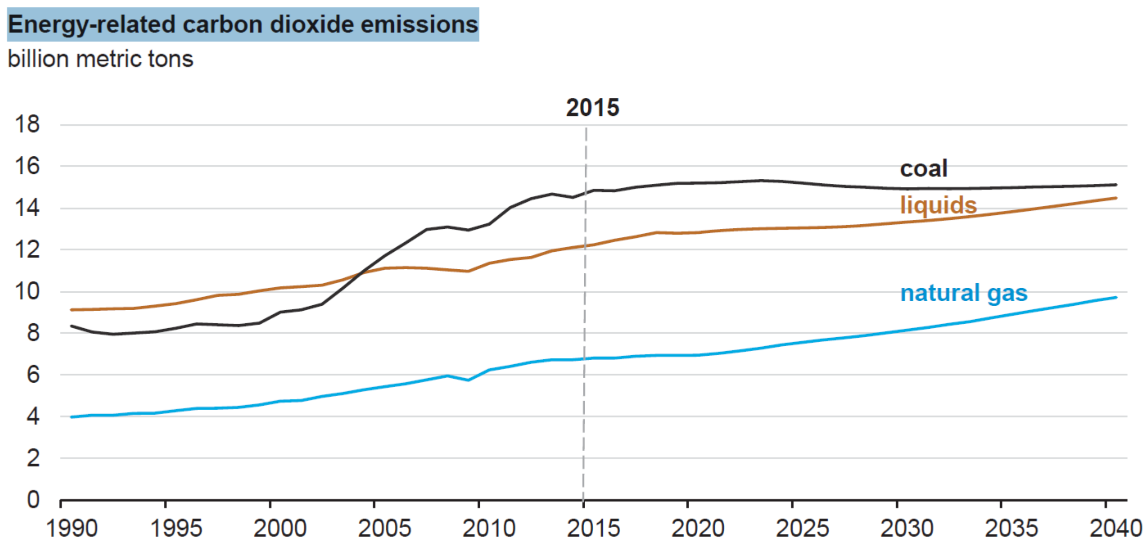

Figure 11. Energy-related carbon dioxide emissions by fuels. [2]

In order to control the anthropogenic global warming, the UNFCC has planned a global stocktaking of countries in which each of them will be reviewed on the progress towards the goal of keeping the global warming below 2°C set by the Paris Agreement in 2015. The next step will concern the reach of the limit under 1.5°C, considered as the most important goal to achieve within 2030 [6].

1.3 Transportation sector

Although the most significant sectors involved on the growth of the global greenhouse gas emissions are industrial, energy production and agriculture with around 60%, smaller contributions like the transport sector must be considered like equally important. As shown in fact by the U.S. Energy Information Administration, transportation contributes as second factor to the world energy consumption and it is predicted that from now to 2040 it will increase by almost 40% going from 100 to around 140 quadrillion Btu [2]. Furthermore, according to the Climate Change 2014, the graph reported below shows the percentage of greenhouse gas emission by sectors, highlighting how transportation influence the global greenhouse gases emissions by around the 14%. [8]

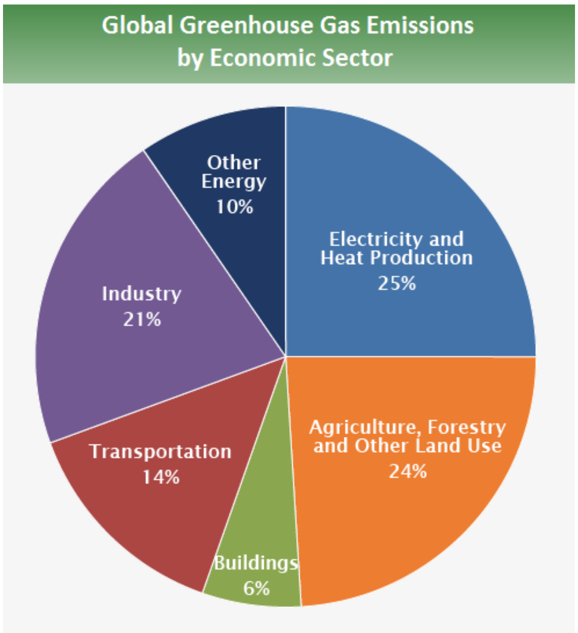

Figure 12. Global GHG Emissions by Economic sector. [8]

Global transport greenhouse gas emissions grew from 2.8 $GtCO_{2,eq}$ to 7 $GtCO_{2,eq}$ between 1970 and 2010 [9]. The OECD countries contributed mostly to rise up emissions: they were responsible by the 60% in 1970, 56 % in 1990, and 46 % in 2010. Although transport emissions have steadily increased through this period, a significant decrease has been noticed around the end of the first ten years of the second millennium. The most important reasons were the high oil prices of 2008 and the global recession in 2009 both involved on the fossil fuel consumption reduction for the OECD countries. GHG emissions in non-OECD countries were not instead affected. The most significant greenhouse gas in transportation is carbon dioxide that amounts almost to the totality of GHG emissions; it is in fact considered as reference for the estimation of the other gas quantity emitted.

In order to make an accurate analysis on the CO_2 emissions growth it is therefore important to consider many political and social-economic factors: urban development, lack of passengers' transportation like bus and rails, quite low oil prices and limited availability of low-carbon.

The growth rate of the world transport emissions in the 2010s was equal to the growth in Chinese exporting industries suggesting an intervention by countries policies and world trade agreements on transport emissions in order to regulate this uncontrollable rise.

With regards only to the carbon dioxide emissions from fuel combustion, according to the "*CO_2 emissions from fuel combustion 2015: highlights*", two sectors are responsible for 2/3 of the global CO_2 emissions from fuel combustion: electricity and heat generation for the 42% and transportation for the 24% [7]. The transport sector can be divided in some contributes: road, domestic navigation, domestic aviation, other transport, marine bunkers and aviation bunkers. The road contribute represents the daily own means of transportation, the navigation and aviation sectors, both domestic and bunker, correspond to the passenger transportation and the commercial transportation through ocean and sky.

As shown in the columns graph reported below the transport energy-related CO_2 emissions have increase from around 4.75 $GtCO_2$ to around 7.8 $GtCO_2$, observing an increase by almost the 65%.

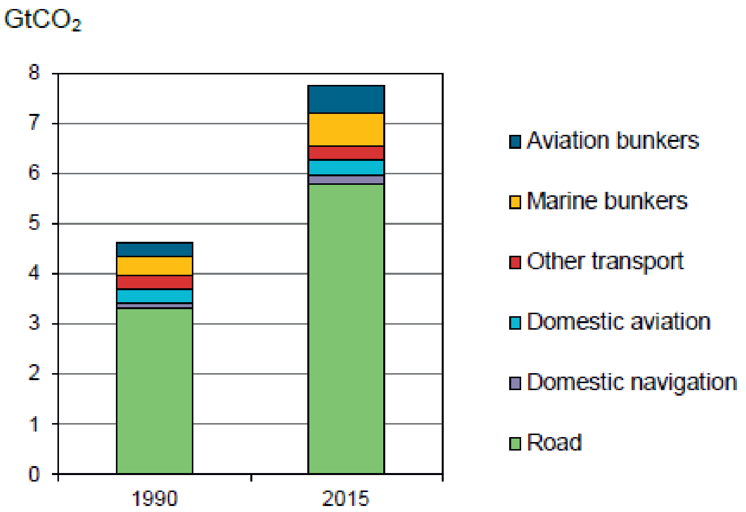

Figure 13. CO2 emissions from transport 1990-2015. [7]

In particular the road sector, coloured in green in the figure, represented for the 68% this rise leading the transport sector to being one of the most responsible for emissions. Although many Protocols and agreements had been signed in the period between 1990 and 2015 in order to limit emissions from international transport, emissions related to marine and aviation bunkers have grown faster than road-related emissions; in particular the marine international transportation has increased by the 77% and the aviation one by the 105%. For these reasons, even though projections are promising about the natural gas growth and the coal abandonment for all the energy production sectors, the CO_2 emissions from liquid fluids are predicted to increase. In transport sector it is warranted by the strong need of liquid fuel, in particular for passengers' transportation. As matter of the fact the percentage of liquid fuel utilization amounts to almost the 55% but forecasts predicted it will stay flat through 2040. Exactly as it has been noticed for the global energy consumption, the natural gas is subjected to a slow but significant growth and it is predicted it will continue his increase through 2040. As a matter of the fact according to the International Energy Outlook 2017 the energy consumption in transportation is predicted to develop following many technology evolution, giving more space to LPG and natural gas, rising up their utilization rate [2]. In the following figure a graph showing the world transportation energy consumption is reported:

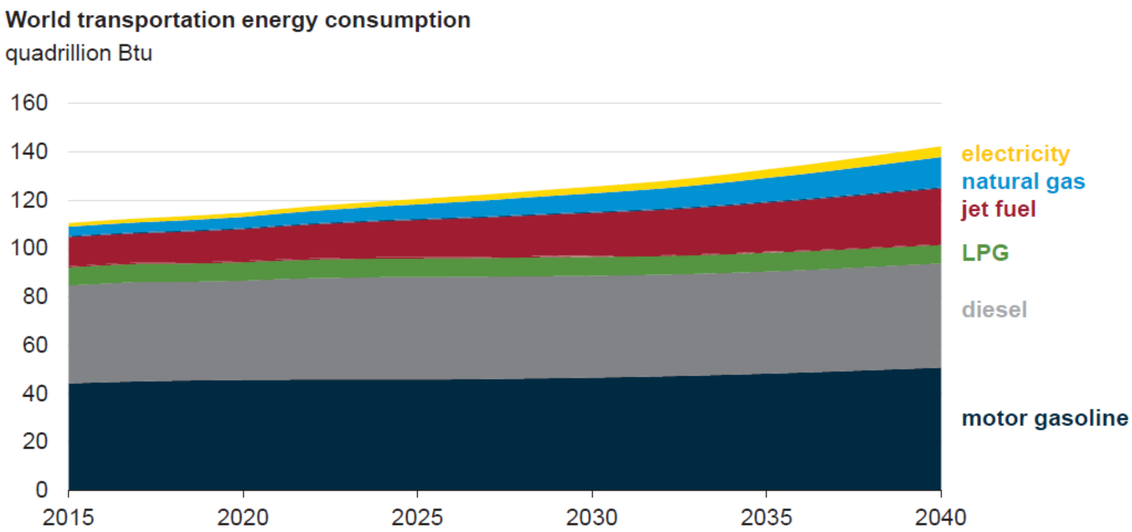

Figure 14. World transportation energy consumption 2015-2040. [2]

Although the development of alternative liquid fluids like LPG and natural gas has already interested almost every OECD countries, most of the total primary transportation energy supply is still attributed to motor gasoline, diesel and jet fuel. In particular the motor gasoline represents the first choice for road transportation and the diesel is mostly used as fuel for marine transportation but in OECD countries it feeds around the 20% of internal combustion light-duty vehicle. The jet fuel, named aviation turbine fuel ATF or avtur, is a mixture of many different hydrocarbons and it is used in aircraft characterized by gas-turbine engines; two examples are Jet A which is included in the kerosene-type jet fuel and the Jet B which is part of the naphtha-type jet fuel.

With regards to the road transportation it is possible to divide the entire group of vehicles according to the weight and it is therefore make the distinction between light-duty vehicles LDVs, medium-duty vehicles MDVs and heavy-duty vehicles HDVs.

Even though the sales of LDVs in OECD countries are predicted to stay flat through the 2040, energy consumption is projected to decrease thanks to the improved vehicle fuel economy. In particular according to the International Energy Outlook, in OECD countries light-duty vehicles will continue to record flat share sales for the motor gasoline vehicles around the 75% and decreasing flat shares for the diesel vehicles by some percentage points. Furthermore, the figure reported below shows a low increasing sales share of EVs and PHEVs but it will transform in 2040 in around a 6% growth; at the same time natural gas and LPG vehicles will be characterized by a light rise. In the other hand, in non-OECD countries the diesel vehicles sales share is and will be flat around the 10%, while the motor gasoline vehicles will continue to feed a big part of vehicles going from the 82% in 2015 to around the 72% in 2040. At the same time, even though the contribute of LPG vehicles will stay flat around low percentages, the natural gas vehicles, already around the 10%, will be subjected to an increase [9].

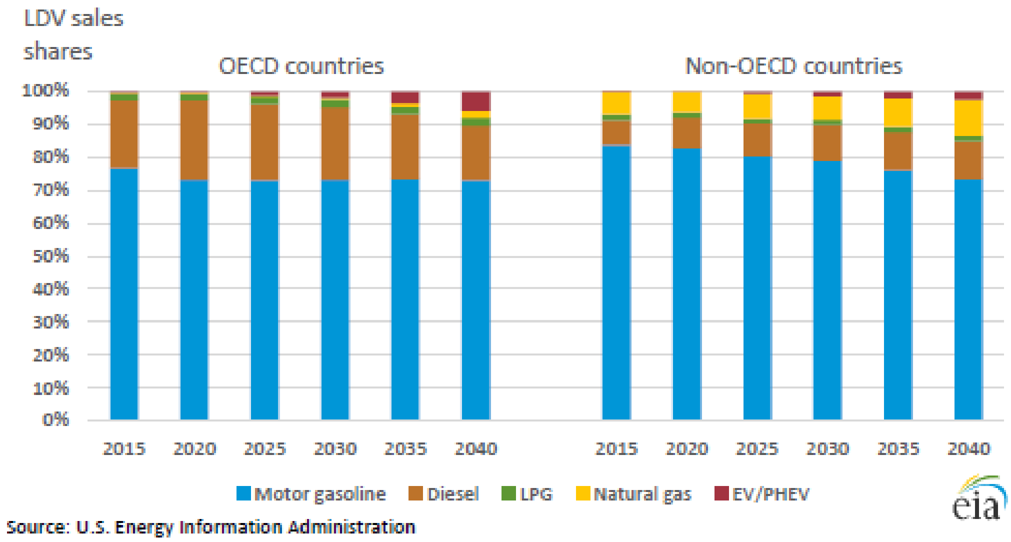

Figure 15. Light-duty vehicles sales share 2015-2040. [9]

The consequences on the energy consumption are actually not always coherent with the sales share. In particular while the OECD countries will be characterized by an LVD fuel consumption reduction through 2040 mostly due to a more gasoline consumption decrease and a more efficient engine economy, in non-OECD countries the development of a more penetrating industrialization will increase the energy penetration in transportation. An important difference predicted by the analysis performed concerns the different percentages related to fuels; in OECD countries motor gasoline and diesel will continue to represent mostly the only way to feed vehicles but in non-OECD countries the natural gas consumption will equal the diesel one. With regards to the EVs and PHVs, both in the OECD and non-OECD countries, the sales share will rise with a low growth rate entailing also electricity consumption increase.

With regards to the medium- and heavy vehicles, data show an energy consumption increase from 10.4 quadrillion Btu in 2015 to 12 quadrillion Btu in 2040. In particular motor gasoline and diesel consumption will stay almost flat in OECD countries with a low decrease of the diesel consumption replaced by a low increase of natural gas consumption. While for the LDVs case the most representative fuel is motor gasoline, for medium- and heavy-duty vehicles the most significant one is diesel, which is responsible for around the 90% of the fuel consumption. In non-OECD countries the motor gasoline consumption will decrease through 2040 and the total fuel consumption will increase mainly because of diesel and a natural gas consumption growth.

1.3.1 CO_2 emission reduction target for 2021

The European Union in order to reduce the carbon dioxide emission in transportation has established a legislation giving emission reduction targets for new cars; according to the European Commission cars are indeed responsible for 12% with respect to the CO_2 emission in EU. In particular the strategy has predicted two targets in order to help the automotive companies to achieve step by step the objectives requested. In 2015 the limit was the reduction by the 18% with respect to the 2017 average emission of 157.7$\left[\frac{g\ CO_2}{km}\right]$; in 2021 the objective to be reached is the reduction by the 40% with respect to same value. These limits correspond to a fuel consumption of around 5.6 $\left[\frac{l\ of\ gasoline}{100\ km}\right]$ or 4.9

$\left[\frac{l\ of\ diesel}{100\ km}\right]$ for 2015 and around 4.1 $\left[\frac{l\ of\ gasoline}{100\ km}\right]$ or 3.6 $\left[\frac{l\ of\ diesel}{100\ km}\right]$ for 2021. The average carbon dioxide of new cars was around 118.5 $\left[\frac{g\ CO_2}{km}\right]$ in 2017, which corresponds to an emission reduction by around the 33% compared to the 2017 average emission [10].

Nevertheless, even if the average 2015 target has been achieved, according to the *PA consulting* report published in 2017 some carmakers are late with respect to the 2021 emission limit of 95$\left[\frac{g\ CO_2}{km}\right]$. As matter of the fact a figure representing prediction and target for each carmaker is reported below, highlighting in green the actual data referred to 2016, in blue the forecasted emission for 2021 and in red the 2021 target:

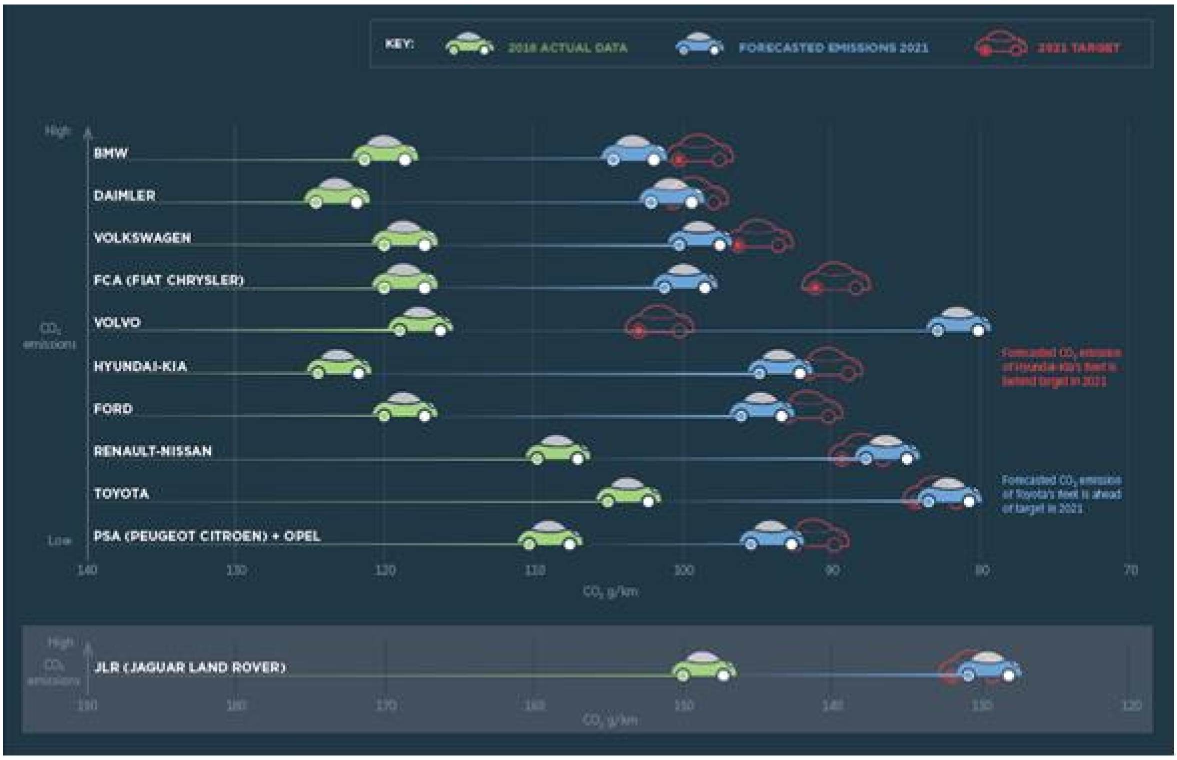

Figure 16. CO_2 emission reduction over time against 2016 actual data and 2021 target. [10]

According to this analysis there are only four big carmakers predicted to respect the 2021 limit: *Volvo*, *Toyota*, *Renault-Nissan* and *JLR (Jaguar Land Rover)* with regards to SUV. In particular *Volvo* has declared the intention to stop launching cars with only combustion engine from 2019 also thanks to the new Chinese owner which is intentioned to focus on electrification; they are therefore predicted to achieve the first place with an average CO_2 emission equal to 83,1 $\left[\frac{g\ CO_2}{km}\right]$. *Toyota* will reach the second place in the ranking thanks to their emission improvement and to the focus on the share of hybrid electric vehicles, even though they have not full electric vehicles in their car fleet. *Renault-Nissan* is focusing on electrification and can count electric vehicles for the 2% of the car fleet (i.e. the Nissan Leaf). *PSA (Peugeot-Citroen + Opel)* has stopped their hybrid diesel program and it is predicted to develop petrol hybrids and plug-in hybrids from 2019 and to obtain a significant EV penetration into their car stock. *Ford* has no electrified vehicle in their portfolio and they will focus their investments on reaching the 40% of EVs of the fleet and on CNGVs (Compressed Natural Gas Vehicles). *Volkswagen* is still subjected to the results of the diesel emission scandal happened in 2015 but it is focusing on a major electric vehicles production (also in Audi and Porsche); furthermore, investments will be done on battery production and on the electrification of all models reducing CO_2 emissions without probably reaching the 2021 target. *FCA Group* is very far from the achievement of this goal because of the production of SUV with high emission rate; two projects on the electrification of vehicles can be noticed with the announcement of launching an electric-driven Maserati and the development of the electric Fiat 500. *Mercedes Benz Daimler* will probably miss their target because of their late focus on alternative engines; nevertheless, a program for the production of electric vehicles has already been undertaken, planning to increase their BEV sales to 25% through 2025. *BMW* is predicted to miss their goal because of their low fuel consumption improvement and their insignificant electric vehicle sales. *Jaguar Land Rover* has increased their improvements on emission reduction and it has focused on the announcement that by 2020 50% of the entire fleet will be available as hybrid as well [10].

1.3.2 Towards the EVs

In 2009 the Clean Energy Ministerial (CEM) has proposed one of the best several initiatives in order to introduce and accelerate the knowledge of the electric vehicles world: the Electric Vehicles Initiative (EVI), a multi-government policy forum coordinated by the International Energy Agency and participated by the most representative countries in EVs like China, Finland, France, Norway, UK and United States.

An electric vehicle EV is a vehicle which uses an electric motor for propulsion. The electric motor is powered by electricity which can be generated by many integrated technologies: batteries, solar panels, fuel cells or hybrid propulsion systems. EVs don’t include only light-duty vehicles but, in many developed countries, gather every kind of transportation vehicle. The most significant examples of electric vehicles are given by prototypes realized around the world which use many electric power systems. In particular:

- In the United States class 8 electric trucks and an electric bike;
- In Brazil electric trolleybus and electric scooters;
- In China a battery electric bus with a LiFePO4 battery on board;
- In Switzerland an electric solar-powered aircraft which has successfully circumnavigated the globe.

With regard to the electric light-duty vehicles they can be divided in three categories according to the different characterizing technologies: BEVs, PHEVs and FCEVs.

- Battery electric vehicles or BEVs use electric motors instead of internal combustion engines for propulsion and they are characterized by battery packs that produce the whole power the vehicles need.
- Plug-in hybrid electric vehicles or PHEVs are hybrids and their battery can be recharged by plugging it thanks to an electric power external source or by the on-board engine of the vehicle.
- Fuel cell electric vehicles FCEVs are instead characterized by a fuel cell which produces electricity in combination with a battery or a supercapacitor in order to power the electric motor. Usually the fuel cells use oxygen and compressed hydrogen.

The first example concerning the EVs technology in Europe is represented by countries of the Nordic region in which since 2010 the stock of electric cars has been growing substantially. In particular in 2016 Norway has achieved the most successful goal with a 29% market share; to follow the Netherlands with a 6.4% and Sweden with a 3.4%. Generally, the whole Nordic region can be considered as the third large-producer of electric vehicles with around 90000 vehicles inserted in the global market. The first producer is China with almost the 40% of the world electric vehicles sold, accounting the double of the amount sold in the United States [11]. Globally the world electric car stock amounted to almost 2 million vehicles in 2016 and it is predicted to continue to rise up. In the figure reported below the trend of the electric car stock between 2010 and 2016 is shown for the most significant producers. BEVs and PHEVs represent mainly the world of the passengers' light-duty electric vehicles today. With regards to the FCEVs, the technology is more complex because of the hydrogen production and stock; furthermore, while the technology related to BEVs is mostly clean, FCEVs depend on the hydrogen production systems which have as product of the reaction carbon dioxide.

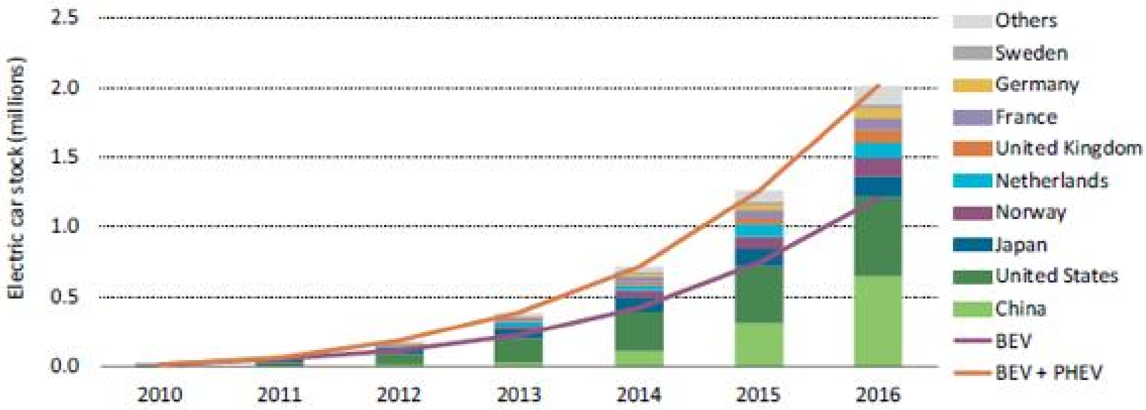

Figure 17. Light-duty vehicles sales share 2010-2016. [11]

<<*EVs are coming fast, but it is still too early to write the obituary for oil*>> [1] is the introduction to the strong theme of the transition toward the EVs used by the International Energy Agency in the World Energy Outlook 2017. It represents the real state of art of the worldwide position with respect to the EVs which concerns the switch from a transportation sector led by oil to a cleaner sector, led by the renewables and zero emissions. Even though the United States have been the most EVs producer in 2015, according to the New Policies Scenario (which is based on the energy policies and strategies declared by the leaders of the world countries) they indeed will account for 80% of the increase in global oil supply in 2025, demonstrating that the transition to EVs will be a difficult, steep and long-lasting itinerary. In particular the demand growth remains flat around significant quantities but it is characterized by a marked decrease of the rate thanks to a greater efficiency and to the variation of alimentation for passenger vehicles. One of the most significant sources of increase for the oil demand concerns indeed the consumption for aviation, for marine and for trucks which are involved in the fuel-efficiency policies less than the global road car fleet. Nevertheless, according to the two possible IEA scenarios for the next century, the world needs rapidly to reach the net-zero emissions and it is predicted to be reached around in 2090 or 2060 respectively according to Two Degree Scenario or Beyond Two Degree Scenario. [1]

CHAPTER II: HVAC SYSTEMS AND THERMAL COMFORT

2.1 Thermal Comfort

Comfort has become a significantly treated theme since the time in which the need of realizing most of tasks in a thermal, acoustic and visual comfort has begun to represent an important factor influencing the problem-solving capability. In particular, the thermal comfort can be gathered to many applications and in each of them it is regulated by legislation that set the thermal conditions reducing as much as possible the energy waste.
Thermal comfort and energy savings are in fact controlled by the EN 15251 (*Indoor environmental input parameters for design and assessment of energy performance of buildings addressing indoor air quality environment, lighting and acoustic, May 2007*) for buildings, UNI EN ISO 7730 (*Ergonomics of thermal environment – Analytical determination and interpretation of thermal comfort using calculation of the PMV and PPD indices and local thermal comfort criteria, 2005*) and ASHRAE Standard 55 – ANSI/ASHRAE 55-2010 (*Thermal Environmental Condition for Human Occupancy, 2010*) [12]. The last one is the latest edition of ASHRAE Standard 55 and it will be taken as reference for the definition of the main parameters and indices which the thermal comfort is based on.
The ASHRAE Standard 55 defines the thermal comfort as "*that condition of mind that expresses satisfaction with the thermal environment*" [13]; in fact, it concerns the personal reaction to a particular thermo-hygrometric condition and it changes from person to person because physiological and psychological reactions are totally individual.
It is important to subdivide factors in environmental ones and personal ones: the former are strictly related to the environment and they are temperature, thermal radiation, humidity and air speed, the latter are human-related and they concern activity and clothing.
With regards to the environmental factors, it is important to consider at least two distinctions between thermal types of environment. In particular, in thermally moderate environments like offices, shops and residences, the temperature and the other factors can be slightly different with respect to the thermal comfort; hence the aim concerns the reaching of the thermal comfort of the space in order to have a higher satisfaction by

occupants. Otherwise in thermally severe environments, like industries and workshops, all the environment factors are totally out of target because of the difficult ambient conditions; thermal comfort is impossible to be achieved and then the goal is preserving the health of person reducing the thermal stress. In moderate environments the objective of an accurate thermal comfort study is the achievement of thermal neutrality, absence of heat storage and of any shivering or sweating, thanks to suitably dimensioned HVAC systems. The thermal comfort analysis for moderate environments is based on the Fanger's theory, thought by the Professor Ole Fanger in 1960s and 1970s after having realized an experiment controlling environmental and personal factors in a climate chamber. He varied the air temperature and assessed the value of temperature corresponding to a state perceived by people of no thermal difference between themselves and the environment [12]. Thereafter, Fanger introduced two indices:

- Predicted Mean Vote (or PMV) index which "*predicts the mean value of votes of large group of persons on the seven-point thermal sensation scale*" [13];
- Predicted Percentage Dissatisfied (or PPD) index which "*establishes a quantitative prediction of percentage of thermally dissatisfied people determined from PMV*" [13].

PMV value	Thermal sensation
-3	Cold
-2	Cool
-1	Slightly cool
0	Neutral
+1	Slightly warm
+2	Warm
+3	Hot

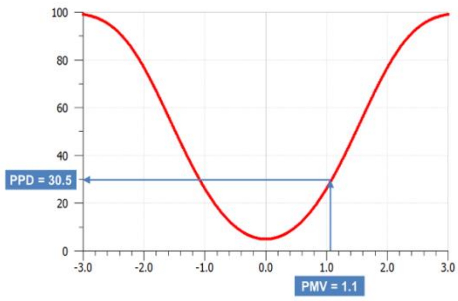

Figure 18. Seven-point thermal sensation scale and behaviour of PPD as function of PMV. [14]

The comfort zone is therefore defined thanks to the integration of the six environmental and individual factors with the assessment of the PMV and PPD indices. In particular the air temperature and mean radiant temperature with metabolic rate, clothing insulation, air speed and humidity, are used to determine the indices [13].

In order to estimate the thermohygrometric conditions related to the thermal comfort, an assessment of the energy balance of the human body is mandatory to understand how it reacts when subjected to a thermal discomfort and which are the parameters involved.

In particular the human body can be considered as divided in two main zones at different temperatures: the outer zone is the skin and it has a temperature depending on the environmental conditions, the inner zone contains vital organs and it has a constant temperature of 37 °C [12]. Furthermore, the heat production of a human (named metabolic heat or metabolism) is strongly depending on the type of task: in a condition of sedentary activity it produces 100 W; in a stressed condition it can produce heat up to 1000 W in order to regulate the body temperature. Then it is possible to consider the human body as a thermodynamic system and therefore to impose an energy balance:

$$S = M - W - E_{sk} - E_{sw} - R_{res} - C - R - C_k \quad [12]$$

In particular:

- ✓ S is the heat storage expressed in *W*;
- ✓ M is the metabolism expressed in *met* $\left(1\,\mathrm{met} = 58\frac{\mathrm{W}}{\mathrm{m}^2}\right)$;
- ✓ W is the work expressed in *W*;
- ✓ E_{sk} is the evaporation through the skin expressed in *W*;
- ✓ E_{sw} is the heat loss by swearing expressed in *W*;
- ✓ R_{res} is the latent and sensible heat loss by respiration expressed in *W*;
- ✓ C is the convective heat loss expressed in W/m^2;
- ✓ R is the radiation heat power expressed in W/m^2;
- ✓ C_k is the conduction heat power expressed in W/m^2.

It is possible to gather in two terms all contributes respectively referred to latent and sensible emission:

$$S = M - W - Q_L - Q_S - C_K \quad [12]$$

In particular, since usually W and CK are negligible contributes, the energy balance equation can be written as below:

$$S = M - Q_L - Q_S$$

$$S = 0 \quad \rightarrow \quad M - Q_L - Q_S = 0 \quad \rightarrow \quad \text{energy balance [12]}$$

With regards to the metabolism, it is more or less proportional to the body area which is expressed as below, according to the Dubois formula:

$$A_b = 0.202 * m^{0.425} * h^{0.725} \quad [12]$$

With respect to this dependence, a suitable table has been built up reporting metabolism data with respect to the correct activity and showing an increasing heat production going from sedentary activities to more lively ones.

At the same time an accurate analysis on the heat loss by convection has been realized, focusing on the clothing and its different thermal implications depending on garments with different thermal resistance. In the following tables overall data concerning metabolism and clothing have been reported in order to make a distinction between summer and winter periods with respect to the garments worn.

Clothing	I_{cl}	
	clo	*m² °C/W*
Naked	0	0
Light summer clothing	0.5	0.08
Light office clothing	0.7	0.11
Typical indoor winter clothing	1	0.16
Traditional heavy office suite	1.5	0.23

Activity	Metabolism	
	met	*W/m²*
Laying	0.8	46
Seated, relaxed	1	58
Sedentary activity	1.2	70
House work activity	2	116
Moderate activity	2.8	165

Table 1. Typical values of clothing and metabolism according to the garments and activity. [12]

The energy balance equation becomes:

$$M - W + \quad \rightarrow \text{ Metabolic heat}$$
$$-0.31[\,57.4 - 0.07 * (M - W) - P_a] + \quad \rightarrow \text{ Evaporation through skin}$$
$$-E_{sw} + \quad \rightarrow \text{ Sweating}$$
$$-0.0017 * M * (58.7 - P_a) - 0.0014 * M * (34 - T_a) + \quad \rightarrow \text{ Respiration}$$
$$-3.9 * 10^{-8} * f_{cl} * (T_{cl}^4 - T_r^4) + \quad \rightarrow \text{ Radiation}$$
$$-f_{cl} * h_c * (T_{cl} - T_a) = 0 \quad \rightarrow \text{ Convection}$$

In particular:

- f_{cl} is the ratio between clothed and nude surface area;
- p_a the water vapour pressure in mbar;
- h_c is the convection heat transfer coefficient.
- T_a is the air temperature in °C;
- T_r is the mean radiant temperature in °C;

- T_{cl} is the clothes temperature in °C and it is function of the skin temperature T_{sk} and the clothes thermal resistance R_{cl}.

In comfort conditions skin temperature T_{sk} and sweating E_{sw} have different expressions:

$$T_{sk} = 35.7 - 0.0275 * (M - W) \qquad E_{sw} = 0.42 * (M - W - 58.15) \text{ [12]}$$

According to the energy balance equation, the definition of parameters and the explanation of variables involved, Fanger finally gave the formulation of the "*load on the human thermal control system*" L and of the PMV index obtained introducing the T_{sk} and the E_{sw} as formulated above:

$$M - Q_L^* - Q_S^* = L$$

$$PMV = 0.303 * L * e^{-0.036*M+0.028} \text{ [12]}$$

According to the ASHRAE Standard 55, it is possible to verify the thermohygrometric conditions thanks a suitable open source tool which need as input the six environmental and individual parameters in order to carry out the thermal thermohygrometric status in a graph. In the y-axis there is the humidity ratio expressed in $\left[\frac{g\ of\ water\ vapour}{kg\ of\ air}\right]$, in the x-axis there is the dry-bulb temperature in °C. With respect to the input data introduced in the tool, the thermo-hygrometric point can fall in two zones: the central one, coloured in violet, corresponds to the thermal comfort zone, the outer zone corresponds to uncomfortable conditions. In the following figure an example of thermal comfort study through the ASHRAE tool is reported, showing the input data and the PMV and PPD indices which therefore define the type of sensation with respect to the thermal scale:

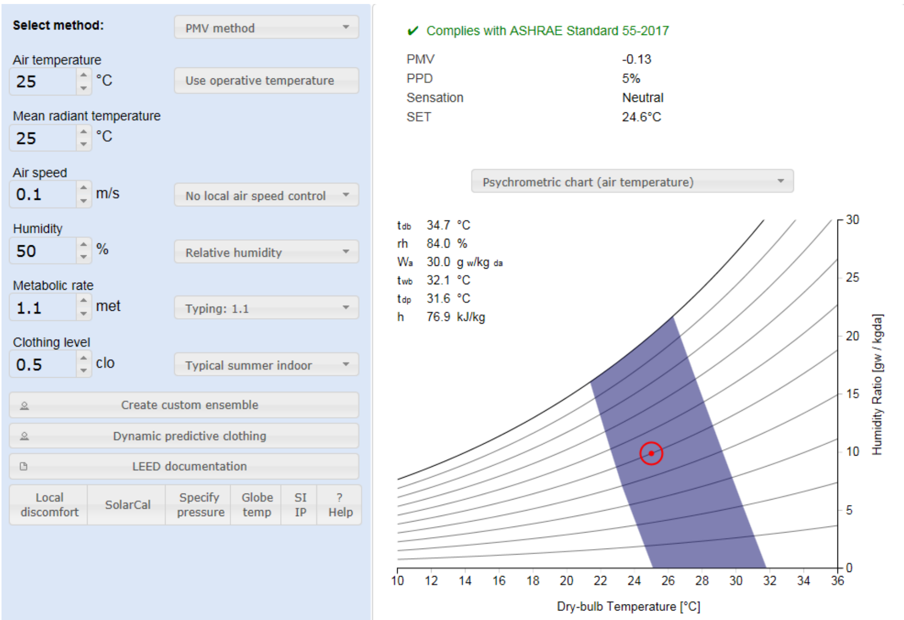

Figure 19. ASHRAE tool for the estimation of PMV and PPD. [15]

2.2 HVAC systems for passenger cars

The HVAC (or Heating Ventilation and Air Conditioning) systems are systems used in order to obtain an environmental thermal comfort for people during both summer and winter periods; in automotive applications they grant visible requirements with respect to defrosting and defogging operation times. Furthermore, according to the ASHRAE Standard 55 the A/C system has the mandatory job concerning the air change in the cabin in order to respect the CO_2 concentration deriving from human activities. They are suitably projected to guarantee specific thermohygrometric conditions in a space occupied by humans. In particular, HVAC systems include generally:

- thermostat, a thermal sensor that measure the ambient temperature and trigger the heating or air conditioning system when the ambient conditions are far from the comfort ones;
- furnace, a heater component which warm up the temperature of an air supply. This component can be a combustion chamber, electric resistance, heat pump or a local solar collector.
- heat exchanger, a system containing an operating fluid which absorbs the heat power produced by the heater component;
- evaporator coil, a heat exchanger in which the refrigerant fluid evaporates and the air supply cools down;
- condensing unit, a heat exchanger in which the refrigerant fluid condenses giving heat away to environmental air forced in thanks to a ventilation system;
- compressor and pump, mechanical components which carry on respectively the refrigerant vapour and liquid water;
- thermostatic valve, a totally dissipative constriction which allows the refrigerant to cool down and reducing its pressure without any external energy supply;
- refrigerant lines, the system carrying the refrigerant fluid to complete its thermal cycle passing from compressor, evaporator, condenser and thermostatic valve;
- ductwork, the system carrying the air to warm up and/or cool down and bringing it into the space to be conditioned.
- vents, the outlets which introduce the treated air into the space.

2.2.1 Air conditioning systems properties

A typical air conditioning system is realized with a compressor, a condenser, an orifice for the Joule-Thompson expansion and an evaporator; each of them is represented and schematized in the figures below, showing the working and the thermodynamic diagrams, highlighting every transformation and function.

- *Transformation 1-2*: the refrigerant enters in the evaporator in the condition of point 1, where the temperature T_1 is the saturated temperature for the inlet evaporator pressure $p_{in,\ evap}$. The point is in saturated conditions and it is characterized by a gas mass fraction x_1. For this reason, every thermodynamic property is linked to the gas mass fraction:

$$x_1 = \frac{h_1 - h_{l,p_{in,evap}}}{h_{lv,p_{in,evap}}}$$

$$h_1 = h_{L,p_{in,evap}} + x_1 * h_{lv,p_{in,evap}}$$

$$s_1 = s_{L,p_{in,evap}} + x_1 * s_{lv,p_{in,evap}}$$

$$v_1 = v_{L,p_{in,evap}} + x_1 * v_{lv,p_{in,evap}}$$

- *Transformation 2-3*: the refrigerant is compressed and led from the lower pressure p_2 to the higher pressure p_3 by a volumetric compressor according to its efficiencies. The outlet temperature of the refrigerant is the highest temperature of the whole cycle and it must be controlled in order to avoid problems with the viscosity of the lubricant which can lead to the separation of the chemical components affecting the heat transfer in the heat exchangers.

- *Transformation 3-4*: the refrigerant enters in the condenser where it condenses thanks to the heat transfer with moist air forced to pass into the condenser by a vent.

- *Transformation 4-1*: in the last transformation of the cycle the refrigerant enters in an orifice in which the refrigerant pressure drops and the temperature decrease. The transformation is isoenthalpic and so the inlet enthalpy of the refrigerant is equal to the outlet one.

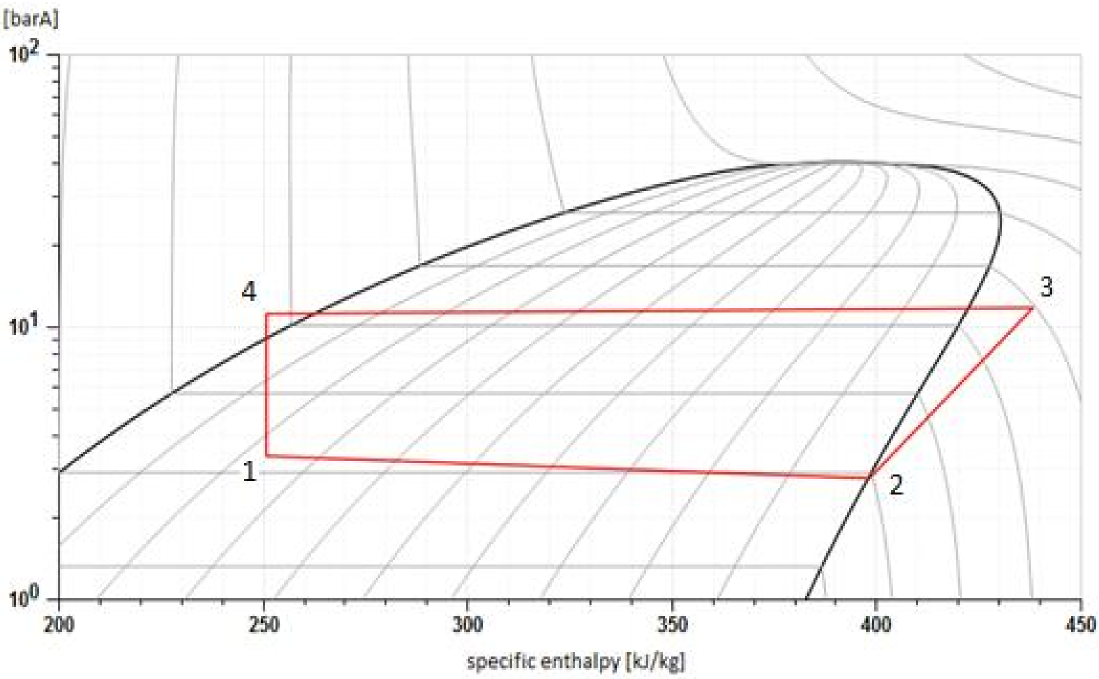

Figure 20. Thermodynamic diagram of a refrigerant operating an air conditioning cycle. [14]

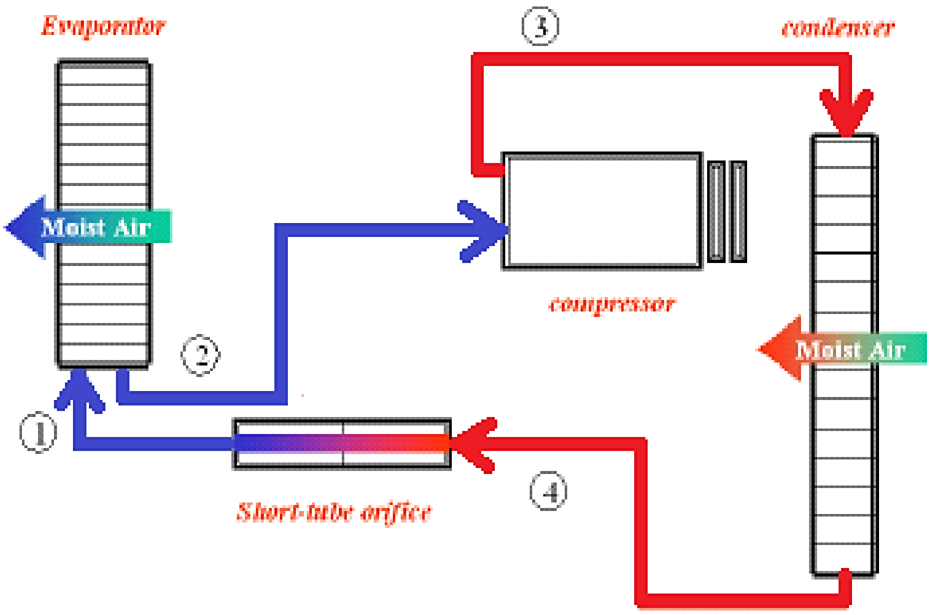

Figure 21. Functional diagram of a refrigerant operating an air conditioning cycle. [14]

Evaporator

The evaporator is the heat exchanger responsible of the evaporation of the refrigerant and therefore it cools down the air flow rate circulating in the car cabin. During the heat transfer, depending on the inlet thermohygrometric condition, air temperature can drop down through the reaching of the dew point. Hence it implies the condensation of a part of the water vapour contained by the air and the consequent water content reduction. The evaporator is characterized by a two-phase fluid at the inlet condition due to the Joule-Thompson expansion and by a saturated fluid at the outlet condition, usually overheated in order to avoid liquid drops which could ruin the compressor. In this way furthermore, the outlet enthalpy at the evaporator is greater than the saturated vapour one, increasing the specific energy absorbed q_L. During the evaporation the refrigerant is subjected to pressure drops which lead the pressure to decrease from the p_1 through the p_2 (with $p_2 < p_1$). The pressure drop causes therefore a greater inclination of the transformation and so the outlet temperature is lower than the temperature related to the case in which the pressure drops are null. In the following figure, an example of evaporator is shown:

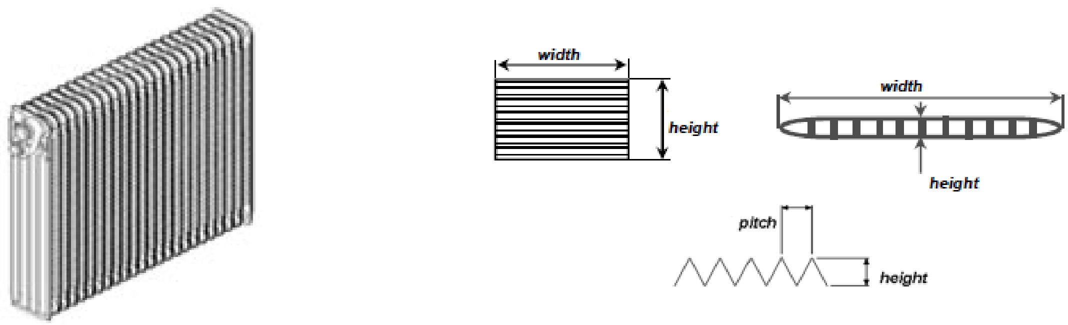

Figure 22. Characteristics of an evaporator.

The evaporator is characterized by length, height and thickness; varying the geometrical characteristic, it is possible to increase or reduce the frontal area and then the air flow rate. The evaporator can include one or more rows depending on the dimension and on the heat transfer requested; each of them can be constructed with tubes or plates according to the producer and they are organized in order to achieve a suitable inner path which can maximize the cooling power production. Tubes and plates are furthermore characterized by channel cross-sectional area with respect to the refrigerant side and hydraulic diameter of the channel in order to obtain an estimation of the refrigerant inner path. In both the applications fins are applied in order to increase the air-side heat exchange area and so to increase the heat exchanger efficiency. Fins are installed with a specific criterion in terms of quantities, pitch, length and height. In fact, the more fins are dense the more heat exchange increases and air-side pressure drops are high; otherwise the more fins are far the more heat exchange is worse and air-side pressure drops decrease.

Compressor

The compressor is a mechanical component which needs to be moved with a mechanical power; applications are various and so the alimentation of the compressor is also various. Compressors can be subdivided in “open compressors” and “hermetic compressors”.
Open compressors are characterized by two separated boxes containing respectively engine and compressor and connected by an axle; this kind of compressors are hence characterized by fluid losses and they use refrigerant fluids which are incompatible with the copper of the electric engine but compatible with the environment and therefore not pollutant. The hermetic compressors are instead characterized by a unique box containing both the engine and the compressor; they are not characterized by fluid losses and they use refrigerant fluids compatible with the copper of the electric engine but possibly incompatible with the environment [5].
In particular, in civil or industrial applications it is usually triggered by an electric engine which absorbs electric energy and converts it in mechanical power thanks to an alternator. In these applications, many refrigerants can be used like: zeothropic mixtures, azeothropic mixtures, HFC, HCFH, CFC or hydrocarbons. Otherwise in automotive applications the compressor is connected to the engine axle which transmits to it the mechanical power necessary to trigger it and to obtain a torque profile coherent with the air conditioning system operation; the refrigerant must therefore be compatible with the

environment. The refrigerant fluid enters in the compressor and it is compressed through a higher pressure according to the pressure ratio β and its efficiencies: $\beta = \frac{p_3}{p_2}$

Figure 23. Example of compressors. [16] [17]

Compressors used in internal combustion vehicle applications can be subdivided in at least two typologies depending on their control system: fixed displacement or variable displacement. The former usually can be realized with pistons, palette or scrolls according to the kind of volumetric compressor, the latter are basically constituted by many pistons which change the displacement of the compressor. In this case the heat load variation is regulated thanks to the displacement reduction, controlled by regulation valves. According to the type of regulation, it is possible to distinguish two kinds of regulations: internal controlled and external controlled. In the former the compressor is self-regulated with characteristics of the valves fixed by the constructor, in the latter the compressor is regulated with valves which change their settings according to an electric signal coming from a sensor measuring the outlet air temperature from the evaporator [15]. Usually it can be possible to subdivide the compressor efficiency in: volumetric (related to the gas remaining in the compressor at the end of the compression and to the pressure ratio β), isoentropic (depending on the irreversibility of the compression) and mechanical (related to the connection of the system engine - axle - compressor). Volumetric and isoentropic efficiencies are strictly depending on the pressure ratio β and on rotary speed of the engine, the mechanical efficiency is usually high enough and it can be assumed constant. In particular volumetric and isoentropic efficiency expressions are:

$$\eta_v = \frac{V_{max} - V_{min}}{V_{max} - V_c} \qquad \eta_{is} = \frac{\Delta h_{ideal}}{\Delta h_{actual}}$$

where V_c is the dead centre volume, V_{max} is the maximum displacement, V_{min} is the minimum displacement, Δh_{ideal} is the isoentropic enthalpy variation and Δh_{actual} is the non-isoentropic enthalpy variation.

Condenser

The condenser is the heat exchanger responsible of the liquefaction of the refrigerant which enters in it after having been compressed by the compressor to the highest pressure of the system. In this heat exchanger the refrigerant reduces its energy rejecting heat power to the environment thanks to the external moist air forced to pass through the rows by a vent. In order to obtain an efficient heat rejection, it is mandatory for the refrigerant to have a temperature sufficiently greater than the environmental air temperature. This condition is obtained by the compression; in this way the violation of the pinch point is avoided and the system operation is preserved. In particular the refrigerant enters in the condenser as overheated vapour and leaves it as sub-cooled liquid, ready to pass through the expansion component. Hence, similarly to the evaporator for the overheating, in the condenser a sub-cooling is realized in order to reduce the inlet enthalpy at the evaporator (maximizing the q_L) and to reduce the refrigerant inlet temperature at the expansion component under the maximum inversion temperature. At the same time both evaporator and condenser are characterized by pressure drops which reduce the outlet temperature from heat exchangers. In the condenser pressure drops are a critical point because they decrease the fluid temperature risking to reach the violation of the pinch point and compromising the whole system operation. In order to avoid this problem, the pressure ratio of the compressor is increased taking into account the pressure drops; in this way the temperature at the end of sub-cooling is always greater than the temperature of environmental air.

In civil applications the condenser is the simplest component to notice; in fact, it is located outside, usually attached to the perimeter walls because of the simpler way to sucked environmental air. In automotive applications it is located in front of the engine radiator.

In the following figure a typical condenser is shown:

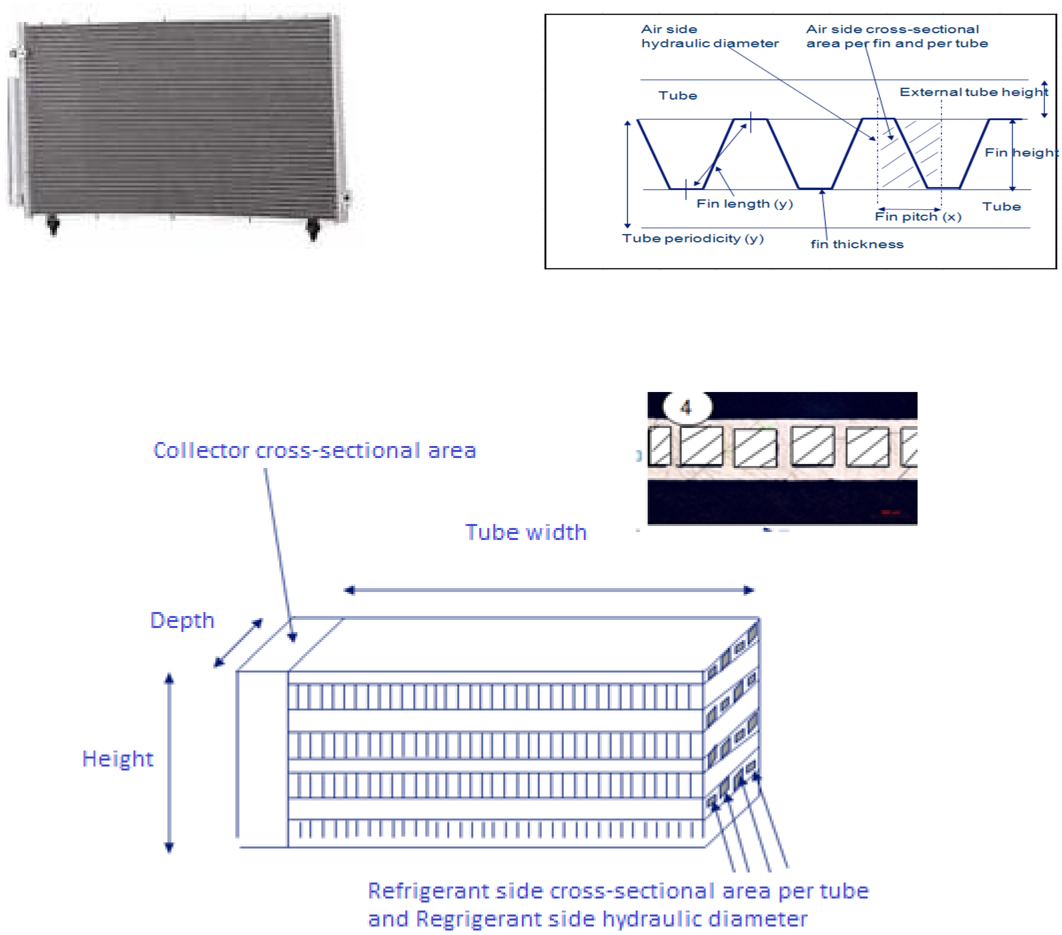

Figure 24. Example of a condenser

With respect to the geometrical characteristic, they are almost equal to the evaporator ones except for the presence of tubes instead of plates. The condenser is finned and fin properties are shown in the figure above.

Joule-Thompson expansion component

The Joule-Thompson expansion is an isoenthalpic transformation and so the enthalpy of the refrigerant leaving the condenser is equal to its enthalpy when it enters into the evaporator. The refrigerant is sub-cooled liquid at the input but during the transformation the chemical and physical processes cause a pressure reduction and a consequent temperature reduction which leads the fluid to pass to the two-phase condition. At the end of the thermal expansion the refrigerant is therefore in a condition under the saturation curve of the diagram (log p – h).

The Joule-Thompson expansion can be realized with a simple calibrated short-tube orifice or with a thermostatic expansive valve: the former is a mere orifice in which the refrigerant decreases its pressure and temperature, the latter is more complex compared to the simple orifice but it's characterized by the possibility to regulate the refrigerant mass flow rate and to control the overheat at the end of the evaporation in the evaporator [16]. In the following figures a thermostatic expansive valve TXV with integrated bulb and a simple orifice are shown:

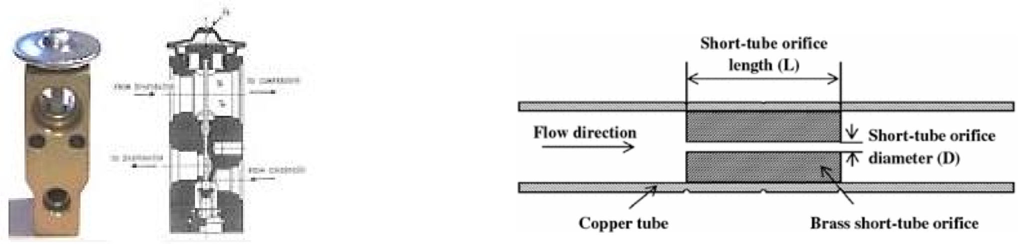

Figure 25. Representation of a TXV (on the left) [16] and of a short-tube orifice (on the right).

In order to obtain a temperature reduction consequent to the pressure reduction realized by the Joule-Thompson expansion, the refrigerant inlet temperature and the Joule-Thompson coefficient have to be controlled. The Joule-Thompson coefficient is expressed as reported below:

$$\mu = \frac{\partial T}{\partial p} \quad for\ h = cost \qquad [5]$$

$$\mu > 0 \quad "cooling\ zone"$$

$$\mu > 0 \quad "heating\ zone"$$

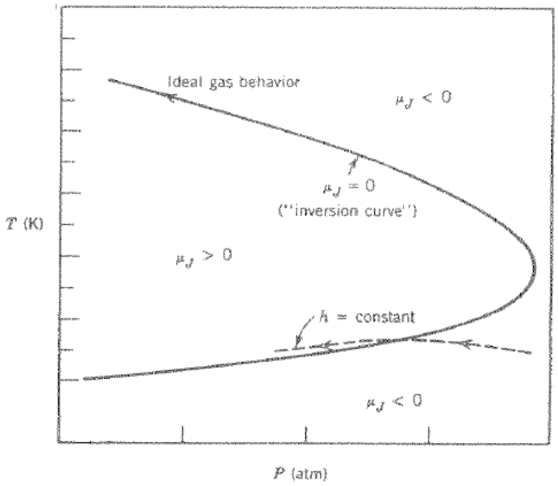

Figure 26. Diagram T – log p – inversion curve [20].

The graph reported above represents the variation of the temperature with respect to the pressure evolution. In this graph isoenthalpic curves are drawn; in particular each curve is characterized by a maximum and, connecting all the maximum points, it is possible to find the *inversion curve*, limited on the upper side by the *maximum inversion temperature*. On the left of this curve every pressure reduction causes a temperature reduction ("cooling zone"), on the right every pressure reduction causes a temperature increase ("heating zone") [20]. In order to obtain the transition from the high-pressure line to the low-pressure line coupled to a temperature reduction, it is necessary that the thermal expansion occurs in the cooling zone conditions and therefore that the refrigerant fluid has characterized by a sufficiently high maximum inversion temperature.

2.2.2 HVAC systems and thermal comfort for passengers' car

In the following figure a typical HVAC system for a car is shown:

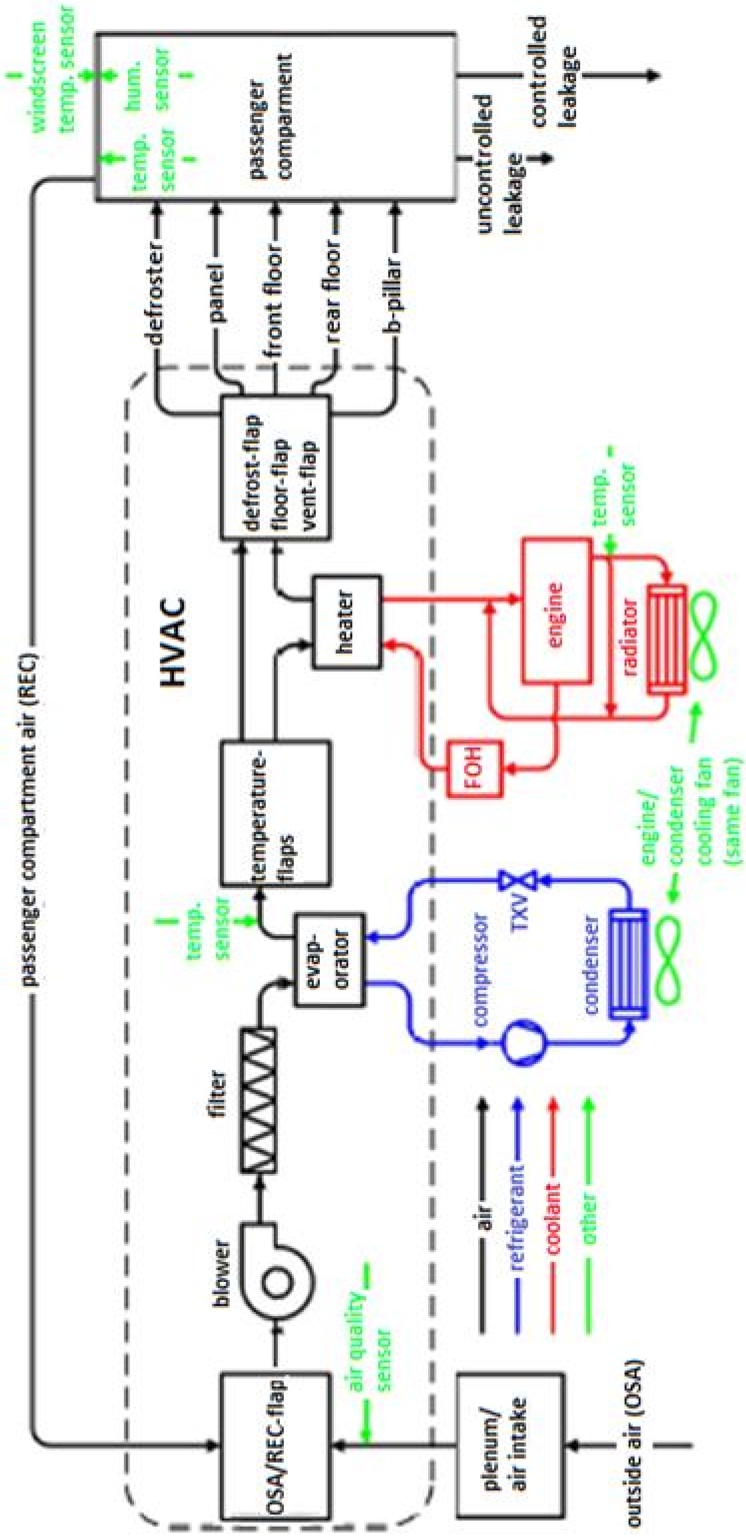

Figure 27. Functional diagram of a typical HVAC system for a car [21].

The air conditioning system is characterized by three different but cooperating systems: air system, coolant system and refrigerant system.

The air system is regulated by an actuator which switches two flaps in order to control the amount of outside air (OSA) and recirculated air (REC) sucked by the blower and led through the passenger compartment after having made mandatory steps [21]. The moist air is at first treated by a filter in order to stop all the particles which get worse the air quality and then it enters in the evaporator where it exchanges heat in order to get the evaporation of the refrigerant. After that, in order to regulate the inlet air temperature, the air can be heated by a heater; in particular it can be a secondary system which uses the engine coolant thermal charge or an electric component (particularly indicated for EVs applications). The heater is controlled thanks to temperature and humidity sensors which transmit to it a signal (mechanical or electric according to the heater typology) in order to regulate the coolant flow rate or the electricity.

The coolant system is the system used by the vehicle in order to reduce the engine temperature; it is characterized by a radiator located in the front end of the car where a vent forces the environmental air to pass through it in order to reduce the coolant temperature. In order to reduce as much as possible the waste coming from the engine, the heat rejection can be employed in order to feed the air conditioning system heater. Since this heat amount could not be sufficient, especially for the start-up, a fuel operated heater (FOH) is provided; it is an electrical component which is used also to ignite fuel.

The refrigerant system is used for the air conditioning and it can be possible to observe in the following figure:

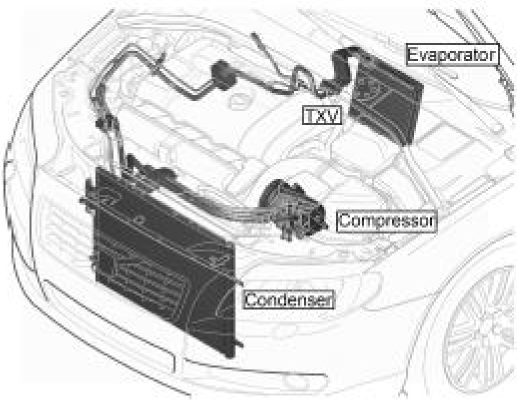

Figure 28. Example of an air conditioning system in a car [21]

The condenser is located in front of the engine radiator, in the front end of the car, and it removes heat from the system thanks to the environmental air forced to pass through the condenser channels by the blower that feeds the radiator. The heat flow removal is strictly depending on the air flow rate; if the vehicle is moving with a sufficient velocity the air flow rate allows a suitable heat removal, if the car velocity is lower than a particular value the flow rate would be insufficient. In this case the blower fan starts to work in order to reach the necessary air flow rate [21].

The evaporator is in the inner part of the motor compartment near to the dashboard in order to reduce the heat loss in the ducts which lead the air treated into the cabin. In this heat exchanger hence, the air is cooled thanks to the evaporation of the refrigerant.

The compressor is always coaxial with the internal combustion engine which transmits it the mechanical power necessary to compress the refrigerant. According to the kind of compressor it can be regulated by different ways: rotary speed regulation, internal cabin temperature or outlet evaporator air temperature. In particular in the first case the compressor has a fixed displacement and the regulation is operated by the alternator which reduces or increases the rotary speed, in the second case the compressor has a variable displacement and the control is made basing the regulation on the internal cabin target temperature, in the third case the compressor has also a variable displacement and the control is made with respect to the outlet evaporator target temperature of the air.

The Thermal eXchange Valve (TXV) is situated between the condenser and the evaporator and it is aimed to control the refrigerant flow rate in the system after having measured the outlet temperature and pressure from the evaporator. The purpose of this component is to regulate the superheat at the evaporator outlet thanks to a force balance acting on a rod via a diaphragm.

In the following figure the valve diagram is shown. In particular it provides: the refrigerant saturation curve and the valve opening curve as function of the thermal sensing bulb fluid in the first quadrant, the evaporator outlet pressure as a function of the valve lift for different constant temperature values in the second quadrant, the evolution of the reference mass flow rate as a function of the valve limited to the maximum mass flow rate in the third quadrant, the evolution of the reference mass flow rate as a function of the evaporator outlet temperature in the fourth quadrant [14].

These curves depend on each other and therefore knowing the curve of the third quadrant all the other curves can be deduced.

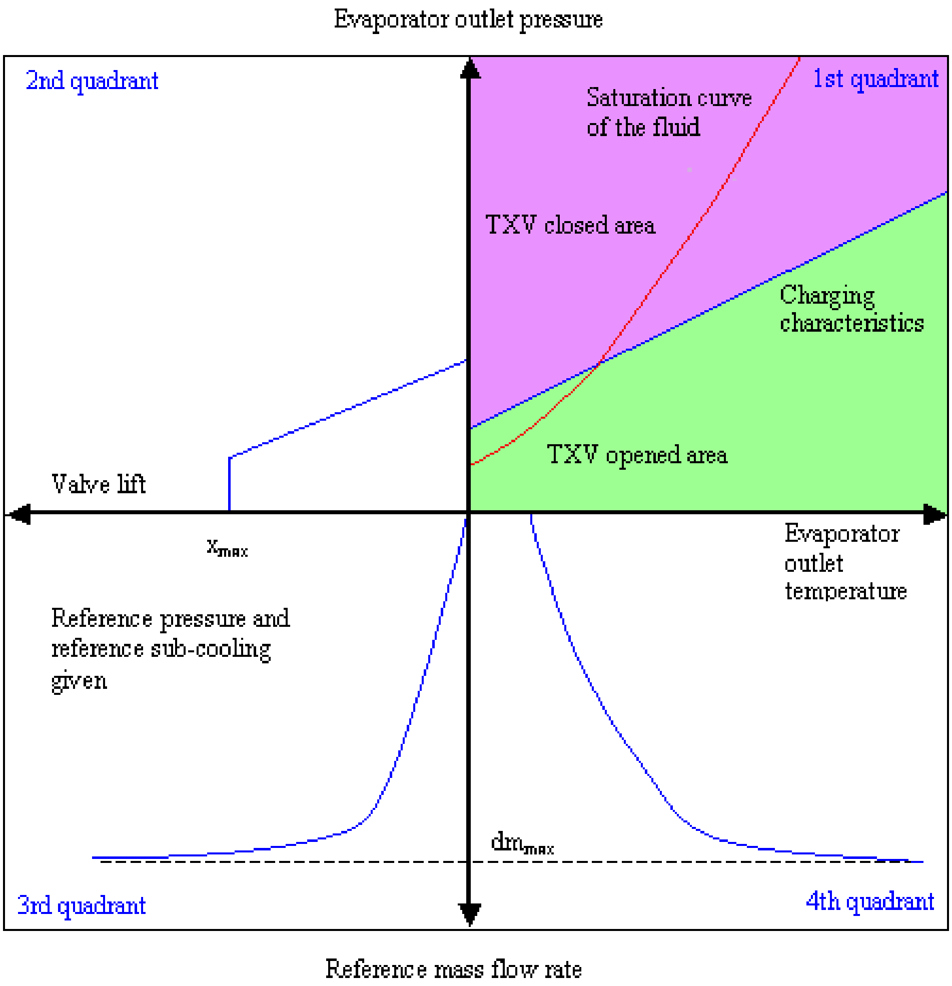

Figure 29. Four-dimension diagram of a thermostatic expansion valve [14]

According to ASHRAE Standard 55 – Thermal environmental conditions for human occupancy, it is possible to introduce approximate comfort conditions in automotive applications [13]:

Values for inside temperature and RH with respect to the outside conditions			
Outside temperature	*Outside RH*	*Comfort temperature*	*Maximum RH*
+20 °C	60 %	22 °C	70 %
+25 °C	60 %	23 °C	65 %
+30 °C	60 %	25 °C	60 %
+32 °C	60 %	26 °C	55 %

Table 2. Comfort thermo-hygrometric conditions with respect to outside temperature [13]

CHAPTER III: VEHICLE CHOICE

The project work has been focused on a particular vehicle according to the need of the carmaker to improve the knowledge of all the materials and systems' operation in order to achieve a suitable basis to perform other studies. In particular, the strongest need to reduce the fuel consumption concerns certainly a research of ways to improve energy savings both in the cabin and in the engine system. It is obvious how all improvements studied for an internal combustion engine vehicle can be used as starting point in order to enhance the autonomy of an electric vehicle. The differences concern only the particular kinds of technologies implemented. For example, with respect to this project thesis it is possible to deal with the different compressors used in the air conditioning system of an internal combustion engine vehicle and in the air conditioning system of an electric vehicle.

As described in the paragraphs written above the variety of compressors used in automotive applications for air conditioning systems depends mostly on the displacement characterization. In particular it is possible to consider fixed displacement compressors or variable displacement compressors according to the type of the control system.

With regards to the differences between electric and internal combustion applications, the compressor used for this automotive application is a variable swash plate and the electric application is characterized by an electric compressor. In the following figures these two compressors are reported with the only intention to show the different details.

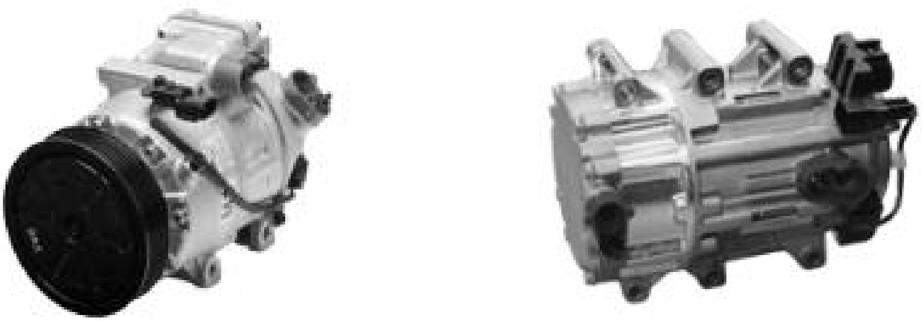

Figure 30. Overview of a variable swash plate compressor (on the left) and an electric compressor (on the right) [22].

For internal combustion vehicles the air conditioning compressor is triggered by a belt connected to the engine and so it depends on the engine operation. For electric and hybrid vehicles the compressor is a scroll controlled by the electric motor and the integrated power control. It operates independently and therefore it is possible to ensure the air conditioning operation even though the electric engine is switched off [22].
With regards to the system control, the internal combustion compressor is regulated according to the evaporator discharge air temperature, improving the power consumption and the fuel economy guarantying comfort to passengers. When the target temperature is reached the regulation varies the displacement of the compressor, reducing the refrigerant mass flow circulating and then the cooling power absorbed. On the other hand, the electric compressor is regulated varying the rotary speed with a frequency converter. Furthermore, while the maximum rotary speed amounts around 5000-6000 rpm for internal combustion, the maximum rotary speed of an electric vehicle compressor can reach 8600 rpm.

3.1 Vehicle

The choice the vehicle is reserved and will not explained in this thesis. In particular the choice has been done according to the need of the carmaker and to the internal available data. The description of the choice of the vehicle will involve only the engine, accounted in the FCA engine stock:

2.0 l Multijet Common-rail 103 kW E5

In the following paragraphs the engine and the air conditioning group are listed and characterized, specifying the choice of the refrigerant fluid describing roughly the obligations involved in the choice. At the same time every component will be described according to the internal policy of the carmaker on the privacy of sensible data, omitting data which could be identify particular operations or the supplies involved in the project management of the vehicle.

3.2 Engine

Figure 31. Engine Multijet 2.0 l Common-rail [23].

The vehicle is provided with a 170 CV engine which is able to produce a maximum torque of 350 Nm and it can be combined with a nice-speed automatic gearbox or a six-speed manual gearbox. It ensures a maximum velocity of 196 km/h and an acceleration 0-100 km/h in 9.5 seconds; the urban, combined and extra-urban consumption are shown in the table below:

Engine performance	
Combined consumption [l/100 km]	5.1
Extra-urban consumption [l/100 km]	4.6
Urban consumption [l/100 km]	6.0
CO_2 emission [g/km]	134

Table 3. Performance of the engine Multi-jet 2.0 l.

CO_2 emission values are defined according to the obligations established by the European Union with the Regulation (EC) 692/2008 which implements and modifies the “*Regulation (EC) 715/2007 of the European Parliament and of the Council […]*” concerning “*[…] the approval of motor vehicles with respect to the emissions from light passenger and* *commercial vehicles (Euro 5 and Euro 6) and […]"* concerning "*[…] the vehicle repair and maintenance information"* [23].

In particular the evaluation of the fuel consumption and of the carbon dioxide emission is realized according to many driving cycles, different by countries. The Europe driving cycles are the New European Driving Cycle (NEDC), referred to the assessment of emission levels of light passenger vehicles. It is realized repeating four ECE-15 urban driving cycles (UDC) and one Extra-Urban Driving cycle (EUDC). Although the NEDC is supposed to represent the typical operation of a car in Europe, it has been continuously criticized because accelerations realized in the test are weak and they don't represent an actual drive [24].

According to this problematic the Worldwide harmonized Light vehicles Test Procedure (WLTP) has been introduced in order to harmonize the global standard for the assessment of pollutants and CO_2 emissions, energy consumption and electric range [25].

In this work three driving cycles will be considered:

- NEDC or New European Driving Cycle;
- WLTC belonging to the WLTP or Worldwide harmonized Light vehicles Test Procedure;
- SC03 a cycle belonging to the Supplemental Federal Test Procedure (SFTP) in which the test is performed with the air conditioning system switched on.

The engine is fed by Diesel fuel, its displacement is 1956 cc (or 2.0 litres) and it is able to produce 103 kW with a maximum rotary speed of 3750 rpm.

3.3 Evaporator data

The evaporator employed in the present vehicle application is shown before, characterized by the geometrical properties:

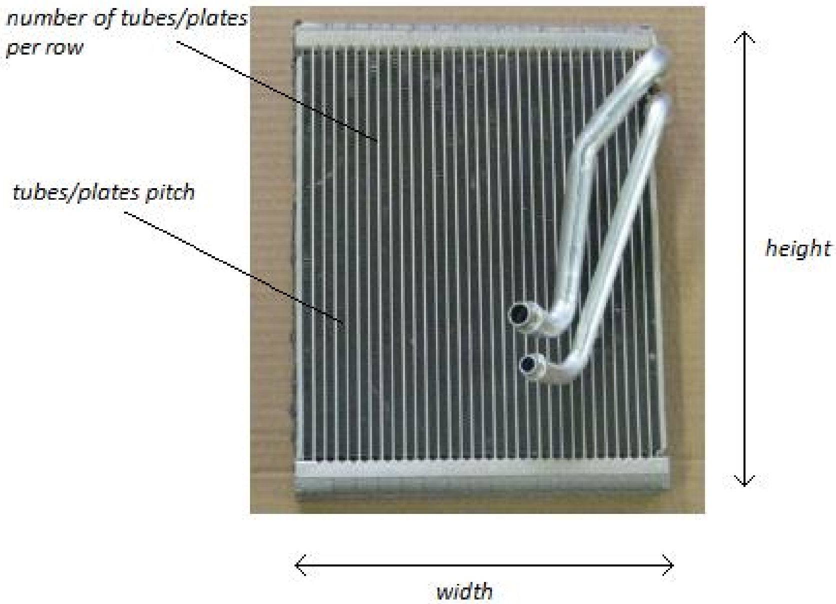

Figure 32. Evaporator

Geometrical data of the evaporator		
	Unit	
Frontal area	dm^2	5.34
Height	mm	251
Width	mm	212.7
Thickness	mm	38
Number of rows	n	2
Number of tubes/plates per row	n	31

Table 4. Geometrical input data for the evaporator in Amesim.

The thermodynamic characteristics are reported with the following tables in which all the initializing data for the component are reported; according to them it has been edited by the supplier a study for the assessment of heat rejection of the heat exchanger and the pressure drops related to refrigerant and air.

R1234yf	$T_{out, condenser}$ outlet condenser temperature	(°C)	57,5
	$p_{out, condenser}$ outlet condenser pressure	(barG)	18,387
	$p_{out, evaporator}$ outlet evaporator pressure	(barG)	2,287
	OH over-heating	(°C)	5
AIR	$T_{in, evaporator}$ inlet evaporator temperature	(°C)	35
	RH relative humidity	%	60

Table 5. Thermodynamic input data for the evaporator in Amesim.

The following table reports the heat rejection and the pressure drop:

AIR MASS FLOW		HEAT REJECTION		AIR SIDE PRESSURE DROP		REFRIGERANT MASS FLOW		REFRIGERANT SIDE PRESSURE DROP	
G_a (kg/h)	ε(*)	Q (kW)	ε(*)	Δp_a (daPa)	ε(*)	G_{ref} (kg/h)	ε(*)	Δp_{ref} (bar)	ε(*)
220		3.552		1,6		0		0	
330		4.896		3,9		100		0,5	
440		5.952		6,5		150		1	
550		6.624		9,6		180		1,4	
660		6.912							

Table 6. Heat rejection and pressure drops air-side and refrigerant-side

3.4 Compressor data

The compressor employed in the HVAC module used for the present vehicle is a variable displacement compressor characterized by a maximum displacement of 140 cm^3.

Figure 33. Variable displacement compressor

In the following figure the table related to the performance of the compressor employed in this application is reported:

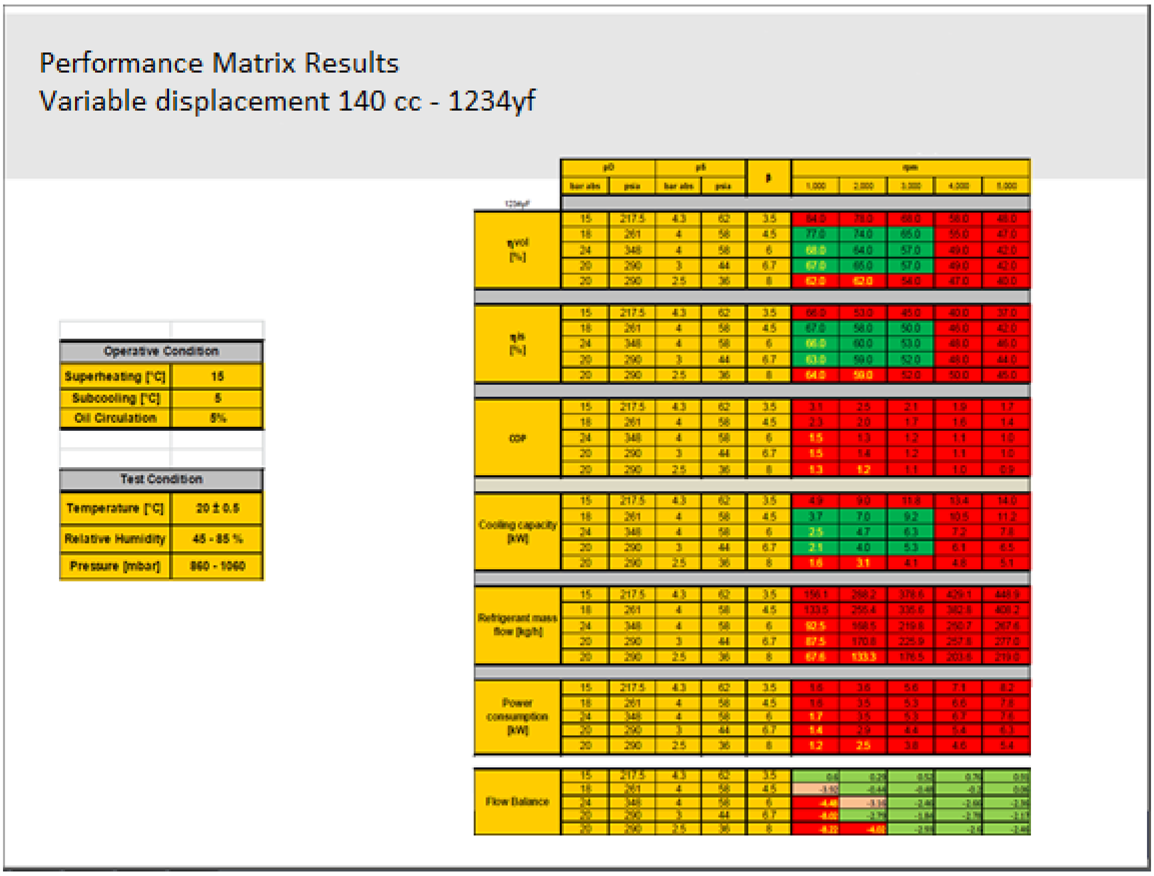

Performance Matrix Results
Variable displacement 140 cc - 1234yf

Operative Condition	
Superheating [°C]	15
Subcooling [°C]	5
Oil Circulation	5%

Test Condition	
Temperature [°C]	20 ± 0.5
Relative Humidity	45 - 85 %
Pressure [mbar]	860 - 1060

1234yf	p0		pc		β	rpm				
	bar abs	psia	bar abs	psia		1,000	2,000	3,000	4,000	5,000
ηvol [%]	15	217.5	4.3	62	3.5	84.0	78.0	68.0	58.0	48.0
	18	261	4	58	4.5	77.0	74.0	65.0	55.0	47.0
	24	348	4	58	6	68.0	64.0	57.0	49.0	42.0
	20	290	3	44	6.7	67.0	65.0	57.0	49.0	42.0
	20	290	2.5	36	8	62.0	62.0	54.0	47.0	40.0
ηis [%]	15	217.5	4.3	62	3.5	66.0	53.0	45.0	40.0	37.0
	18	261	4	58	4.5	67.0	58.0	50.0	46.0	42.0
	24	348	4	58	6	66.0	60.0	53.0	48.0	46.0
	20	290	3	44	6.7	63.0	59.0	52.0	48.0	44.0
	20	290	2.5	36	8	64.0	59.0	52.0	50.0	45.0
COP	15	217.5	4.3	62	3.5	3.1	2.5	2.1	1.9	1.7
	18	261	4	58	4.5	2.3	2.0	1.7	1.6	1.4
	24	348	4	58	6	1.5	1.3	1.2	1.1	1.0
	20	290	3	44	6.7	1.5	1.4	1.2	1.1	1.0
	20	290	2.5	36	8	1.3	1.2	1.1	1.0	0.9
Cooling capacity [kW]	15	217.5	4.3	62	3.5	4.9	9.0	11.8	13.4	14.0
	18	261	4	58	4.5	3.7	7.0	9.2	10.5	11.2
	24	348	4	58	6	2.5	4.7	6.3	7.2	7.8
	20	290	3	44	6.7	2.1	4.0	5.3	6.1	6.5
	20	290	2.5	36	8	1.6	3.1	4.1	4.8	5.1
Refrigerant mass flow [kg/h]	15	217.5	4.3	62	3.5	156.1	288.2	378.6	429.1	448.9
	18	261	4	58	4.5	133.5	255.4	335.6	382.8	408.2
	24	348	4	58	6	92.5	168.5	219.8	250.7	267.6
	20	290	3	44	6.7	87.5	170.8	225.9	257.8	277.0
	20	290	2.5	36	8	67.6	133.3	176.5	203.6	219.0
Power consumption [kW]	15	217.5	4.3	62	3.5	1.6	3.6	5.6	7.1	8.2
	18	261	4	58	4.5	1.6	3.5	5.3	6.6	7.8
	24	348	4	58	6	1.7	3.5	5.3	6.7	7.6
	20	290	3	44	6.7	1.4	2.9	4.4	5.4	6.3
	20	290	2.5	36	8	1.2	2.5	3.8	4.6	5.4
Flow Balance	15	217.5	4.3	62	3.5	0.6	0.29	0.52	0.76	0.91
	18	261	4	58	4.5	-3.10	-0.44	-0.48	-0.2	0.06
	24	348	4	58	6	-4.48	-3.16	-2.46	-2.66	-2.96
	20	290	3	44	6.7	-4.00	-2.79	-1.84	-1.79	-2.17
	20	290	2.5	36	8	-4.22	-4.00	-2.99	-2.4	-2.46

Figure 34. Data sheet compressor

3.5 Condenser data

The condenser employed in the HVAC module of this application is shown in the following figure, combined with preliminary geometrical data extracted by the data sheet.

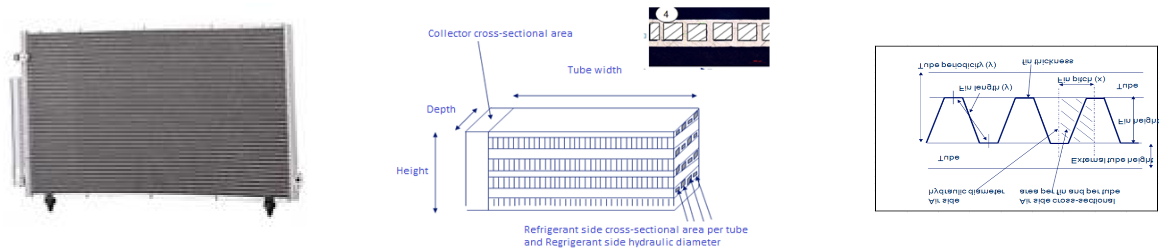

Figure 35. Overview of the condenser geometrical data

Similarly to the evaporator, the data sheet is not integrally reported but an overview of the most characterizing data is showed in the following table:

Geometrical data of the evaporator		
	Unit	
Mass	kg	1.8
Inner volume	cm^3	507
Frontal area	dm^2	23.7
Height	mm	357
Width	mm	663
Thickness	mm	12
Inner path		44 – 11
Channels number	n	17

Table 7. Geometrical input data for the condenser in Amesim

In the following figure a table showing the thermodynamic properties is reported; starting from this point heat rejection and pressure drops have been estimated. The original case is provided by two set of input data for the test in order to make a more accurate assessment of the behaviour of the refrigerant in the inner path of the condenser. Nevertheless, in this project thesis only a set of input data has been considered and it is reported in the tables shown in the following page.

R1234yf	$T_{refr,IN}$ Inlet condenser temperature	(°C)	100
	$P_{refr,IN}$ Outlet condenser pressure	(barA)	19.4
	SC Sub-cooling	(°C)	10
AIR	$T_{IN,condenser}$ inlet condenser temperature	(°C)	45
	$V_{a,IN}$ Inlet air velocity	(m/s)	1 ÷ 5

Table 8. Thermodynamic input data for the condenser in Amesim

AIR SPEED		**HEAT REJECTION**		**AIR SIDE PRESSURE DROP**		**REFRIGERANT MASS FLOW**		**REFRIGERANT SIDE PRESSURE DROP**	
V_a (m/s)	ε(*)	Q (kW)	ε(*)	Δp_a (Pa)	ε(*)	G_{ref} (kg/h)	ε(*)	Δp_{ref} (bar)	ε(*)
1		5.6		15		100		0.25	
1.5		7.7		22		110		0.29	
2		9.5		30		120		0.33	
2.5		10.9		41		130		0.38	
3		12.2		55		140		0.43	
3.5		13.4		72		150		0.48	
4		14.4		92		160		0.53	
4.5		15.3		115		180		0.65	
5		16.1		142		200		0.77	

Table 9. Heat rejection and pressure drop air-side and refrigerant-side

3.6 Thermal eXpansion Valve data

With regards to the thermal expansive valve a small overview is now reported, followed by the data sheet of the valve which includes only the four-dimensional diagram that regulate its operation.

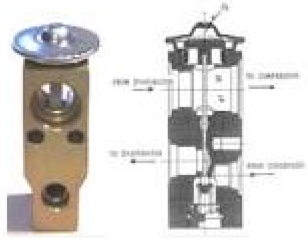

Figure 36. Overview of a TXV for automotive application [16]

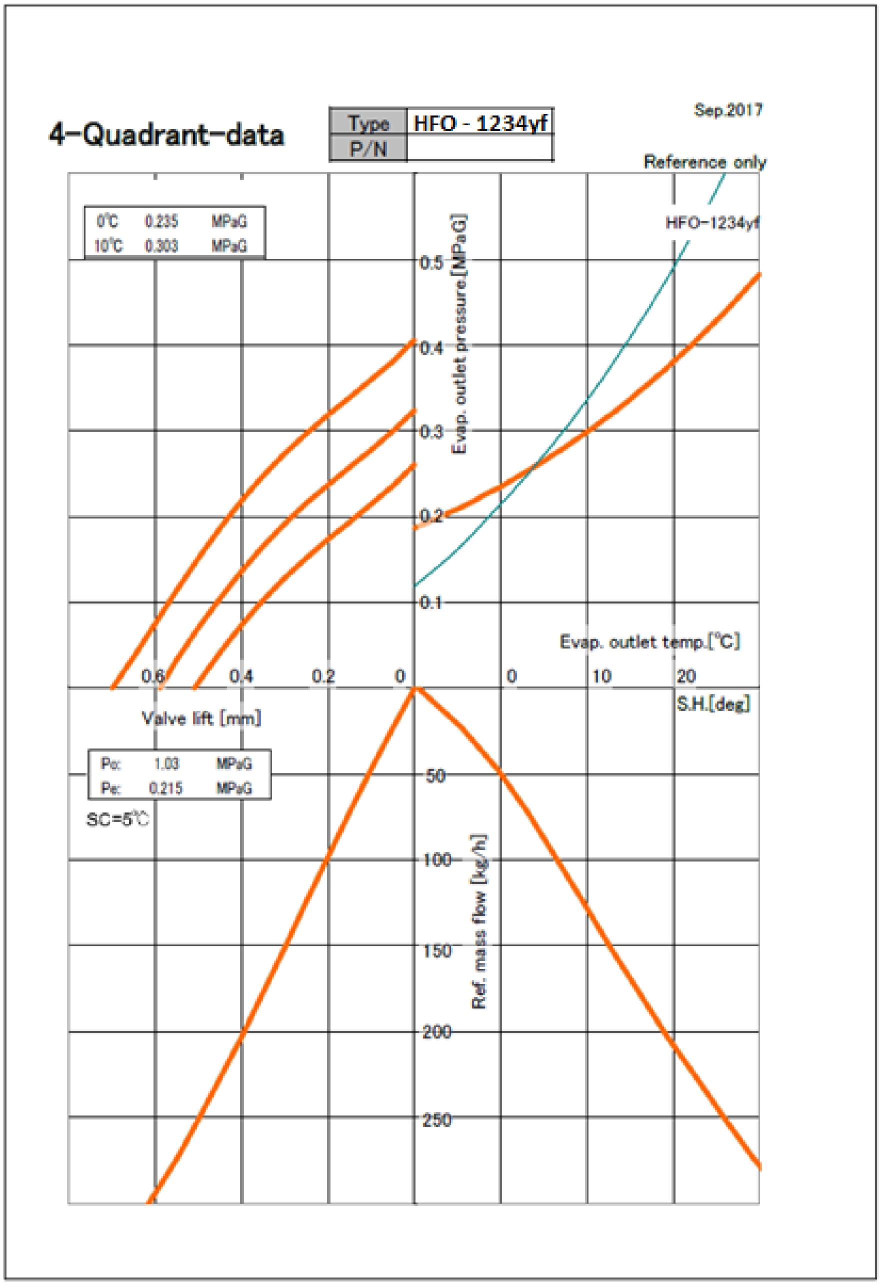

Figure 37. Overview of a TXV data sheet

3.7 Choice of refrigerant

The design of a refrigerating system is strongly dependent on the type of fluid refrigerant employed for the operative work cycle and then on its properties. Refrigerants used for the air conditioning have changed many times since the first utilizations to today according to legislations concerning their thermo-physical properties and incompatibility with the environment. At the same time the development of the concept “energy savings” and “thermal comfort” has increased the need to find a compromise aimed to satisfy environmental and thermal comfort requirement simultaneously.

CFCs and HCFCs were the most used refrigerants, but the consequence on climate change, mostly concerning the ozone depletion, has represented the fundamental reason why the AHRI Standard 700 banned them, except for existing plants. In order to limit the negative consequences of the employment of these refrigerants, the European Parliament and Council have established the Regulation (EU) n. 517/2014 focused on the F-gases and on the greenhouse effect. According to this regulation, EU has confirmed the need of reducing the greenhouse gases emission by 80-90% with respect to the 1990s data. As mentioned in the previous chapters the most significant greenhouse gas is the carbon dioxide but, in order to obtain the emission reduction requested by the European Union, it is important to not neglect contributes like F-gases. In fact, the control on plants using them has been improved in order to monitor the F-gas emission and then to assess the impact of the regulation [26]. It is possible to show a simple overview of the evolution of refrigerants employment occurred in the last 30 years:

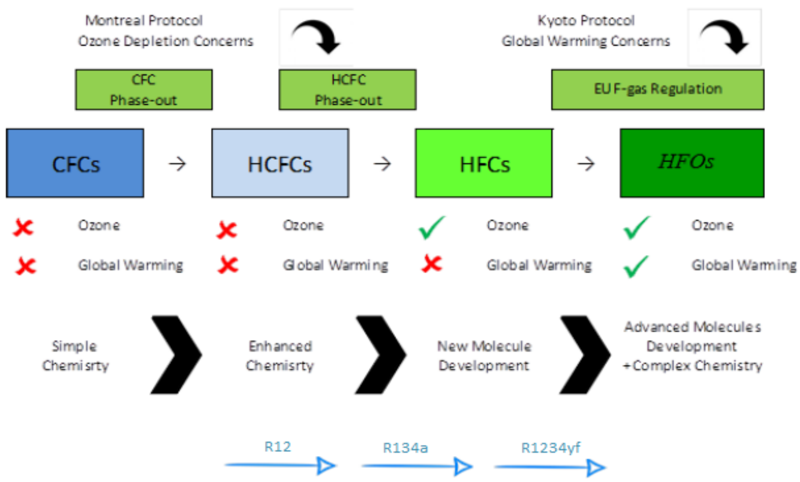

Figure 38. Historical evolution of refrigerants employment [27].

In automotive applications the refrigerant fluid employed since 1990s to last years was the Freon R-134a (1,1,1,2 Tetrafluoroethane), a haloalkane refrigerant non-flammable and with a boiling point of -26.3 °C. Its thermodynamic properties are similar to R-12 (diclorofluoromethane), but it is characterized by a significantly lower ODP index. That was the reason why the R-12 was banned and the R-134a replaced it. Although the limits on the chlorine-gases established by legislations were perfect for the control of the ozone depletion, the global warming was going on carrying the global temperature to increase by a rate significantly high. According to the last edition of the IPCC occurred in 2007 the need of reducing this temperature increase rate has been defined with the target 2 °C per year. For this reason, the R-134a has been banned for air conditioning applications because of its GWP of 1300. In particular the European Union has established:

- Since January 1st, 2011 any validation CE is possible for vehicles with the air conditioning system using as refrigerant F-gases with a GWP > 150 [26];
- Since January 1st, 2017 new vehicles with air conditioning system containing F-gases with GWP > 150 cannot be registered and it is forbidden their sale and circulation [26].

Scientific community has found possible substitutes of the R-134a in natural fluids and HFO (Hydro-Fluoro-Olefin). In particular natural fluids gather: water H_20, ammonia NH_3 and carbon dioxide CO_2 and hydrocarbons.

NATURAL FLUID		
Fluid	Pro	Cons
Water H_2O	*Easy to find* *Low-cost* *Compatible with the environment*	*Freezing temperature of 0°C at* p_{atm} *Boiling temperature of 100 °C at* p_{atm} *Whole cycle under* p_{atm} *High specific volume and heat capacity* *Expensive operation*
Ammonia NH_3	*Freezing point of -77 °C at* p_{atm} *Non-pollutant, compatible with the environment*	*Slightly flammable in vapor conditions* *Toxic for concentration > 50 ppm* *Non-compatible with copper*
Carbon dioxide CO_2	*Low freezing point* *Non-pollutant* *Easy to find* *Non-toxic*	*Critic temperature low (around 31 °C)* *Hypercritic cycle* *Structural problems due to holds*
Hydrocarbons		*Compatible only with hermetic compressors* *High flammability* *Employed only in low-power systems*

Table 10. Pro and cons for natural fluids [5].

With regards to synthetic refrigerants, first researches have been edited studying the thermodynamic and chemical properties of R152a. It is a hydrofluorocarbon characterized by a GWP of 140 (fitting with the legislation limit of GWP < 150), great efficiencies and a significant compatibility with the plants employing the R134a. Despite these positive factors the R152a is slightly flammable and the plants should have needed modifications which have led the scientists to leave this option.

Studies were therefore directed to HFOs, synthetic fluids characterized by a double hydrogen bond. The instability given by the double hydrogen bond is the strong point for HFOs; in particular the half-life of these fluids is low and the decomposition occurs when it is located in atmosphere without being involved in the global warming phenomenon. In particular the HFO on which studies converged is the R1234yf which represents now the refrigerant fluid used in most automotive applications. On the other hand, it is important to assess the thermodynamic and chemical properties in order to verify the compatibility with the existing plants and with lubricants employed:

Chemical properties			
		Refrigerant	
Properties	**Unit**	***R134a***	***R1234yf***
Critic pressure	[bar]	40.593	33.822
Critic temperature	[K]	374.21	367.85
Critic density	$\left[\frac{\mathrm{kg}}{\mathrm{m}^3}\right]$	511	475.55
Molar mass	$\left[\frac{\mathrm{kg}}{\mathrm{kmol}}\right]$	102.03	114.04

Table 11. Overview of chemical properties differences between R134a and R1234yf [27].

Thermodynamic properties					
Properties		***Refrigerant***			
		R134a		***R1234yf***	
Temperature	[K]	313.15	278.15	313.15	278.15
Saturation vapor pressure	[bar]	10.166	3.4966	10.0184	3.7292
Saturated liquid density	$\left[\frac{\mathrm{kg}}{\mathrm{m}^3}\right]$	1146.7	1278.1	1033.8	1160.4
Saturated vapor density	$\left[\frac{\mathrm{kg}}{\mathrm{m}^3}\right]$	50.085	17.131	57.753	20.744
Specific latent heat	$\left[\frac{\mathrm{kJ}}{\mathrm{kg}}\right]$	163.02	194.74	132.27	160.02

Table 12. Overview of thermodynamic properties differences between R134a and R1234yf [27].

Since the density of R1234yf is lower than the R134a one, considering an equal cooling power produced by the evaporator, the refrigerant optimal charge for R1234yf is lower than the charge of R134a. It implies energy and economic savings because when leakages occur, the refrigerant quantity lost is lower.

3.7.1 Diagram log p – h: R134a

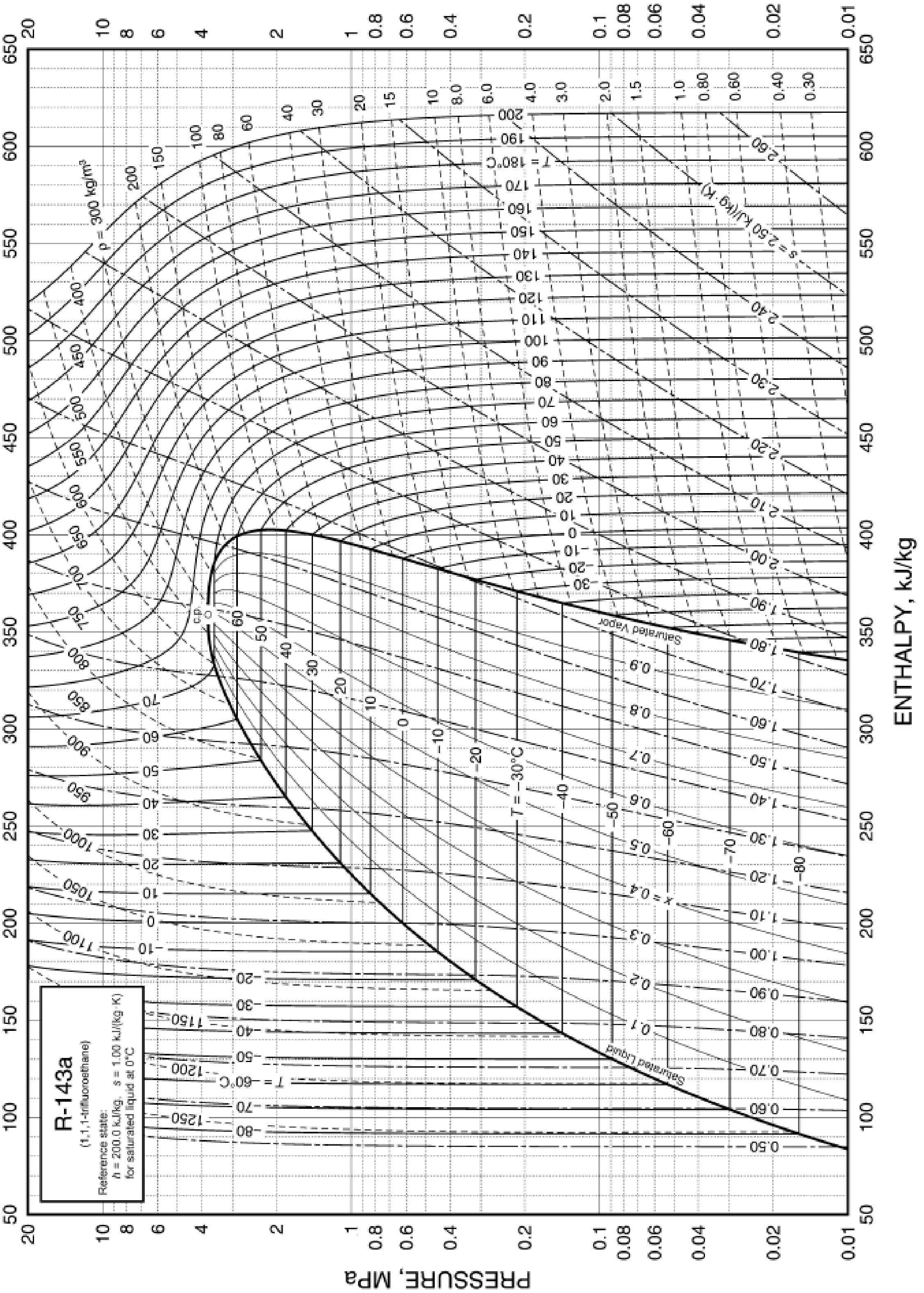

Figure 39. R134a - Diagram log p – h [28].

3.7.2 Diagram log p – h: R1234yf

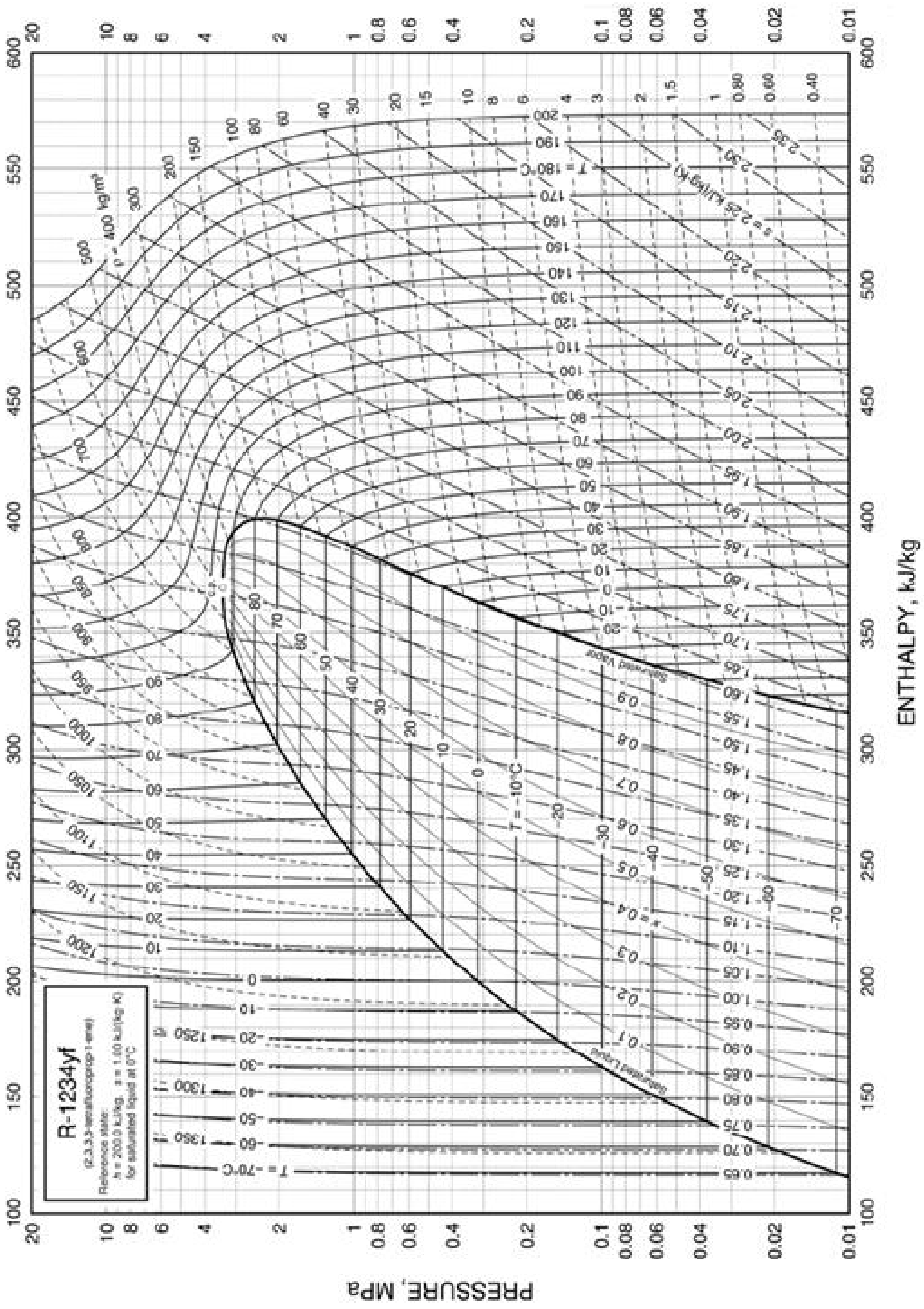

Figure 40. R1234yf – Diagram log p – h [28].

CHAPTER IV: PROJECT STUDY. PART I

The project thesis has been edited with the software ***LMS Imagin.Lab Amesim 15.0.1***, produced by Siemens. It is based on the evaluation of energy savings due to the introduction of thermal insulation and reflective glasses in the car cabin and therefore on the estimation of the reduction of the mechanical power requested by the compressor. This is translated into the assessment of the fuel consumption reduction and of the consequent CO_2 emission reduction. With respect to this aim, the thesis work has been divided in two parts and then structured in many steps in order to obtain a global result coherent with the reality as much as possible. The first part of the project work concerns the validation of the model:

- Production of a sketch containing the equivalent car cabin model;
- Validation of the car cabin model, assessing the internal cabin temperature and comparing it with the internal cabin temperature measured during a Cooldown test;
- Production of two sketches containing respectively the condenser and the evaporator and calibration of them according to the data sheets;
- Production of a sketch containing the whole air conditioning system and estimation of the optimal refrigerant charge;
- Production of a global sketch including the air conditioning system and the car cabin model;
- Validation of the whole model comparing it to the internal cabin temperature with the temperature assessed in the validation of the car cabin model and to the measured temperature resulting from a Cooldown test.

4.1 Introduction to LMS Imagine.Lab Amesim

LMS Amesim is a powerful software which enables the modeling and analysis of multi-physics systems and components in all the engineering fields. It combines 1D simulation and physical testing with an intelligent and confident presentation of the results. LMS Amesim is based on libraries written in C language containing a large quantity of predefined components belonging to different domains. In particular in this project work the libraries used concern the thermal domain but the most important and always used in each field is the control library which represents the link between systems and components. In particular the libraries employed are reported below:

- Signal and Control: 

  It contains all the components involved in the control systems like signal and block components and it allows to realize also complex signals to pilot systems.

- Hydraulic: 

  It is dedicated to the design of general hydraulic systems for a large range of applications such as automotive, aerospace and industrial equipment.

- Thermal Hydraulic: 

  It is used for the design of hydraulic systems in which variations of fluid temperature have a great influence on the overall behavior. This library is based on the transient heat transfer approach and then it is used to model thermal phenomena in liquids considering energy transport and convection.

- Thermal: 

  It is dedicated to solid material and it is based on the transient heat transfer approach. This library is employed to model the heat transfer (conduction, convection and radiation) between solids and to estimate their thermal evolution.

- Two-Phase Flow: 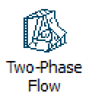

  It is used to model any system where a phase change occurs and hence it is compatible with Thermal and Air-Conditioning library to consider interactions between refrigerants and solid walls.

- Air conditioning: 

- This library deals with the refrigerant loop and therefore it is dedicated to the modelling of a refrigerant thermal evolution incluiding phase changes. For this reason it is compatible with the Two-Phase Flow library [14].

4.2 Car cabin model

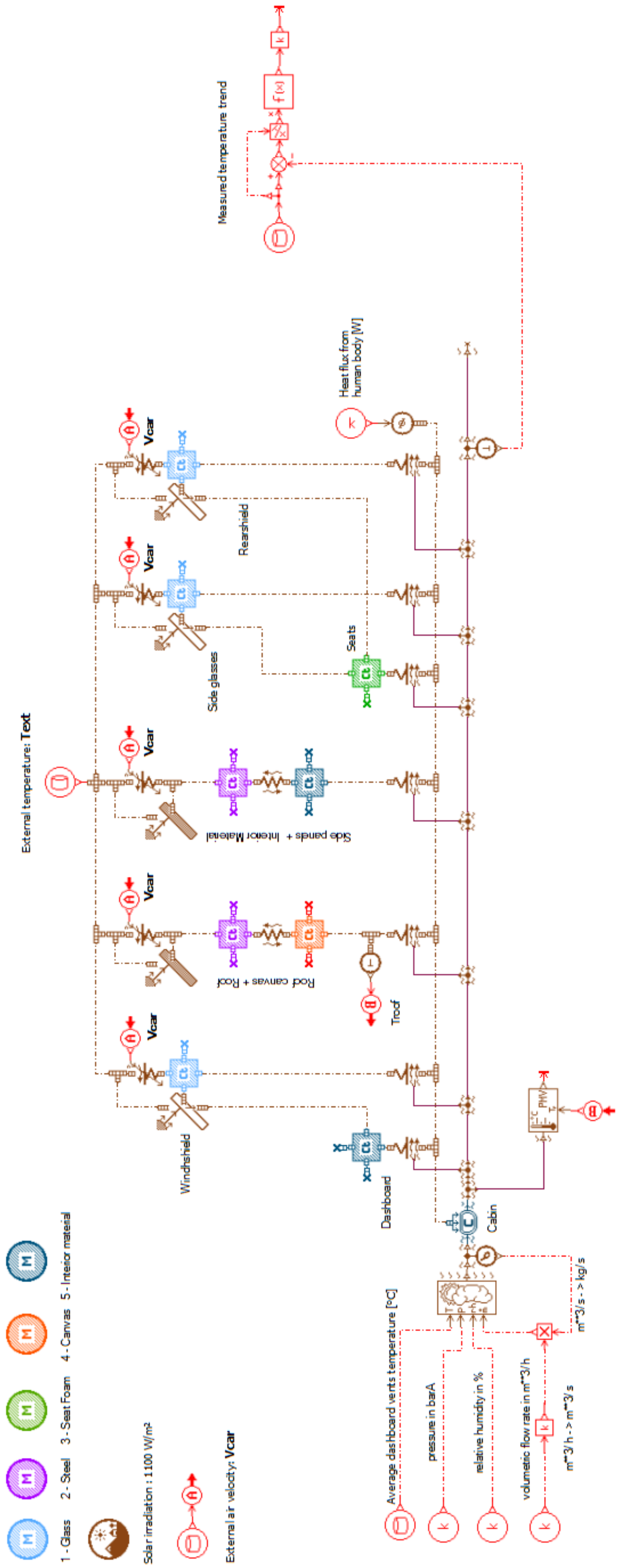

Figure 41. Car cabin model.

In order to characterize the components, a group of global parameters has been produced reporting all the data used: density of materials, surfaces, absorption coefficient, mass flow rate, initial temperature and relative humidity. In particular the geometric data have been extracted by a car cabin model deriving by a Warm – Map test as shown in the following figure:

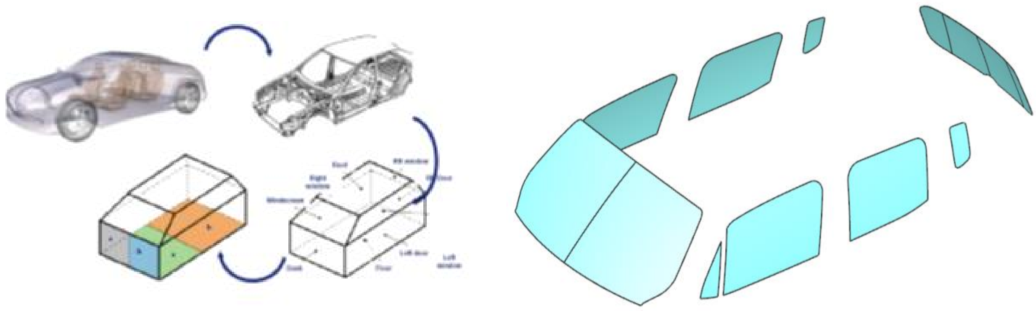

Figure 42. Overview of the geometry of the car cabin model.

The geometrical data employed for the car cabin model realized with Amesim are reported below:

Geometric data employed for the cabin model geometry			
Type of surface	**Surface**	**Unit**	
Steel surfaces	*Roof*	$[m^2]$	2.6
	Side wall & door	$[m^2]$	4.754
	Dash & plenum	$[m^2]$	1.5
Window surfaces	*Windshield*	$[m^2]$	0.84
	Side glasses front	$[m^2]$	0.5
	Side glasses rear	$[m^2]$	0.4
	Third window	$[m^2]$	0.048
	Nolder (4^{th} window)	$[m^2]$	0.04
	Rear glasses	$[m^2]$	0.297

Table 13. Overview of the geometrical data employed for the car cabin model.

The global parameter setup for the sketch of the validation of the car cabin is reported in the following figure, defining all the geometrical and thermodynamic properties of the materials of the components involved in the production of the model:

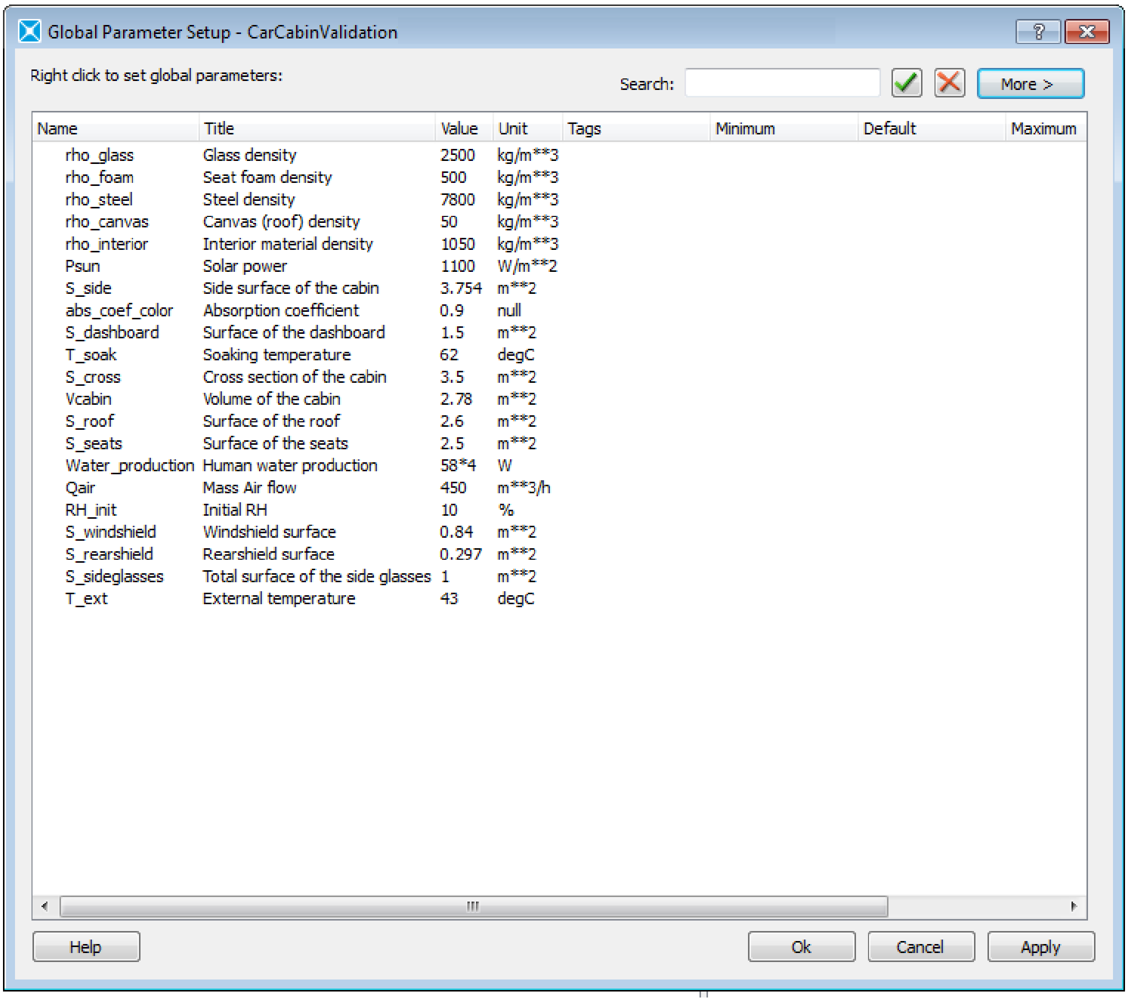

Name	Title	Value	Unit	Tags	Minimum	Default	Maximum
rho_glass	Glass density	2500	kg/m**3				
rho_foam	Seat foam density	500	kg/m**3				
rho_steel	Steel density	7800	kg/m**3				
rho_canvas	Canvas (roof) density	50	kg/m**3				
rho_interior	Interior material density	1050	kg/m**3				
Psun	Solar power	1100	W/m**2				
S_side	Side surface of the cabin	3.754	m**2				
abs_coef_color	Absorption coefficient	0.9	null				
S_dashboard	Surface of the dashboard	1.5	m**2				
T_soak	Soaking temperature	62	degC				
S_cross	Cross section of the cabin	3.5	m**2				
Vcabin	Volume of the cabin	2.78	m**2				
S_roof	Surface of the roof	2.6	m**2				
S_seats	Surface of the seats	2.5	m**2				
Water_production	Human water production	58*4	W				
Qair	Mass Air flow	450	m**3/h				
RH_init	Initial RH	10	%				
S_windshield	Windshield surface	0.84	m**2				
S_rearshield	Rearshield surface	0.297	m**2				
S_sideglasses	Total surface of the side glasses	1	m**2				
T_ext	External temperature	43	degC				

Figure 43. Overview of the global parameter setup concerning the validation model of the cabin.

According to the sketch produced in the previous page, in the upper side the indication of the solar irradiation, the car velocity and the properties of the component materials are reported. In particular:

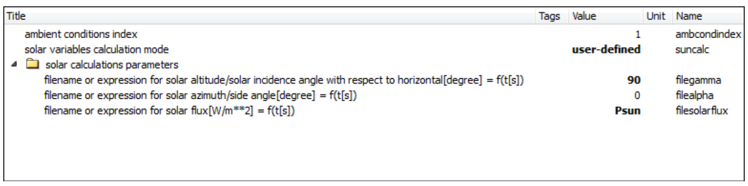

Title	Tags	Value	Unit	Name
ambient conditions index		1		ambcondindex
solar variables calculation mode		**user-defined**		suncalc
solar calculations parameters				
filename or expression for solar altitude/solar incidence angle with respect to horizontal[degree] = f(t[s])		**90**		filegamma
filename or expression for solar azimuth/side angle[degree] = f(t[s])		0		filealpha
filename or expression for solar flux[W/m**2] = f(t[s])		**Psun**		filesolarflux

Figure 44. Overview of the solar irradiation.

1 - Glass

Title	Tags	Value	Unit	Name
solid type index		1		soli
material definition		**user defined**		materialType
type of definition		**constant values**		materialDefType
validity domain: minimal temperature (for warning only)		-100	degC	tMin
validity domain: maximal temperature (for warning only)		660	degC	tMax
density of the material		**rho_glass**	kg/m**3	rho0
specific heat of the material		**800**	J/kg/K	Cp0
thermal conductivity of the material		**0.7**	W/m/K	lam0
name of the solid		**glass**		materialName

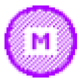

2 - Steel

Title	Tags	Value	Unit	Name
solid type index		**2**		soli
material definition		**user defined**		materialType
type of definition		**constant values**		materialDefType
validity domain: minimal temperature (for warning only)		-100	degC	tMin
validity domain: maximal temperature (for warning only)		660	degC	tMax
density of the material		**rho_steel**	kg/m**3	rho0
specific heat of the material		**500**	J/kg/K	Cp0
thermal conductivity of the material		**50**	W/m/K	lam0
name of the solid		**steel**		materialName

3 - Seat Foam

Title	Tags	Value	Unit	Name
solid type index		**3**		soli
material definition		**user defined**		materialType
type of definition		**constant values**		materialDefType
validity domain: minimal temperature (for warning only)		-100	degC	tMin
validity domain: maximal temperature (for warning only)		660	degC	tMax
density of the material		**rho_foam**	kg/m**3	rho0
specific heat of the material		**1000**	J/kg/K	Cp0
thermal conductivity of the material		**0.3**	W/m/K	lam0
name of the solid		**foam**		materialName

4 - Canvas

Title	Tags	Value	Unit	Name
solid type index		**4**		soli
material definition		**user defined**		materialType
type of definition		**constant values**		materialDefType
validity domain: minimal temperature (for warning only)		-100	degC	tMin
validity domain: maximal temperature (for warning only)		660	degC	tMax
density of the material		**rho_canvas**	kg/m**3	rho0
specific heat of the material		**1300**	J/kg/K	Cp0
thermal conductivity of the material		**0.04**	W/m/K	lam0
name of the solid		**canvas**		materialName

5 - Interior material

Title	Tags	Value	Unit	Name
solid type index		**5**		soli
material definition		**user defined**		materialType
type of definition		**constant values**		materialDefType
validity domain: minimal temperature (for warning only)		-100	degC	tMin
validity domain: maximal temperature (for warning only)		660	degC	tMax
density of the material		**rho_interior**	kg/m**3	rho0
specific heat of the material		**1300**	J/kg/K	Cp0
thermal conductivity of the material		**0.2**	W/m/K	lam0
name of the solid		**interior**		materialName

Figure 45. Overview of materials properties.

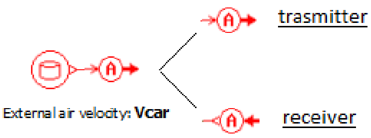

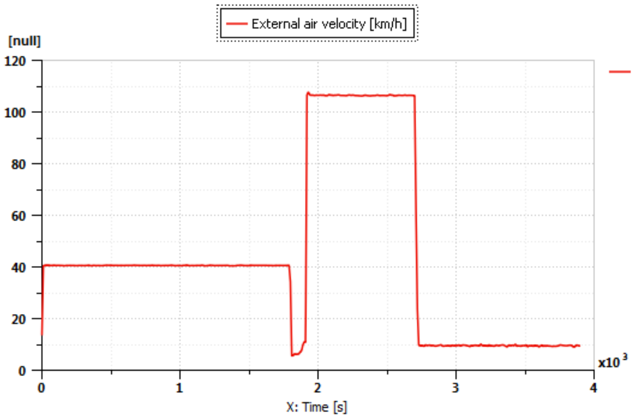

Figure 46. Air velocity trend.

The dynamic time table reported references to the external air velocity which characterize the external heat convective coefficient; in particular it is essentially equal to the actual velocity of the vehicle when it is moving and to the wind velocity when it is stationary. In fact, it is possible to compare the external air velocity introduced in the model with the car velocity measured during the Cooldown test:

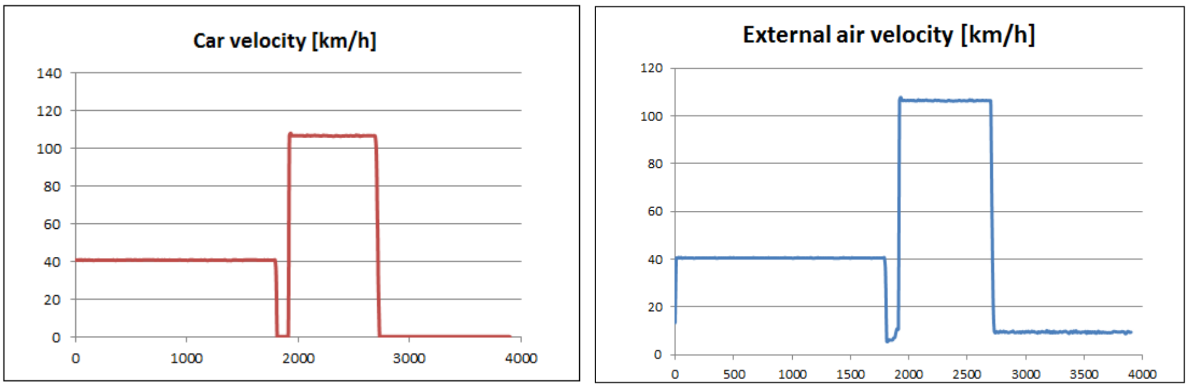

Figure 47. Comparison between car velocity and external air velocity.

It is reported now the most significant components of the sketch in order to explain their meaning and functionality:

Title	Tags	Value	Unit	Name
mass flow rate at port 1		**Qair/3600*1.2396**	kg/s	dms1
pressure at port 1		1.013	barA	p1
temperature at port 2		**T_soak**	degC	t2
setting of chamber dynamics		basic		dynSetting
(#) initial relative humidity		**RH_init**	%	rhinit
chamber volume		**Vcabin**	m**3	vol
filename or expression for water production[g/h] = f(t[s])		**Water_production*(t>0)**		wp1

Figure 48. Cabin properties in Amesim.

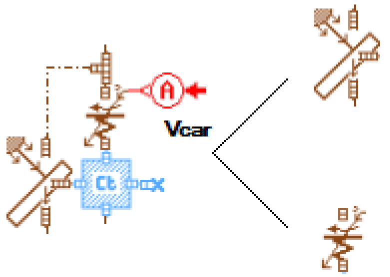

Title	Tags	Value	Unit	Name
solar radiation setting mode		**using ambient conditions**		soldef
ambient conditions index		1		ambcondindex
exchange area		**S_windshield**	m**2	area
transmission factor		**0.9**	null	transcoeff
absorption factor		**0.09**	null	abscoeff
equivalent emission factor gas/surface		0.95	null	epsilon
filename or expression for surface inclination angle with respect to horizontal[degree] = f(t[s])		**39.4**		filebeta
filename or expression for surface angle with respect to the North[degree] = f(t[s])		0		filezeta

Title	Tags	Value	Unit	Name
calculation type		flat plate with predefined correlation		ctype
inclination angle with respect to horizontal (fluid is above port 2 if angle = 0)		**39.4**	degree	theta
width		**sqrt(S_windshield*1e6)**	mm	width
length		**sqrt(S_windshield*1e6)**	mm	length
fluid properties				
fluid properties		environmental moist air		fluidprop
pressure (absolute) of the fluid		1.013	barA	pFluid
moist air relative humidity (%)		40	null	rh
heat exchange				
gain on heat exchange		1	null	kHeat

Figure 49. External thermal loads for glass surface in Amesim. Irradiative and convective heat.

The component shown in the previous page corresponds to the modelling of the cabin volume, characterized initialization data such as initial temperature and relative humidity. The first component highlighted in the figure reported above represents the solar radiation component; the last represents the convective heat exchange component which describes the heat exchange between the car cabin and the external air flow. The light-blue component is the mass representing glasses (windshield, rear-shield and side-glasses); At the same time the group of components used to characterize the heat exchange for the other surfaces like side panels and roof is reported in the following figures. The description is also edited for the masses representing foam seats and dashboard.

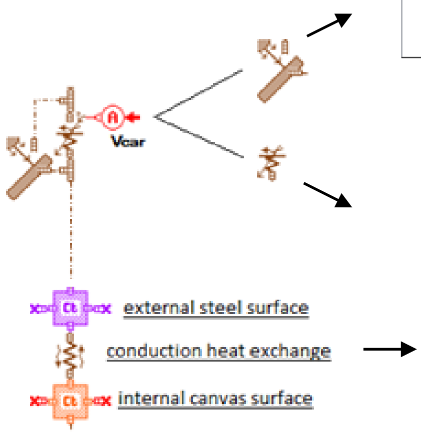

Title	Tags	Value	Unit	Name
solar radiation setting mode		**using ambient conditions**		soldef
ambient conditions index		1		ambcondindex
exchange area		**S_roof**	m**2	area
absorption factor		**abs_coef_color**	null	abscoeff
equivalent emission factor gas/surface		0.9	null	epsilon
filename or expression for surface inclination angle with respect to horizontal[degree] = f(t[s])		**0**		filebeta
filename or expression for surface angle with respect to the North[degree] = f(t[s])		0		filezeta

Title	Tags	Value	Unit	Name
calculation type		flat plate with predefined correlation		ctype
inclination angle with respect to horizontal (fluid is above port 2 if angle = 0)		**180**	degree	theta
width		**sqrt(S_roof*1e6)**	mm	width
length		**sqrt(S_roof*1e6)**	mm	length
fluid properties				
fluid properties		environmental moist air		fluidprop
pressure (absolute) of the fluid		1.013	barA	pFluid
moist air relative humidity (%)		40	null	rh
heat exchange				
gain on heat exchange		1	null	kHeat

Title	Tags	Value	Unit	Name
setting		no specific geometry: dh=f(area, thermal conductance)		conductionSetting
contact surface		**S_roof*1e6**	mm**2	area
thermal contact conductance		**1**	W/m**2/degC	tccond

Figure 50. External thermal loads and conduction heat exchange for the roof.

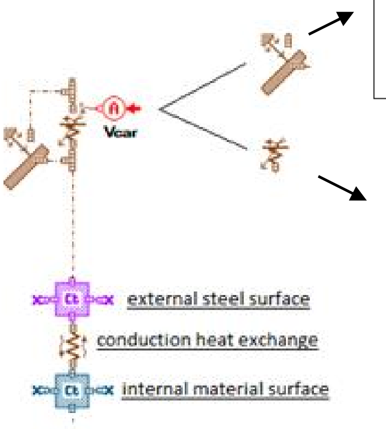

Title	Tags	Value	Unit	Name
solar radiation setting mode		**using ambient conditions**		soldef
ambient conditions index		1		ambcondindex
exchange area		**2*S_side**	m**2	area
absorption factor		**abs_coef_color**	null	abscoeff
equivalent emission factor gas/surface		0.9	null	epsilon
filename or expression for surface inclination angle with respect to horizontal[degree] = f(t[s])		**15**		filebeta
filename or expression for surface angle with respect to the North[degree] = f(t[s])		0		filezeta

Title	Tags	Value	Unit	Name
calculation type		flat plate with predefined correlation		ctype
inclination angle with respect to horizontal (fluid is above port 2 if angle = 0)		**180**	degree	theta
width		**sqrt(2*S_side*1e6)**	mm	width
length		**sqrt(2*S_side*1e6)**	mm	length
fluid properties				
fluid properties		environmental moist air		fluidprop
pressure (absolute) of the fluid		1.013	barA	pFluid
moist air relative humidity (%)		40	null	rh
heat exchange				
gain on heat exchange		1	null	kHeat

Title	Tags	Value	Unit	Name
setting		no specific geometry: dh=f(area, thermal conductance)		conductionSetting
contact surface		**2*S_side*1e6**	mm**2	area
thermal contact conductance		**1**	W/m**2/degC	tccond

Figure 51. External thermal loads and conduction heat exchange for side panels. Irradiative and convective heat.

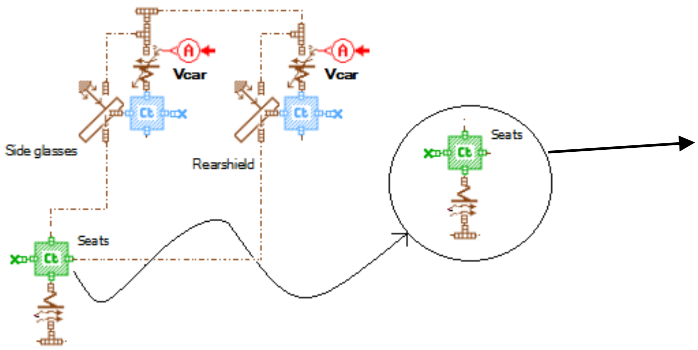

Title	Tags	Value	Unit	Name
calculation type		flat plate with predefined correlation		ctype
inclination angle with respect to horiz...		90	degree	theta
width		**sqrt(S_seats*1e6)**	mm	width
cross sectional area for the fluid flow		**1e6*S_cross**	mm**2	area
length		**sqrt(S_seats*1e6)**	mm	length
heat exchange				
gain on heat exchange		**3.3**	null	kHeat

Figure 52. External thermal loads. Irradiative and convective heat transfer for seats.

4.3 Validation of the car cabin model

The validation of the car cabin model has been edited according to the set of input data listed below:

- Inlet temperature equal to the outlet air temperature profile at the evaporator;
- Relative humidity of the air entering in the cabin equal to 90%;
- Pressure of the air equal to the atmospheric one: p_a = 1.013 [barA];
- Constant air mass flow rate equal to the project one: $Q_{air} = 450 \left[\frac{m^3}{h}\right]$;
- Air velocity equal to the wind velocity profile showed in *Figure 38*;
- External temperature profile to the temperature of the climate chamber;
- Heat flux from human body equal to the heat flux deriving by four persons seated and relaxed: $Water\ production = 4 * 58 = 232\ [W]$.

In particular in the car cabin model, they correspond to the following systems:

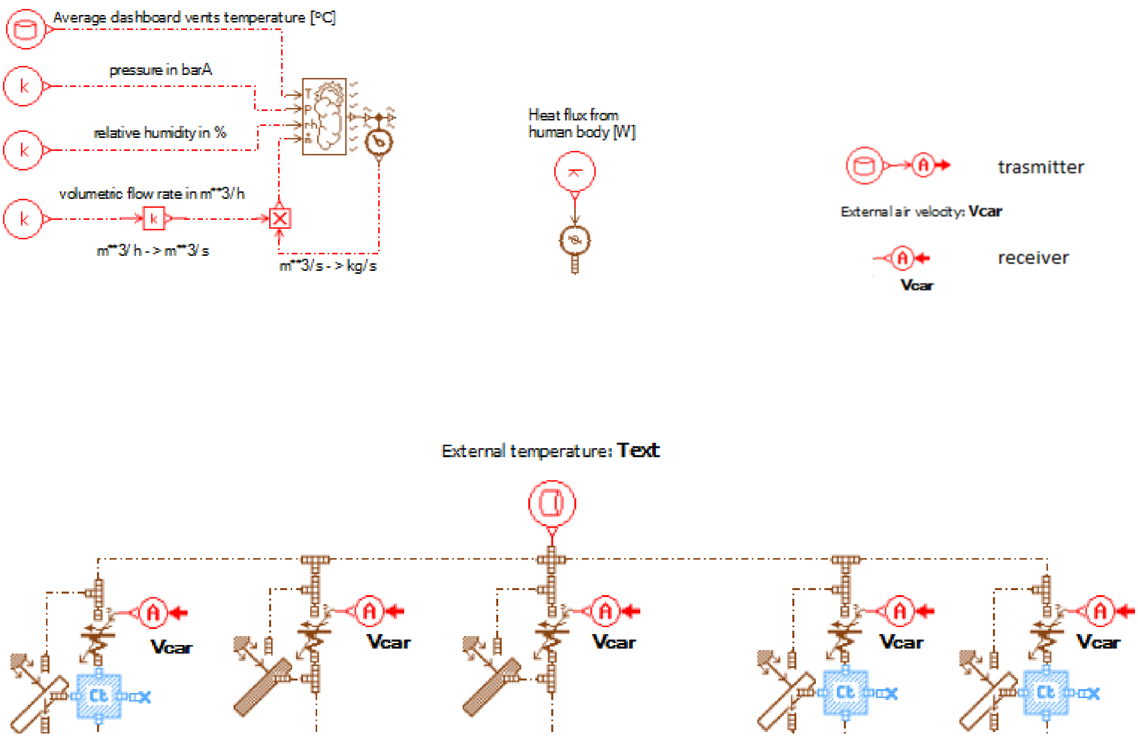

Figure 53. Input data for the validation of the car cabin.

The profiles of the dynamic time-tables concerning the external temperature and the inlet cabin temperature are shown in the figures reported below; the air velocity profile is the same shown in *Figure 46*.

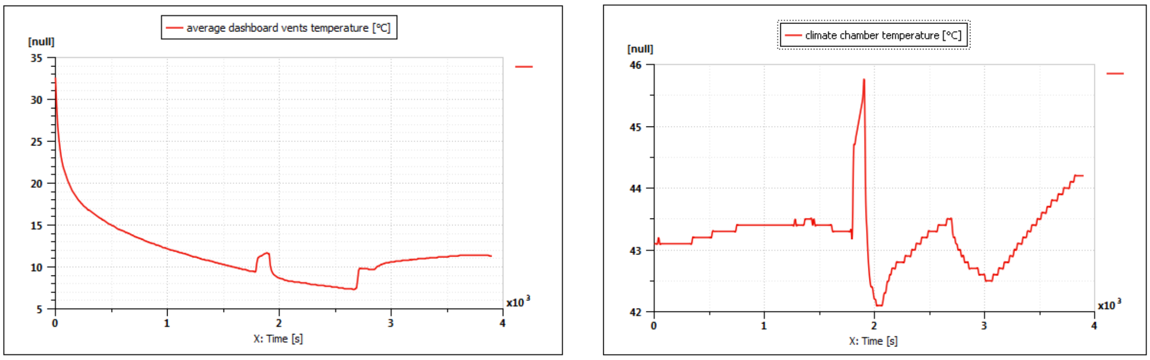

Figure 54. Inlet cabin temperature profile and climate chamber temperature.

Since the simulation model is a transient 1D combined to physical analysis, the validation of the cabin is aimed at the regulation of the heat capacity of the cabin. Varying the coefficients concerning the convective heat transfer and the masses of the components, the heat capacity of the cabin is modelled. The validation is obtained verifying the convergence of the internal cabin temperature of the simulation with the temperature measured with thermocouples during the Cooldown test. In the following figure three graphs are reported:

- Simulated and measured temperature;
- Absolute error;
- Relative error.

It is important to notice that the considerations made on the relative error are not significant because it is not referred to a target value but to a decreasing trend. In fact, an absolute error of 2°C can correspond to a high relative error for low temperature and to a low relative error for high temperature. All validations have been then performed in order to control the absolute error and limiting it to a maximum of around 2°C. The consideration on the absolute error excludes the first 20 seconds of the simulation because the measured temperature depends on many human factors involved in the test and then the measurement is less accurate.

In the following figure the internal cabin temperature evolution is reported, comparing simulated one and measured one.

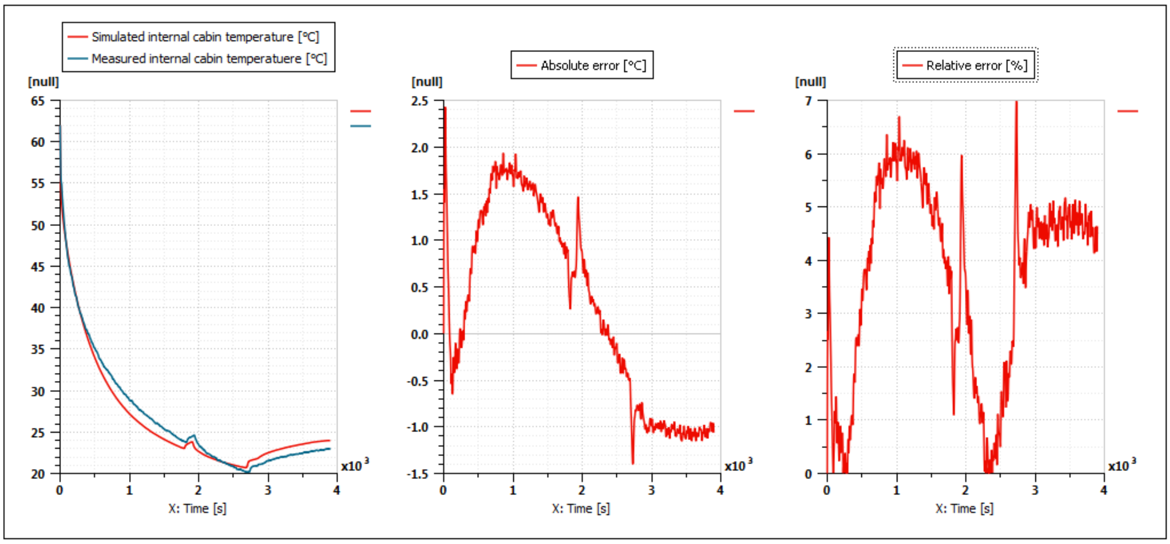

Figure 55. Comparison of the internal cabin temperature simulated in Amesim and measured during the Cooldown test.

4.4 Calibration of the heat exchangers of the AC system

The mandatory step before the validation of the cooldown test concerns the calibration of the heat exchangers and the evaluation of the optimal refrigerant charge. In this way the climate system realized in Amesim is coherent with the actual operation of the AC system.

The calibrations of condenser and evaporator have been edited in two different sketches to simulate the operation of the singular heat exchanger with the input data extrapolated by the respective data sheets.

4.4.1 Condenser calibration

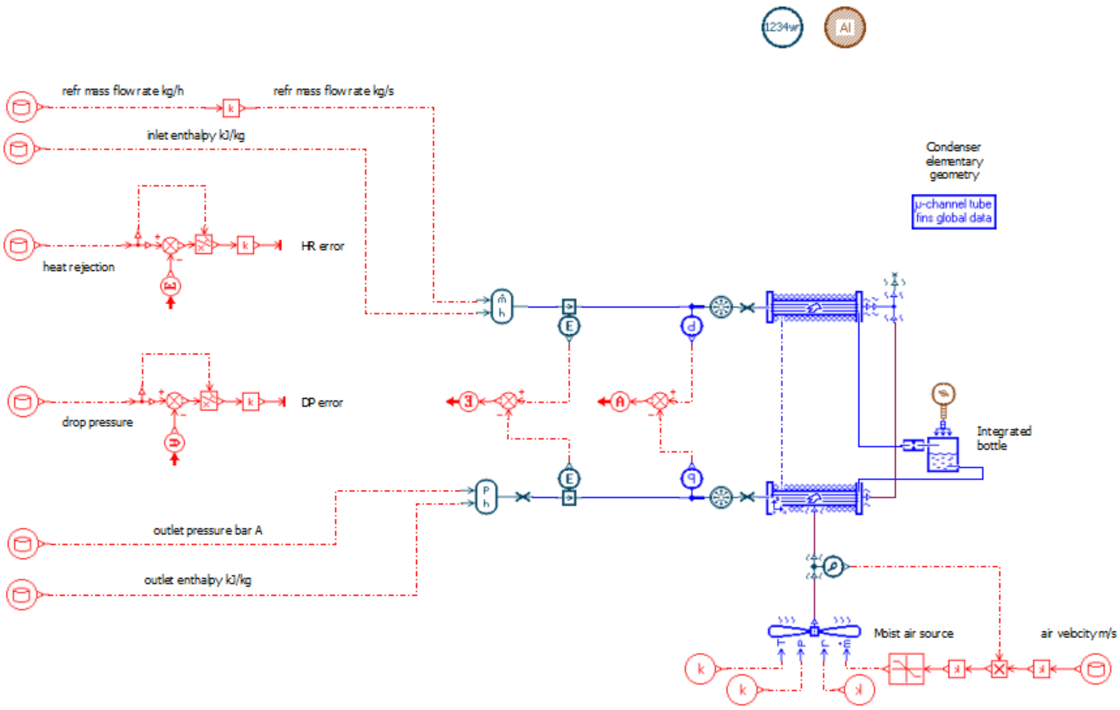

Figure 56. Model for the calibration of the condenser.

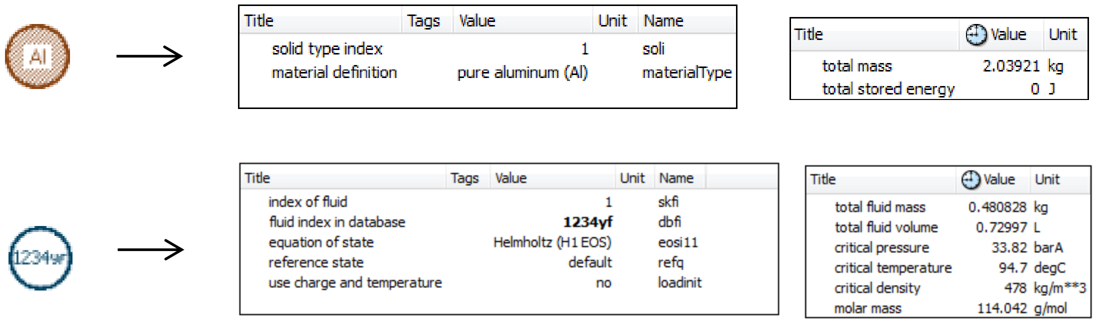

Title	Tags	Value	Unit	Name
solid type index		1		soli
material definition		pure aluminum (Al)		materialType

Title	Value	Unit
total mass	2.03921	kg
total stored energy	0	J

Title	Tags	Value	Unit	Name
index of fluid		1		skfi
fluid index in database		**1234yf**		dbfi
equation of state		Helmholtz (H1 EOS)		eosi11
reference state		default		refq
use charge and temperature		no		loadinit

Title	Value	Unit
total fluid mass	0.480828	kg
total fluid volume	0.72997	L
critical pressure	33.82	barA
critical temperature	94.7	degC
critical density	478	kg/m**3
molar mass	114.042	g/mol

Figure 57. Heat exchanger materials and fluid properties.

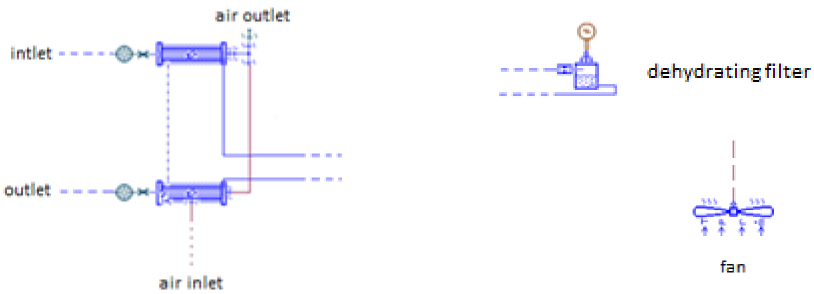

Figure 58. Condenser, dehydrating filter and fan.

The first group of components represents the two rows of the condenser coupled thanks to pipe lines which carry the refrigerant. At the inlet and outlet of the condenser two other components are introduced; the former represents the inlet and outlet section of the condenser; the latter is an adiabatic chamber without internal heat generation used to combine the system with the components containing the boundary conditions applied according to the data extrapolated by the data sheet. In the same representation the air mass flow line is drawn in brown: it enters in the condenser thanks to the fan and passes through the rows before of being rejecting in the atmosphere.

The second group of components represents the dehydrating receiver, important for the reliability of the system thanks to its capability to absorb humidity and organic and inorganic acids.

The geometric data of the condenser inserted in the simulation are reported in the following table:

CONDENSER CALIBRATION DATA	
Geometric data	
Finned tube width [mm]	658
Finned tube depth [mm]	16
Collector cross-sectional area [mm^2]	160
Refrigerant side cross-sectional area [mm^2]	7
Refrigerant side hydraulic diameter [mm]	0.6
Fin pitch [mm]	1.15
Fin thickness [mm]	0.07
Fin length [mm]	5.6
Tube periodicity [mm]	6.4
External tube height [mm]	1.4

Table 14. Overview of the geometrical data employed for the condenser calibration.

For the input data of the calibration it has been adopted a simple method concerning the construction of piece-wise functions representing refrigerant mass flow rate, inlet enthalpy, outlet pressure and outlet enthalpy with respect to air velocity. In particular the procedure followed has been realized performing some iteration until the convergence between heat convergence and refrigerant side pressure drops measured and simulated has been reached. The first step concerns the estimation of the analytical correlation between refrigerant mass flow rate and related pressure drops thanks to a polynomial trend line:

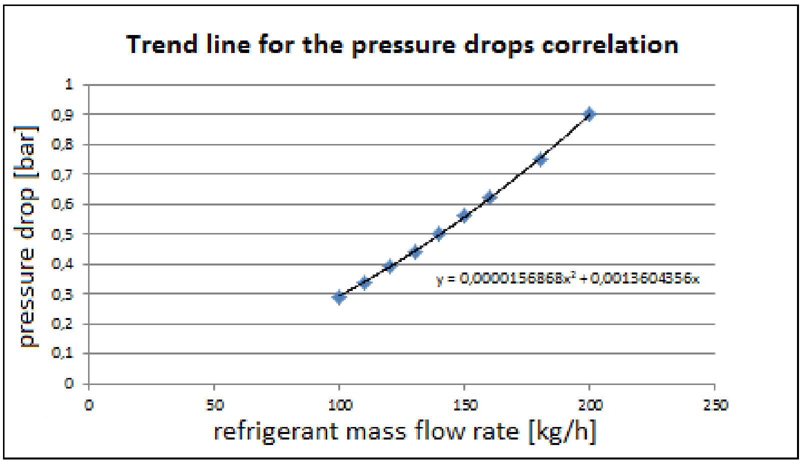

Figure 59. Trend line pressure drops – refrigerant mass flow rate.

According to this analytical correlation, after having performed four iterations starting from pressure drops null, the convergence between simulated and measured heat rejection and pressure drops has been reached. The following table contains all the data obtained at the end of the iterative method and used as input data for the calibration model of the condenser:

Thermodynamic data for the calibration of the condenser						
Air mass velocity [m/s]	Heat rejection [W]	Pressure drops [bar]	Refrigerant mass flow rate [kg/h]	Outlet enthalpy [kJ/kg]	Outlet pressure [barA]	Inlet enthalpy [kJ/kg]
1	5600	0.4127695	124.547	279.943	18.99	441.8
1.5	7700	0.6855646	170.141	278.886	18.71	441.8
2	9500	0.965991	208.551	277.821	18.43	441.8
2.5	10900	1.211888	237.948	276.9	18.19	441.8
3	12200	1.459956	264.776	275.934	17.94	441.8
3.5	13400	1.704615	289.122	274.96	17.69	441.8
4	14400	1.92004	309.17	274.135	17.48	441.8
4.5	15300	2.121681	326.952	273.345	17.28	441.8
5	16100	2.306238	342.511	272.589	17.09	441.8

Table 15. Overview of the input data for the calibration model of the condenser.

In particular the piece-wise functions are reported in the figures below:

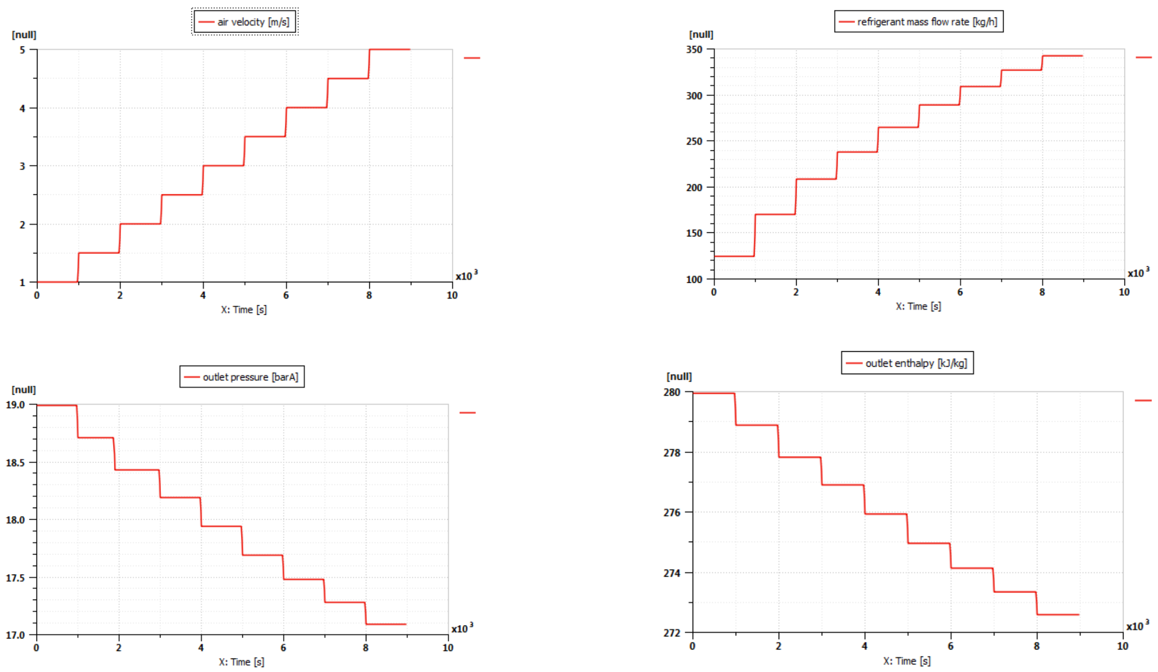

Figure 60. Piece-wise functions for input data to the condenser calibration model.

According to these profiles and to the geometrical data reported in the *Table 14. Overview of the geometrical data employed for the condenser calibration*, the convergence has been achieved thanks to the correct correlation for the air side turbulent Nusselt number and a suitable refrigerant frictional pressure drop gain:

$$Nu = f\,(Re, Pr) = 0.005 * Re^{1.4} * Pr^{0.3}$$

$$k_{dp} = 4.2$$

The convergence of the simulation is considered reached when the relative error is around 10%. In particular, since the simulation has been performed with refrigerant mass flow rates going from 120 $\left[\frac{kg}{h}\right]$to 350 $\left[\frac{kg}{h}\right]$, the convergence has been considered achieved for values of refrigerant mass flow rate lower than 250 $\left[\frac{kg}{h}\right]$ because the air conditioning system does not work with flow rates greater than this limit not even if the external conditions are the most adverse. In the following figure estimated and measured heat rejection and pressure drop are reported, characterizing both with the percentage relative error:

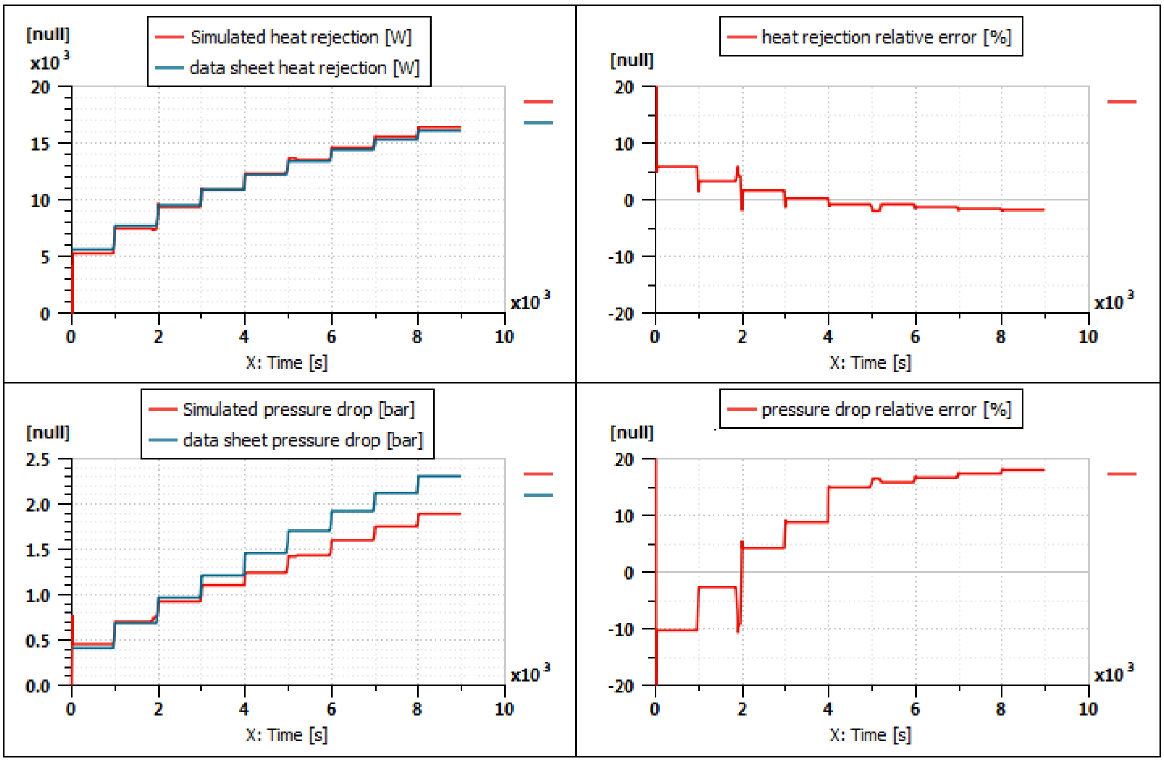

Figure 61. Convergence of heat rejection and pressure drop for the calibration of the condenser.

4.4.2 Evaporator calibration

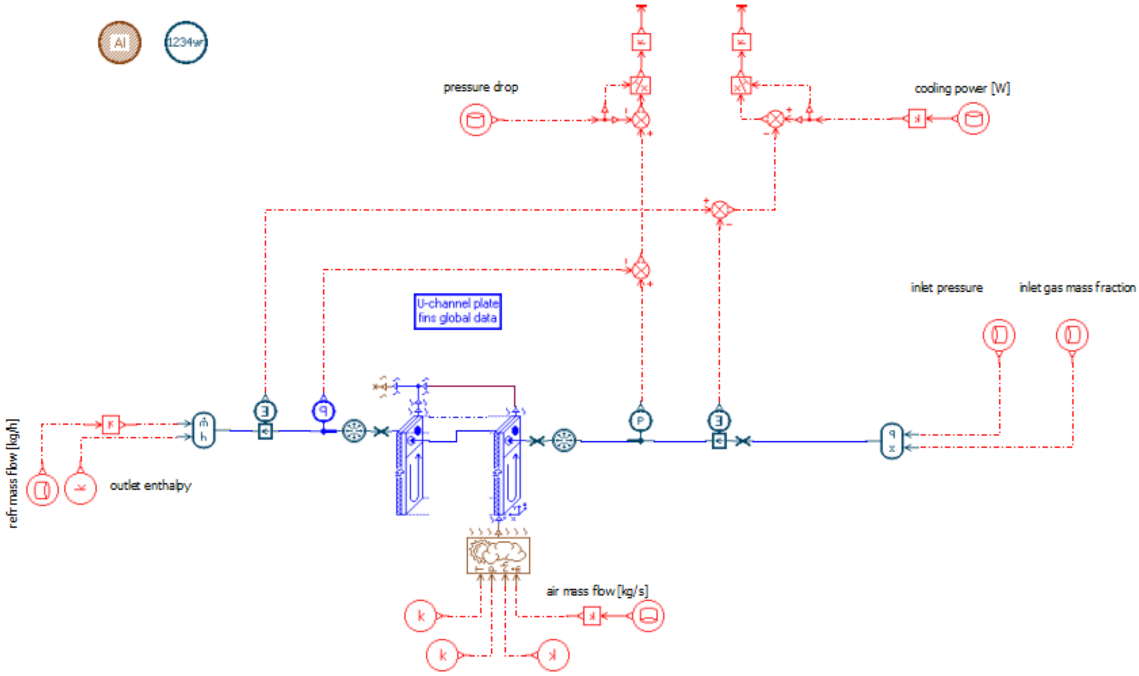

Figure 62. Model for the calibration of the evaporator.

The definition of the heat exchanger material and the fluid properties is the same of the condenser. Nevertheless the mass of aluminum and the total volume of the refrigerant are different because also dimensions are different. In particular the geometrical data of the evaporator inserted in the evaporator calibration model are listed below:

EVAPORATOR CALIBRATION DATA	
Geometric data	
Finned plate height [mm]	256
Finned plate depth [mm]	38
Box cross-sectional area [mm^2]	202.3
Refrigerant side cross-sectional area [mm^2]	14.45
Refrigerant side hydraulic diameter [mm]	2.05
Fin pitch [mm]	1.3
Fin thickness [mm]	0.05
Fin length [mm]	5.666
Plate periodicity [mm]	3.2
Refrigerant channel thickness (thickness of 2 plates + thickness of refrigerant flow) [mm]	2

Table 16. Overview of the geometrical data employed for the evaporator calibration.

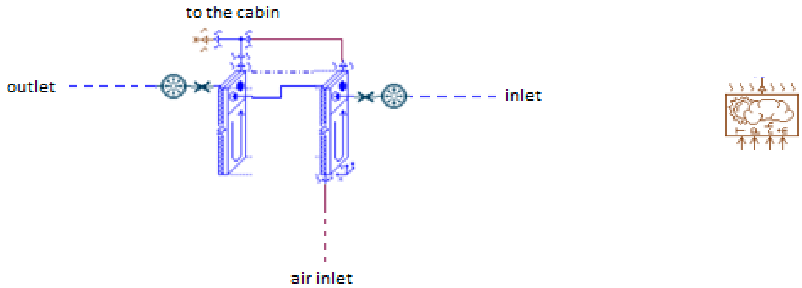

Figure 63. Condenser and blower.

The figure reported above shows the group of components representing the evaporator in which the refrigerant pipe and the air flow line are drawn and the blower characterized by four inputs: temperature, pressure, relative (or absolute) humidity and air mass flow rate.

Adopting the same method employed for the condenser calibration the inputs to the model have been built as piece-wise functions. In particular starting from the condition with pressure drop null and looking for the convergence of the refrigerant mass flow rate, the analytical correlation between pressure drop and refrigerant mass flow rate has been determined thanks to the introduction of the trend line according to the set of data extrapolated by the data sheet. In the following figure the correlation of the trend line for the drop pressure calculation is reported:

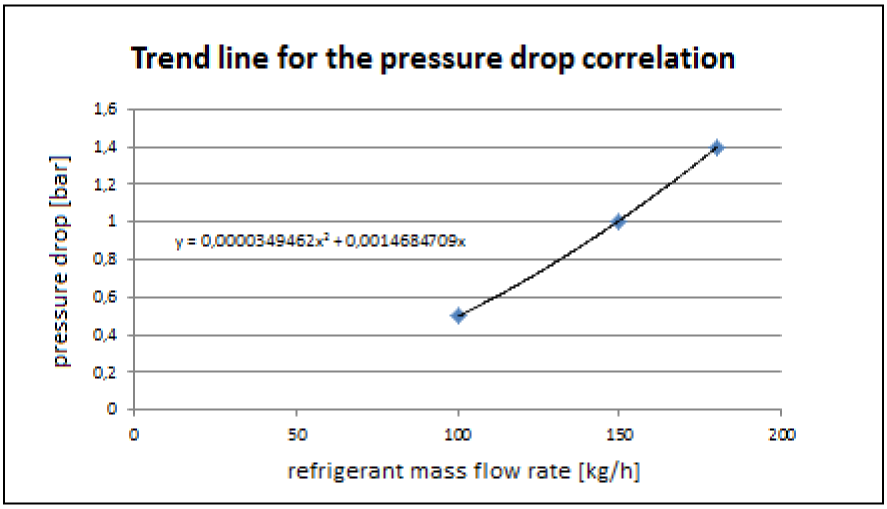

Figure 64. Trend line for the correlation between refrigerant mass flow and pressure drop.

According to the correlation expressed in the figure above, starting from the thermodynamic data listed in *Table 5. Thermodynamic input data for the evaporator in Amesim*, it has been possible the piece-wise functions as shown below:

Thermodynamic data for the calibration of the evaporator						
Air mass flow rate [kg/h]	Heat rejection [W]	Pressure drops [bar]	Refrigerant mass flow rate [kg/h]	Outlet enthalpy [kJ/kg]	Inlet pressure [barA]	Inlet gas mass fraction [null]
220	3552	0.705178	146.01	368.99	4.005	0.4532
330	4896	1.179497	201.25	368.99	4.479	0.43
440	5952	1.632095	244.66	368.99	4.932	0.409
550	6624	1.956729	272.29	368.99	5.257	0.3943
660	6912	2.104575	284.13	368.99	5.405	0.3877

Table 17. Overview of the input data for the evaporator calibration model.

In particular:

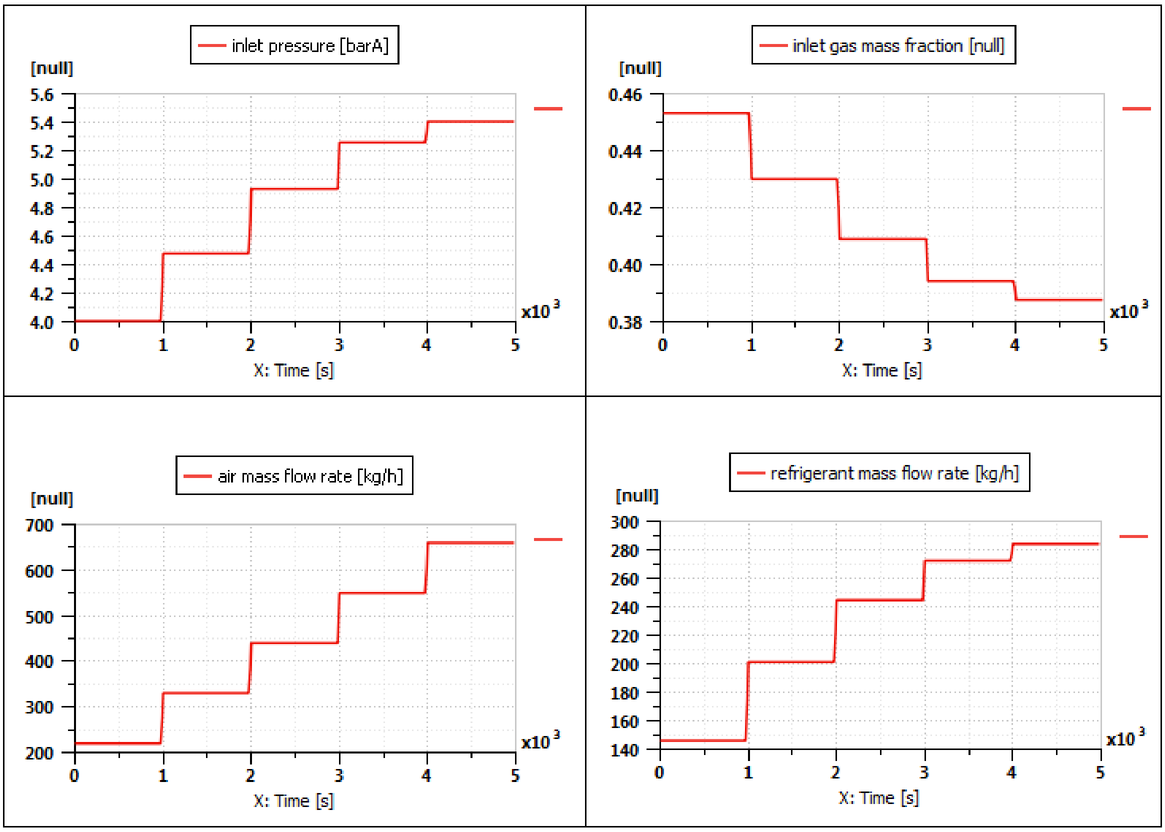

Figure 65. Piece-wise functions for the input to the evaporator calibration model.

According to the geometrical data listed in *Table 16. Overview of the geometrical data employed for the evaporator calibration* and to the piece-wise input function shown above, the calibration has been performed thanks to the correct correlation for the air side turbulent Nusselt number and a suitable refrigerant frictional pressure drop gain:

$$Nu = f\,(Re, Pr) = 0.005 * Re^{1.4} * Pr^{0.3}$$

$$k_{dp} = 1$$

The convergence of the simulation is considered reached when the relative error is around 10%. In the following figure estimated and measured heat rejection and pressure drop are reported, characterizing both with the percentage relative error:

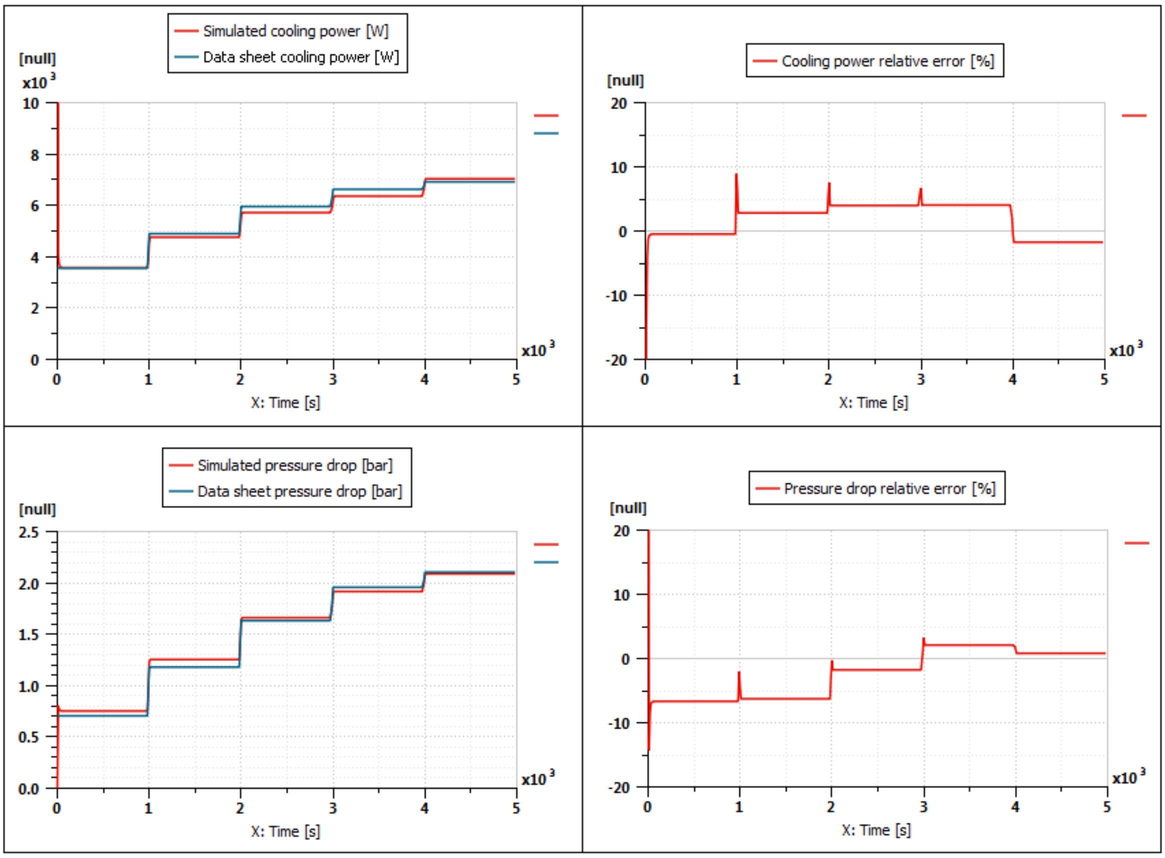

Figure 66. Convergence of heat rejection and pressure drop for the evaporator calibration.

4.5 Optimal refrigerant charge

The evaluation of the optimal refrigerant charge is a procedure aimed at the achieving of the best refrigerant charge of the system. This step is based on the condenser sub-cooling and the evaporator over-heating which vary according to the variation of the charge of the refrigerant. The sketch model used for the evaluation of the optimal refrigerant charge is the representation of the air conditioning group realized as shown in the figure below:

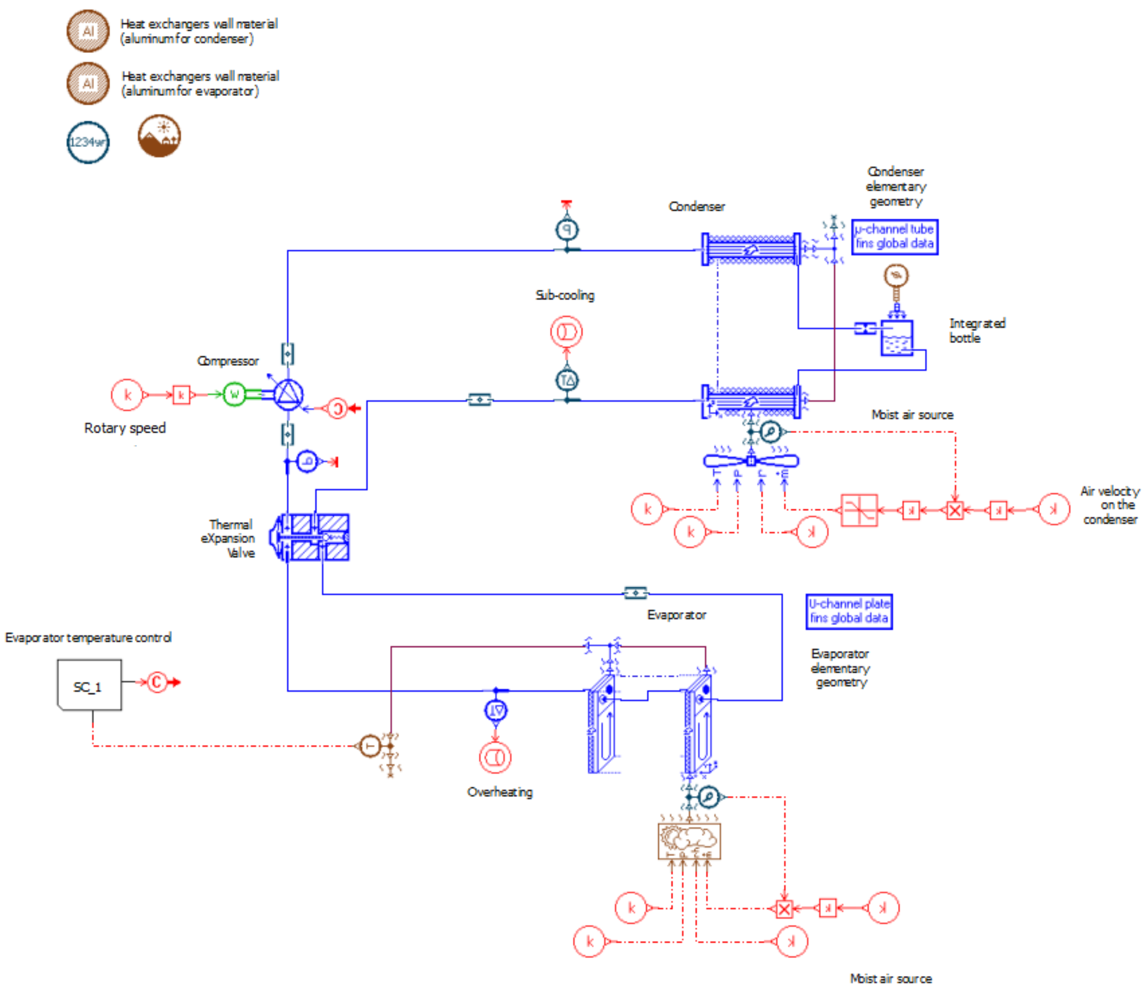

Figure 67. Sketch model employed for the optimal refrigerant charge assessment.

In particular, the control system applied to the compressor is referred to the compressor type; in fact, the compressor employed in this automotive application is a variable displacement externally controlled compressor and therefore the regulation occurs controlling the outlet evaporator temperature. In the present representation the air conditioning system is characterized by inputs which do not cause a temperature decrease under the target and then the control system is not involved in the simulation. For this reason, it will not be described in this section and it will be considered in the following paragraphs.

The input data for the optimal refrigerant charge estimation are:

Data input for the optimal refrigerant charge		
Property	***Unit***	
Evaporator		
Mass flow rate	*[kg/h]*	450
Relative humidity	*[%]*	19
Pressure	*[bar]*	1.013
Temperature	*[°C]*	43
Condenser		
Air velocity on the condenser	*[m/s]*	2
Relative humidity	*[%]*	19
Pressure	*[bar]*	1.013
Temperature	*[°C]*	43
Compressor		
Rotary speed	*[rpm]*	2500

Table 18. Data input to the AC system for the optimal refrigerant charge.

The assessment of the optimal refrigerant charge has been performed thanks to the possibility of using a particular simulation mode which allows to obtain the trends of over-heating and sub-cooling with respect to the variation of the refrigerant charge: "Batch Parameters Simulation". The first step has concerned the communication to the software about the imposition of the charge by the user:

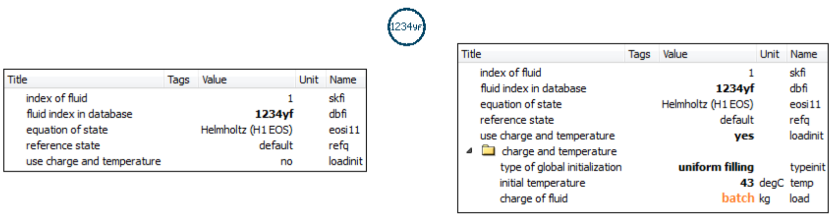

Figure 68. Charge imposed by the user.

The batch simulation of Amesim allows the user to set different values of a parameter and to observe the result of a simulation with respect to its variation. In particular:

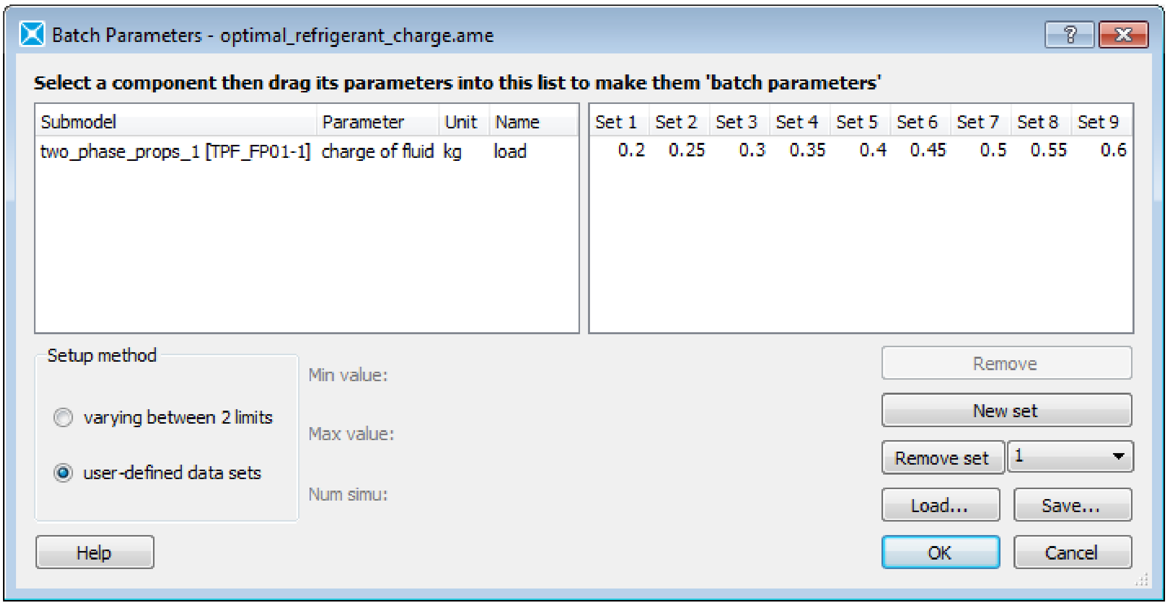

Figure 69. Batch parameters for the refrigerant charge.

The result corresponds to the trend of sub-cooling and over-heating shown below:

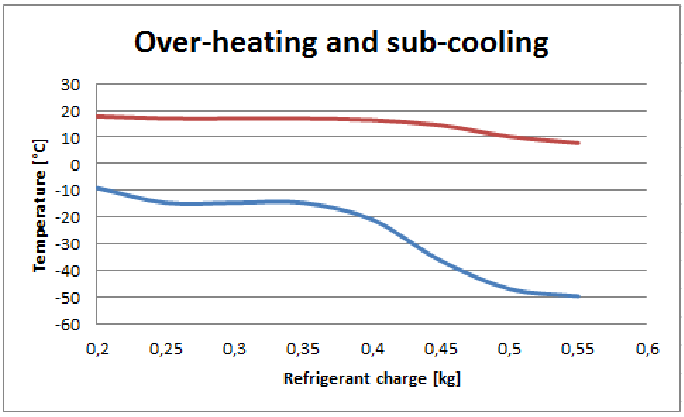

Figure 70. Over-heating and sub-cooling with respect to the refrigerant charge
Refrigerant charge belonging to the interval [0.2; 0.55]

Improving the refrigerant charge interval, it is possible to observe a linearity of the trends of both variables even if the charge rises. After having detected the upper and lower limit of this "plane", the optimal refrigerant is conventionally chosen as the value corresponding to the 75% of the "plane". In particular the definition of the interval including the "plane" and the extrapolation of the optimal refrigerant charge have resulted as reported in the following table:

Optimal refrigerant charge estimation			
"Plane" lower limit	"Plane" upper limit	Sub-cooling	Over-heating
[kg]	[kg]	[°C]	[°C]
0.25	0.35	-14.68868	16.89898

Table 19. Optimal refrigerant charge estimation.

The optimal charge has been estimated as explained above:

$$Optimal\ charge = 0.26 + 0.75 * (0.36 - 0.26) = 0.325\ [kg]$$

4.6 Validation of the Cooldown test

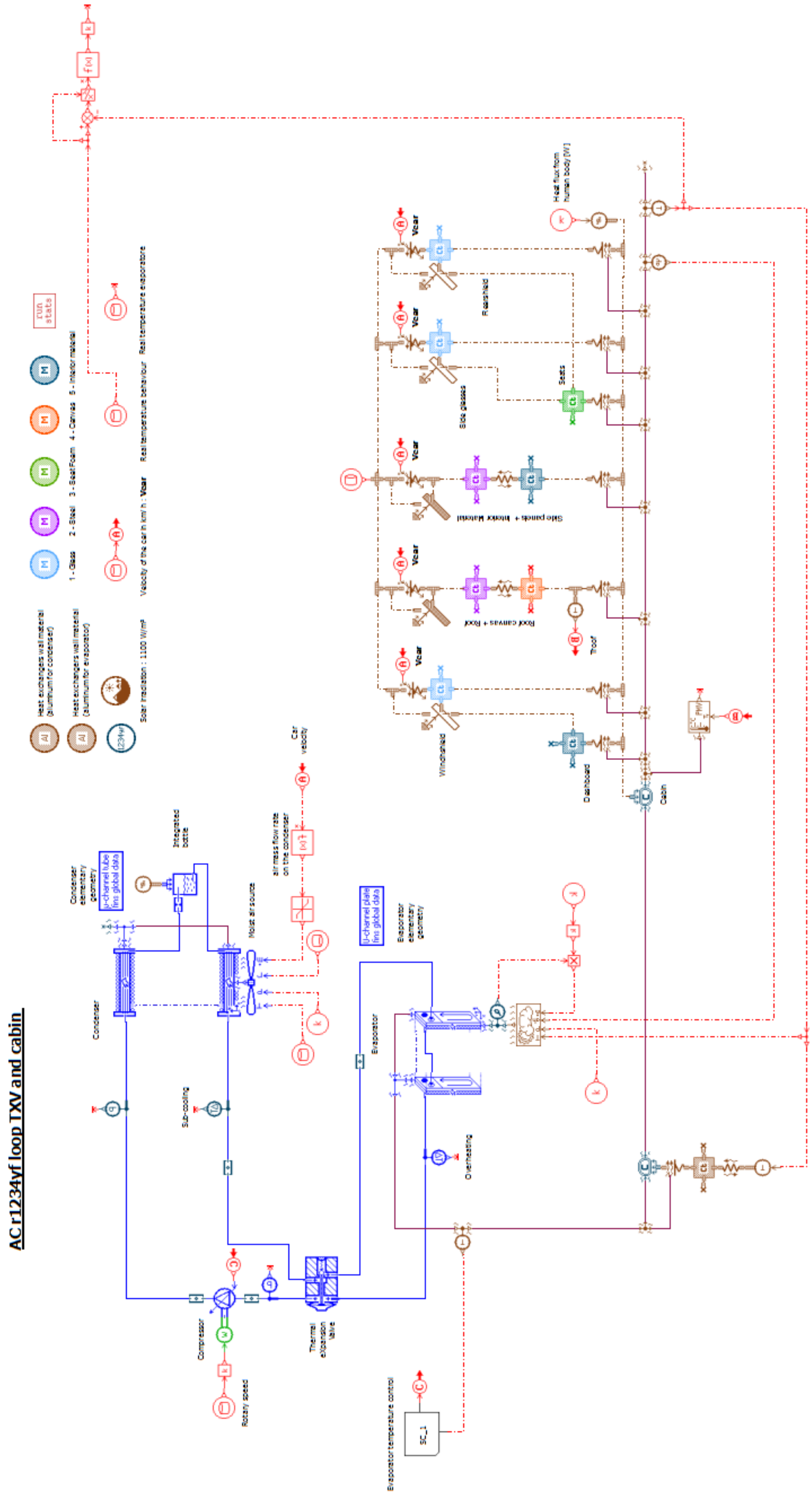

This sketch gathers the air conditioning system sketch and the car cabin sketch but it contains also the compressor control system and the ducts system.

The air conditioning system sketch contains the same components compared to the optimal refrigerant charge; condenser and evaporator have been described during the heat exchangers calibration, but an analysis is mandatory also for compressor and thermal expansion valve.

The compressor has been characterized according to the data sheet shown in *Figure 34 - Data sheet compressor* in terms of displacement and efficiencies as shown in the following figures:

Title	Tags	Value	Unit	Name
index of fluid		1		fi
input data out of range		extrapolate		mode
discontinuity handling		active		disc
compatibility with stop and start		no		sands
coefficient definition		no		CoeffDef
flow rate calculation		displacement		flowRateCal
displacement				
maximum displacement		**140**	cm**3	maxdisp
minimum displacement		20	cm**3	mindisp
efficiencies				
filename or expression for volumetric efficiency = f(tau, N[rev/min])		**D:/users/F21270C/Desktop/Renegade_Cooldown/volumetric_efficiency.data**		volEff
filename or expression for isentropic efficiency = f(tau, N[rev/min])		**D:/users/F21270C/Desktop/Renegade_Cooldown/isentropic_efficiency.data**		isEff
filename or expression for mechanical efficiency = f(tau, N[rev/min])		0.9		mecEff
volumetric efficiency at minimum displacement		0.4	null	veffcmin

Figure 72. Compressor parameters in Amesim.

In particular the files concerning the volumetric and isoentropic efficiencies characterize the compressor efficiency maps:

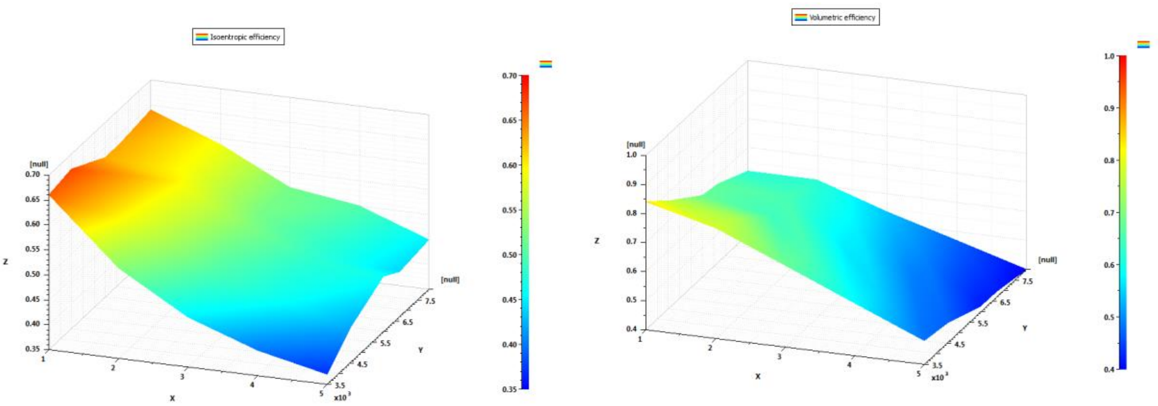

Figure 73. Compressor efficiencies map.

where the *x*-axis corresponds to the rotary speed expressed in *rpm*, the *y*-axis corresponds to the pressure ratio and the z-axis contains respectively the isoentropic and the volumetric efficiencies. The thermal expansion valve has been characterized according to the data sheet reported in *Figure 37 (Overview of a TXV data sheet)*, introducing geometrical and thermal data and the suitable curves compared to the data sheet. In particular:

Title	Tags	Value	Unit	Name
bulb temperature		**T_soak**	degC	tbulb
index of fluid		1		fi
maximum valve lift		**0.7**	mm	liftmax
reference high pressure third quadrant		**11.313**	barA	hpref
reference low pressure in third quadrant		**3.163**	barA	lpref
reference subcooling in third quadrant		5	degC	scref
pressure offset at 0 degC		**0.3**	barA	p0
time constant		1	s	tau
first quadrant		AMETable		
interpolation type		linear		splineq1
linear data out of range mode		**extreme value**		lmodeq1
discontinuity handling		active		discq1
filename of first quadrant curve for valve opening pressure[barA] = f(evaporator outlet temperature[degC])		**../../TESI FCA/Dati Renegade/TXV/first_quadrant_TXV.data**		tableq1
second quadrant		AMETable		
interpolation type		linear		splineq2
linear data out of range mode		**extreme value**		lmodeq2
discontinuity handling		active		discq2
filename of second quadrant curve for evaporator outlet pressure[barA] = f(valve lift[mm])		**second_quadrant.data**		tableq2
third quadrant		AMETable		
interpolation type		linear		splineq3
linear data out of range mode		**extreme value**		lmodeq3
discontinuity handling		active		discq3
filename of third quadrant curve for mass flow rate[kg/h] = f(valve lift[mm])		**third_quadrant.data**		tableq3

Figure 74. TXV parameters in Amesim.

The quadrant curves are shown below:

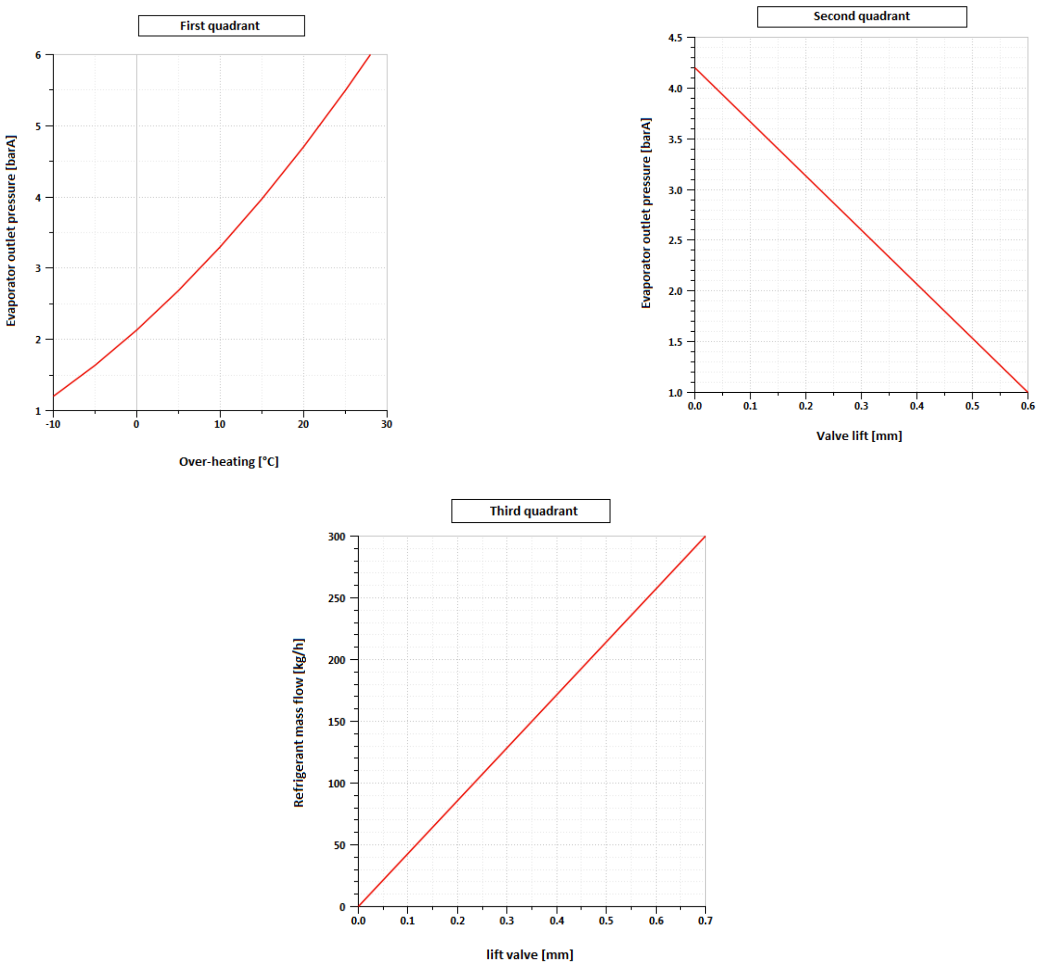

Figure 75. TXV quadrant curves.

The compressor control system has already been introduced in the previous paragraphs; hence it represents the compressor displacement regulation which occurs according to the evaporator outlet air temperature control, as shown in the following figure:

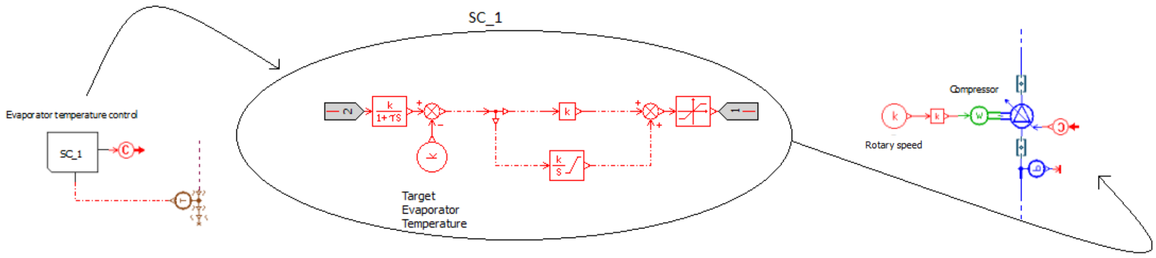

Figure 76. Compressor control system.

In particular the control has been performed using a simple PI (Proportional Integrative) control which receives the difference between the outlet air temperature and the target (set equal to 4 °C) and gives as outcome a signal saturated in the interval [0; 100] which regulates the compressor displacement in order to maintain the air temperature over the target. The cooldown test is performed "*at all cold*" and hence it means that the internal cabin temperature does not respect the condition of thermal comfort in occupied space; nevertheless, the evaporator outlet air temperature must be however controlled in order to avoid the structural problems. In particular, during the Cooldown test the evaporator outlet air temperature behaves as shown below:

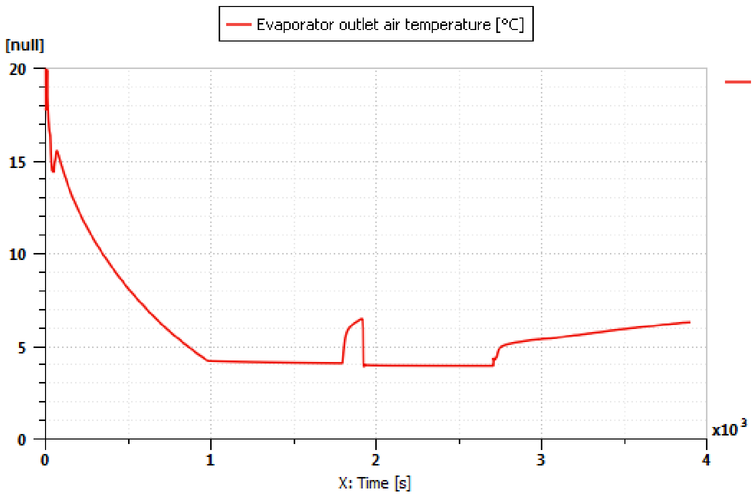

Figure 77. Evaporator outlet air temperature according to the compressor regulation.

In the end the model has been improved with the introduction of a model able to represent the ducts carrying the air from the evaporator to the vents system. In fact, the Car Cabin Validation model discussed in the paragraph **4.3 (Validation of the car cabin model)** the cabin inlet air temperature employed as input to the system was equal to the average dashboard vents temperature shown on the left of *Figure 54. Inlet cabin temperature profiles and climate chamber temperature*. The transition from the evaporator outlet air conditions to the cabin inlet air conditions is warranted by the influence of the thermal capacity of the cabin on the ducts' surfaces. According to this sentence the sub-model has be realized as shown below:

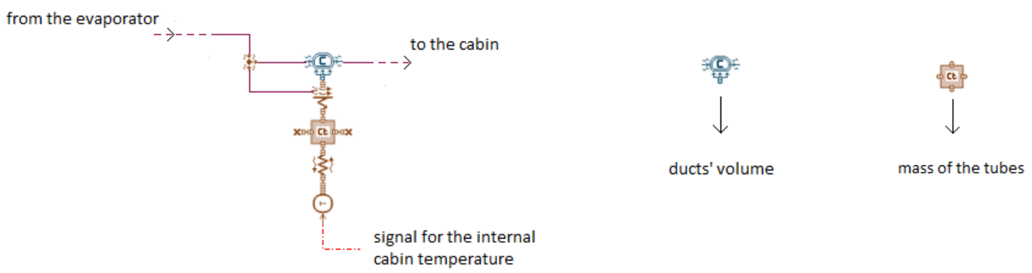

Figure 78. Representation of the sub-model for the ducts' system.

In particular the sub-model describes the heat exchange between the air temperature at the internal cabin conditions and the external surface of ducts (modelled as conductive heat exchange) and the heat exchange between the ducts' surface and the air mass flow rate moving towards the car cabin (modelled as convective heat exchange). In this way the air flow rate is heated up before reaching the vents wasting part of the cooling power produced by the air conditioning system.

The aim of the present study is to produce a model which is able to follow the same thermodynamic trend compared to the actual behavior of car cabin and air conditioning system during external conditions used in the Cooldown test:

Cooldown test		
Property	***Unit***	
External air pressure	[bar]	1.013
External air temperature	[°C]	43
Solar irradiation	[W/m^2]	1100
External air relative humidity	[%]	19

Table 20. External conditions for a Cooldown test.

In order to have a more realistic overview of the Cooldown test, each thermodynamic property has been employed according the data extrapolated by the report edited on an occurred Cooldown test. As matter of the fact external air temperature and relative humidity has been drawn following their oscillations:

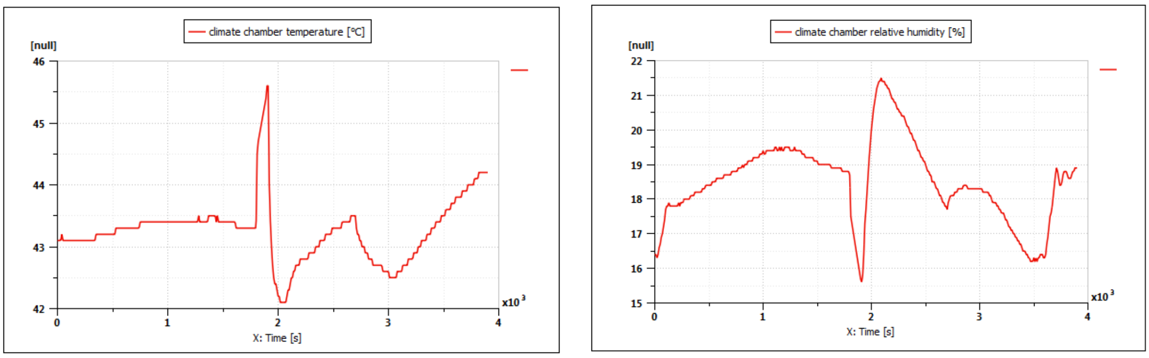

Figure 79. Climate chamber air conditions.

According to the Cooldown test the air mass flow rate sucked by the AC system and then blown towards the car cabin has been fixed to a constant value:

$$\dot{Q}_{air} = 450 \left[\frac{kg}{h}\right]$$

With regards to the dynamic input data deriving by the driving cycle employed during the test, external air velocity and car velocity have already been shown respectively in *Figure 47 (Comparison between car velocity and external air velocity)* and *Figure 54 (Inlet cabin temperature profiles and climate chamber temperature)*. The other dynamic data linked to the driving cycle is of course the engine rotary speed, important for the evaluation of the torque transmitted to the compressor:

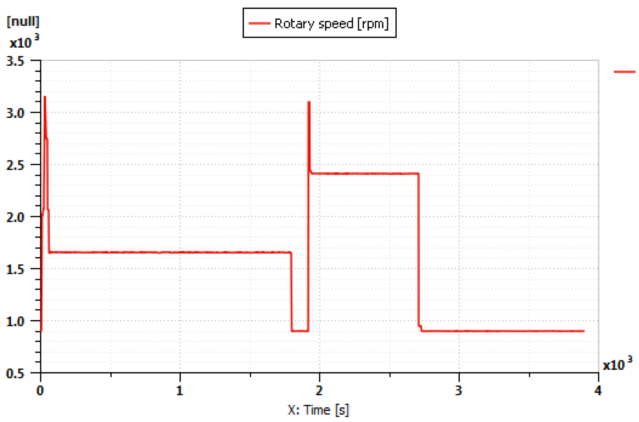

Figure 80. Engine rotary speed.

The last important consideration to be explained concerns the air velocity map on the condenser. In fact, it certainly depends on the car velocity but when the vehicle is moving with a sufficient velocity, all the plastic constituting the car body blocks the air reducing drastically its velocity. On the other hand, when the car velocity is under a certain value or null, the fan is triggered and it drives the air towards the condenser channels. According to this consideration, thanks to a correct fluid-dynamic simulation, the correlation linking the car velocity and the air velocity on the condenser has been employed to simulate accurately the model as much as possible. In particular in the following figure the graph describing the air mass flow rate map is reported, omitting the analytical correlation:

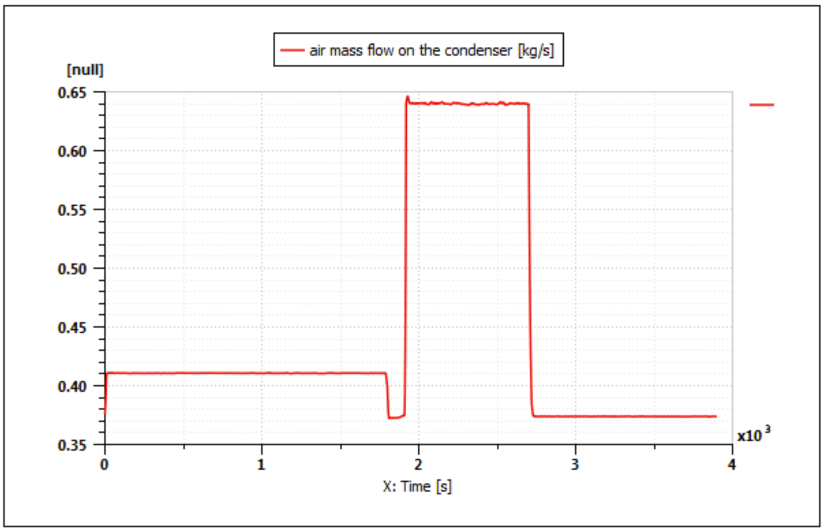

Figure 81. Air mass flow rate on the condenser.

Similarly to the validation of the car cabin model, the validation of the Cooldown test has been edited providing an absolute error between the simulated and the measured internal cabin temperature within 2°C. Furthermore, in order to characterize the combination of the two models, also a comparison between the temperature evaluated in the Car Cabin Model and in the Cooldown Test Model has been performed. Data used for the production of the global Cooldown model are the same compared to the data employed in the previous validations. The first graph explains the accuracy of the simulation on the modelling of a Cooldown test, the second one explains the accuracy of the modelling of the ducts' system which is however intrinsically affected by uncertainties.

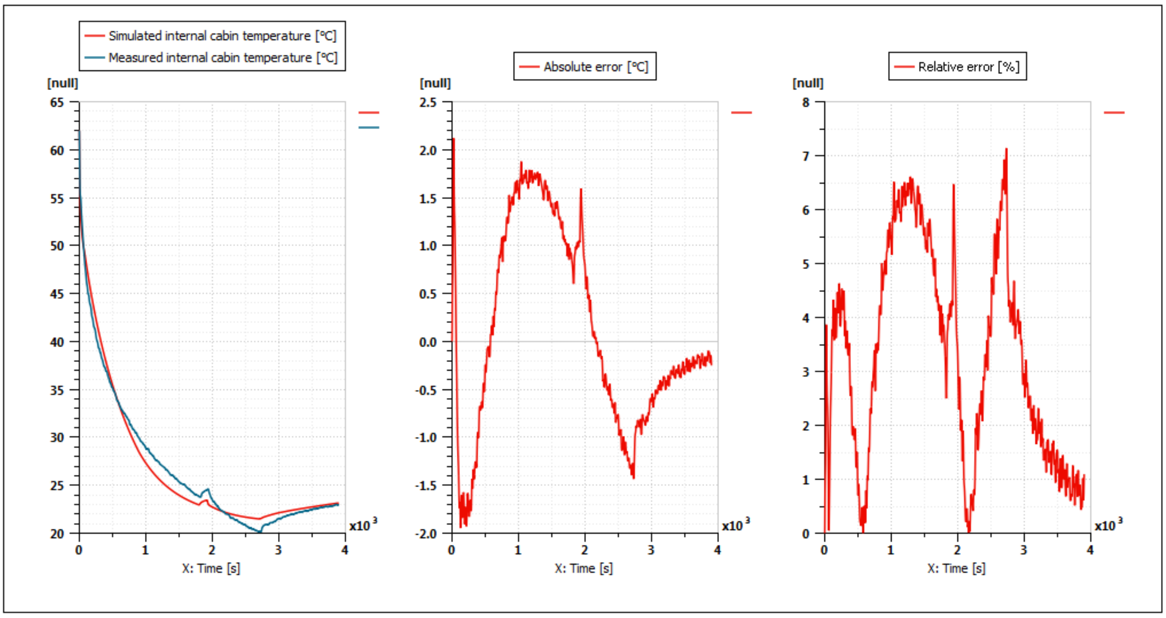

Figure 82. Comparison of the internal cabin temperature simulated in the Cooldown model in Amesim and measured during the Cooldown test.

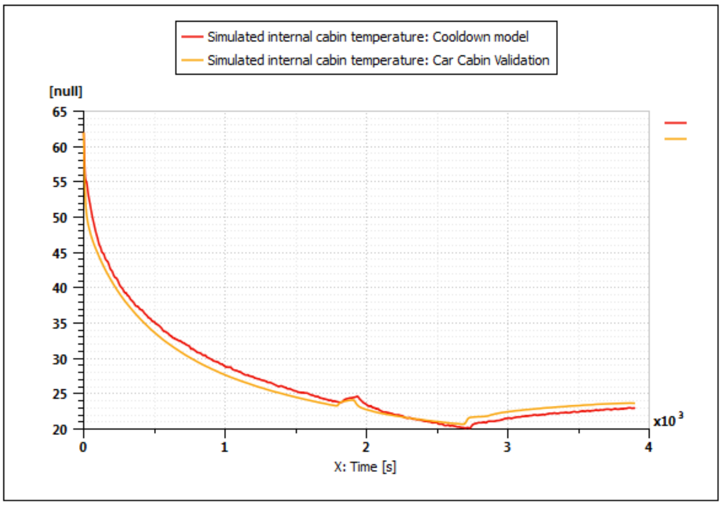

Figure 83. Comparison between the internal cabin temperature simulated in the Car Cabin model and simulated in the Cooldown model in Amesim.

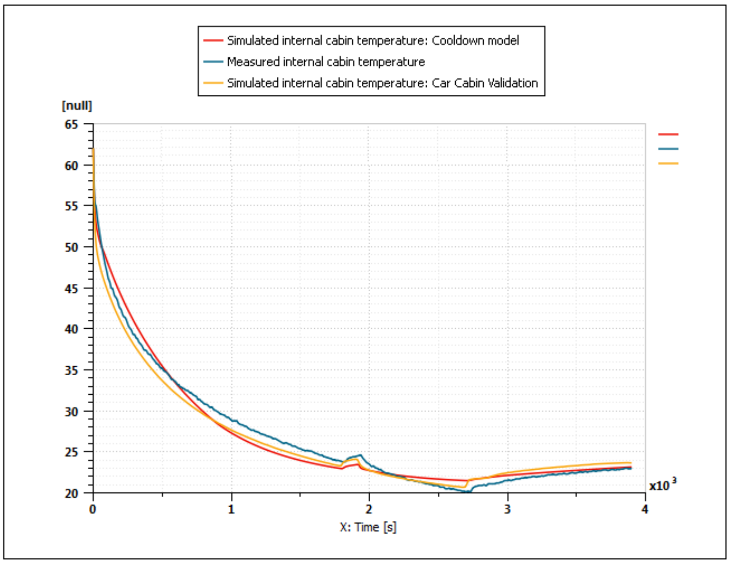

Figure 84. Comparison between the internal cabin temperature simulated in the Car Cabin model, simulated in the Cooldown model in Amesim and measured during the Cooldown test.

CHAPTER V: PROJECT STUDY. PART II

The second part of the project thesis concerns the application of innovative technologies to the car cabin and the evaluation of the energy savings resulted. In particular, three kinds of technological retrofits will be discussed: thermal insulation, reflective glasses and infrared-reflecting (IR) pigments for coatings.

The thermal insulation concerns the increase of the thermal capacity of a vehicle which is more insulated with respect to the heat exchange with the outside conditions. It allows to reach more quickly a comfortable cabin temperature, reducing heat loss and then the energy consumption of the AC system; in the winter period the thermal insulation makes harder to lose warm air, in the summer case it makes harder the heat exchange with the environment. It implies a fuel consumption reduction for an internal combustion vehicle and an electric power consumption reduction for EVs, increasing in both cases the autonomy and reducing the related CO_2 emission [29]. An example of introduction of thermal insulation is referred to Nissan which has analyzed the energy savings deriving from a configuration including thermal insulation in the roof:

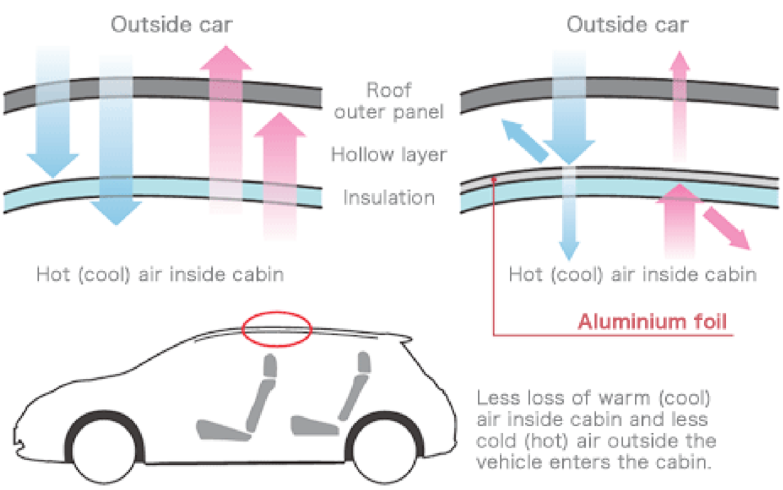

Figure 85. Application of thermal insulation in the roof by Nissan [29].

In particular, the application edited by Nissan concerns the providing of an aluminum foil attached over the internal roof of the vehicle. This application allows a more comfortable temperature in the cabin, maintaining the air hot in the winter period and cool in the summer period.

With regards to glasses the most common solution observed in the last 50 years concerns the employment of a reflective foil when the car is not used in order to reduce the solar radiation transmitted by glasses into the vehicle cabin. This rude application is however used when any driving cycle is occurring reducing the soaking transient but causing any improvement when the car is moving during a sunny hot day. For this reason, the scientific world has focused the attention on the possibility to reduce the irradiative solar load assessing the consequent energy savings deriving from a lower power consumption of the air conditioning system. Thermal studies performed with suitable sensors have shown how the temperature increase of internal cabin surfaces can reach high values; in particular the windshield transmits almost the whole solar load which is totally absorbed by the dashboard components. In particular the steering wheel can reach temperatures greater than 80 °C causing a high local discomfort for the driver when he puts his hands on.

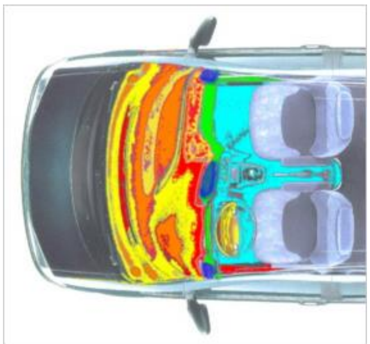

Figure 86. Thermal vision of the internal cabin surfaces at end of the soaking transient [30].

Solutions can therefore be divided in three groups:

- Improvement of glass transmittance;
- Employment of solar reflective coatings for internal surfaces;
- Employment of seats covered with a black solar reflective leather.

With regards to the reduction of glasses' transmittance, the applications employed today are characterized by a spectral transmittance which shows very high values for wave length included in the interval 0 ÷ 3 μm. Furthermore, the solar energy intensity related to visible and infrared radiations amounts to around the 95% and almost the 50% is in the near infrared, demonstrating how improvements on the coats and glasses properties are very powerful [30].

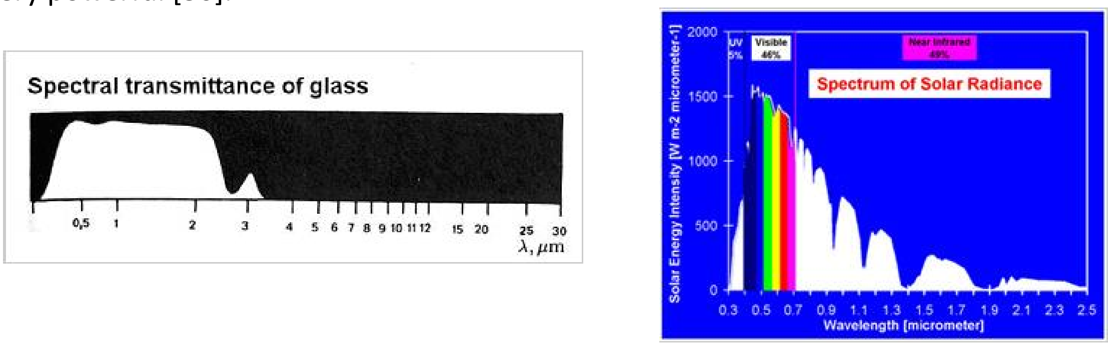

Figure 87. Spectral transmittance of glass [30] and solar energy intensity [31].

PPG Industries’ glass technology group developed a technology, called Sungate EP, which permits to reach a transmission factor of 33%, respecting the requirements for the visibility. It implies a temperature reduction of 12 °C for the internal air, 10 ÷ 12 °C for the seats, 16.8 °C for the dashboard and 20.4 °C for the windshield during the solar-soak test [32].

The solar spectrum can be divided in ultraviolet (UV – wavelengths ϵ [0.295 ÷ 0.400] μm), visible (wavelengths ϵ [0.400 ÷ 0.700] μm) and near – infrared (n – IR – wavelength ϵ [0.700 ÷2.500] μm).

The technology of infrared – reflecting (IR) pigments works on the illumination spectrum; comparing the reflectance curves for the white and the black portion of a virgin card commonly used to test color and opacity of coats, it is possible to observe that the white portion reflects light back in the visible part and keeps on reflecting back into the n-IR part of the spectrum while the black portion absorbs light in the visible part and keep on absorbing into the n-IR part [30].

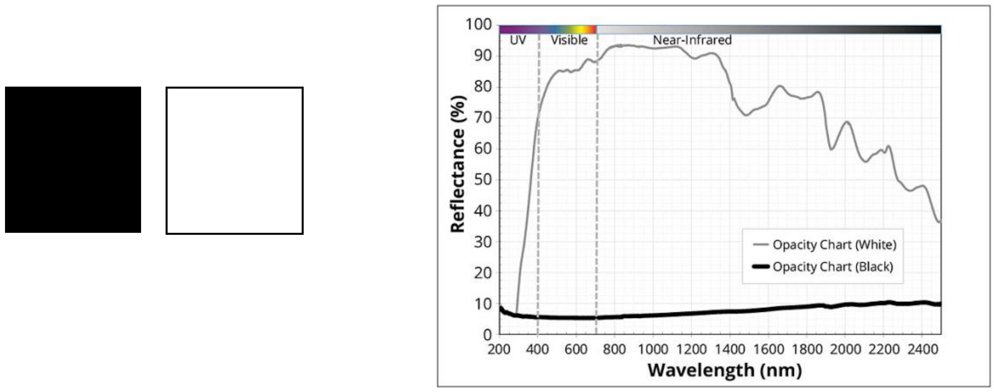

Figure 88. Reflectance of black and white [34].

In this way the white painted coats are cooler and the black painted ones are hotter if subjected to the same solar radiation. The best solution concerns the employment of a material able to absorb in the visible and to reflect in the n-IR in order to maintain a lower temperature. Materials can be distinguished by the Total Solar reflectance (TSR) which represents the ability to reflect the sunlight over the solar spectrum and then the white portion is characterized by a higher TSR while the black portion by a lower TSR. According to studies performed by PCI (Paint & Coatings Industry) the substitution of a standard coating with an IR Pigment coating increases the TSR by 20% reducing the surface temperature by almost 13 °C. It implies hence lower energy consumption by HVAC systems without sacrificing aesthetics [33]. In particular, the PCI presents three different pigment technologies:

- Inorganic IR – reflecting black or CI Pigment Brown 29;
- Organic IR – transmitting black or CI Pigment Black 32;
- IR – optimized titanium dioxide TiO_2.

Inorganic IR – reflecting black pigments represent the principal IR pigments in use and belong to the CICP (Complex Inorganic Color Pigments) family. They are employed since the 1980s when building materials like iron oxide or organic pigments are chromatically limiting; the IR properties of these materials warrant the reduction of the warping of PVC windows induced by the solar irradiation. In the late 1990s they were employed for the "cool roofing" in order to reduce the thermal capacity of the buildings' roof and for motorbike seat covers in order to maintain it cooler and more comfortable.

One of the most significant indices which characterize pigments is the P:B (pigment:binder) ratio; it shows the hiding power of the pigment and it is strictly linked to the opacity. For instance the Pbr29 (CI Pigment Brown 29) is characterized by a P:B ratio varying between 0.1 and 1.2 but this material gains full opacity in the range 0.3 ÷ 0.6 (P:B = 0.4 for visual opacity). The IR range is largely scattering with only a small absorption and so the light can transmit until the P:B is sufficiently high.

The PBr29 pigments have nice IR scattering properties and then it is characterized by a high TSR. On the other hand, the PBk32 (CI Pigment Black 32) is not characterized by appreciable IR scattering properties and achieves high TSR thanks to its IR transmittance. While the Pbr29 has high absorbance in the visible range and high scattering ability in the n-IR range, the PBk32 has a stronger absorbance in the visual (even at low P:B ratios) but low scattering ability in the n-IR region. In particular differences are listed below:

- PBk32 gains visual opacity at a lower P:B ratio;
- The difference for the PBk32 when over black or over white is larger than for the PBr29;
- PBk32 will give higher TSR if the coating is over white;
- PBr29 will give higher TSR if over an absorbing substrate.
- PBr29 products have higher durability and for buildings application gives performance and economic advantages.

With regards to the IR-optimized TiO_2, this technology focuses the attention on white pigments contrarily to the previous ones. In particular the optimization concerns the choice of variants of pigments with a larger particle size in order to obtain a greater scattering ability in the longer-wavelength n-IR region. The IR-optimized TiO_2 has a much flatter reflectance curve and less scattering in the visible region and higher reflectance in the IR range with respect to the standard TiO_2.

PBk32 and IR-optimized TiO_2 can be used to produce optimized TSR performance sacrificing performance in case of different weathers and cost restrictions respectively. The best solution for an application depends on TSR, color, cost and durability requirements which warrant the best performance.

The employment of solar reflective glasses is able to reduce the solar load by almost the 50%, especially if combined with other technologies; in particular in this project only IR-glasses and IR-paints for the vehicle body have been considered, excluding any consideration on the seats and interior materials coatings [33].

5.1 Introduction of retrofits: Thermal insulation, IR-glasses and IR-paint

With respect to the first technology in this project work the application of thermal insulation will involve roof and side panels, neglecting the contribute related to the trunk which is instead considered as a null contribute in terms of heat source. The car cabin model has been modified introducing another mass ($m_{insulation} = 0.2\ kg$) and another conductive heat exchanger. In particular, the sketch has therefore been modified as shown below (it possible to compare it with the *Figure 50 and Figure 51*):

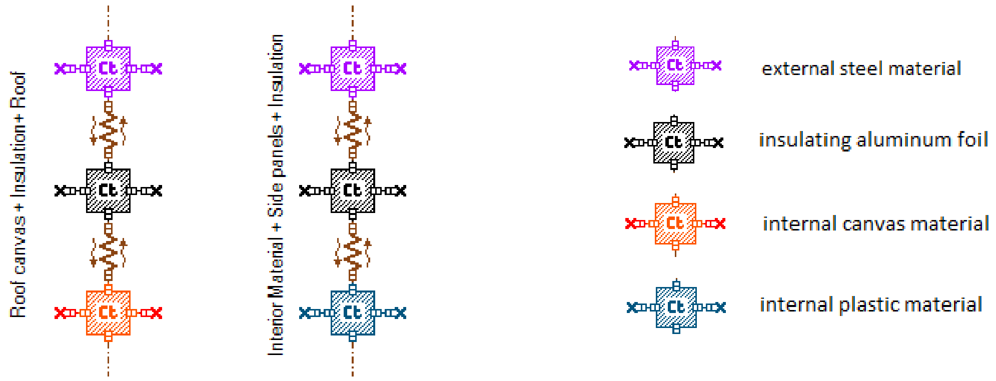

Figure 89. Introduction of the thermal insulation modelled in Amesim.

With regards to the substitution of the standard glasses with IR-reflective ones, according to the data published by IPS innovation, this application may be able to reduce the transmittance until 33%. Nevertheless, trying to perform a conservatory analysis, the choice taken has modified the solar irradiance coefficients as reported below, reducing the transmittance from 90% to 40% [30]:

Title	Value	Tags	Unit	Name
solar radiation setting mode	**using ambient conditions**			soldef
ambient conditions index	1			ambcondindex
exchange area	**S_windshield**		m**2	area
transmission factor	**0.9**		null	transcoeff
absorption factor	**0.09**		null	abscoeff
equivalent emission factor gas/surface	0.95		null	epsilon
filename or expression for surface inclination angle with respect to horizontal[degree] = f(t[s])	**39.4**			filebeta
filename or expression for surface angle with respect to the North[degree] = f(t[s])	0			filezeta

typical glasses:

$$\tau = 0.9; \ \ \alpha = 0.09; \ \rho \ = 0.01$$

Title	Value	Tags	Unit	Name
solar radiation setting mode	**using ambient conditions**			soldef
ambient conditions index	1			ambcondindex
exchange area	**S_windshield**		m**2	area
transmission factor	**0.4**		null	transcoeff
absorption factor	**0.05**		null	abscoeff
equivalent emission factor gas/surface	0.95		null	epsilon
filename or expression for surface inclination angle with respect to horizontal[degree] = f(t[s])	**39.4**			filebeta
filename or expression for surface angle with respect to the North[degree] = f(t[s])	0			filezeta

IR – glasses:

$$\tau = 0.4; \ \ \alpha = 0.05; \ \rho \ = 0.55$$

A method of reducing the heat build-up of a plastic automotive part concerns to provide an infrared reflective pigment and a suitable plastic composition to incorporate the IR-pigment into the plastic composition at a concentration lower than 5 weight percent. In particular a coherent unpainted plastic composition for automotive application includes an infrared reflective pigment and a thermoplastic component in order to cause an increased reflectance of about 300% in the visible and IR wavelength region [34].

The color absorption coefficient of external vehicle body has been modified as below:

Color absorption coefficient	
Standard paints	*IR-reflective paints*
0.9	0.6

Table 21. Colour absorption coefficient variation according to retrofits.

5.2 Car cabin soaking

The first step for the evaluation of the consumption reduction concerns the assessment of the car cabin behavior during the soaking. In particular two sketches have been edited, characterizing them simulating the condition with totally wind absence, higher solar irradiation and any passenger occupying the cabin.

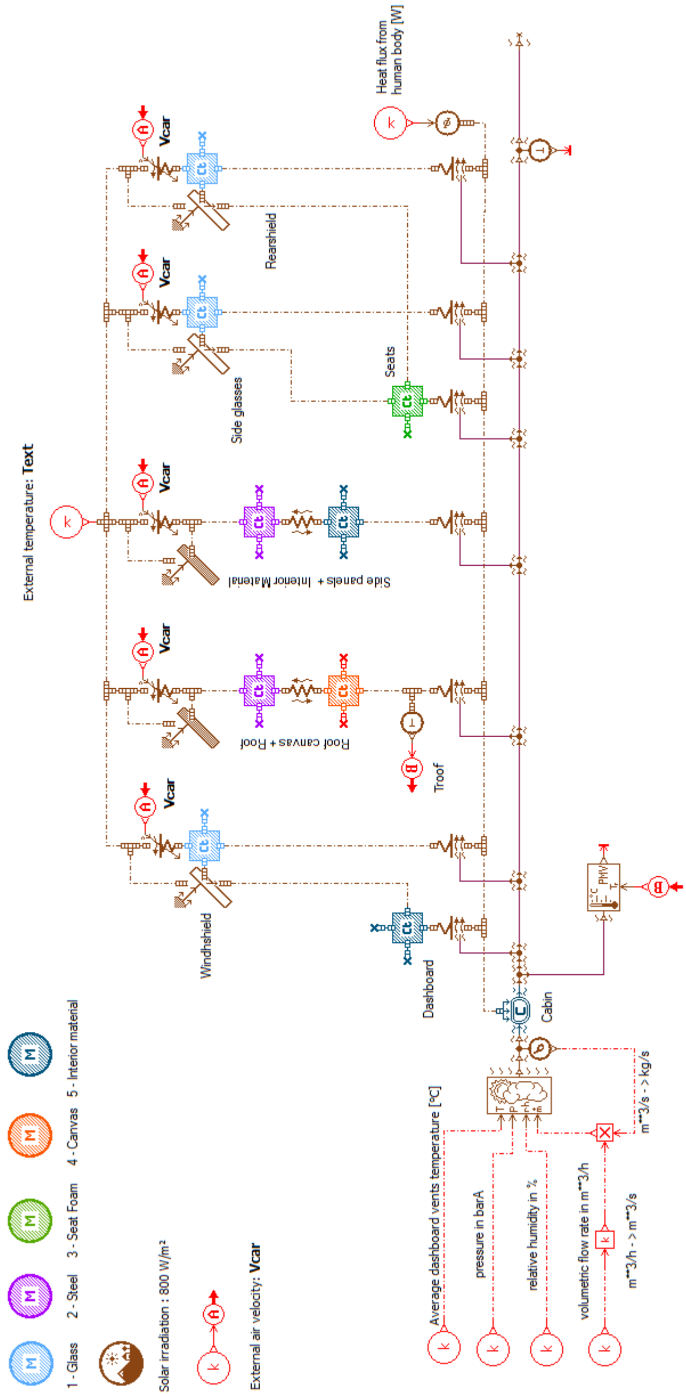

Figure 90. Standard car cabin model for the soaking simulation.

In the following figure the global parameters overview for the standard car cabin is reported:

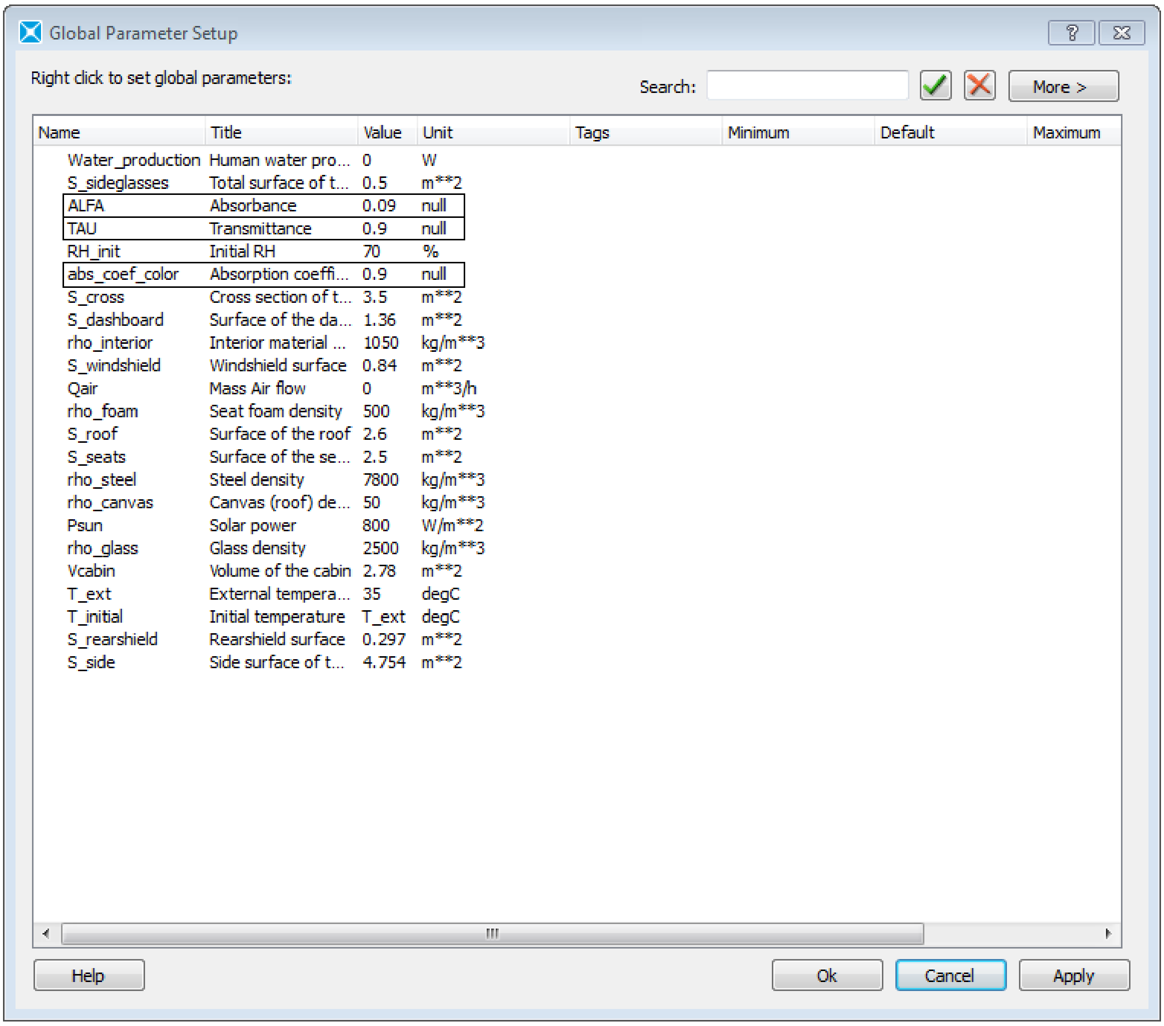

Figure 91. Standard car cabin global parameters.

where *Alfa* corresponds to the absorbance, *Tau* to the transmittance and *abs_coeff_color* to the absorption coefficient of the body painting.

The second model realized is instead provided by the thermal insulation layer in the roof and side panels and IR reflective paints for the vehicle body, varying then the values of *Alfa*, *Tau* and *abs_coeff_color* and introducing the mass representing the aluminum insulation foil. The figure of the sketch of the improved cabin is reported in the following page.

The soaking simulations have been performed for a time-step of 3600 seconds (one hour), considering the vehicle subjected to the maximum solar irradiation in the hottest day in wind absence.

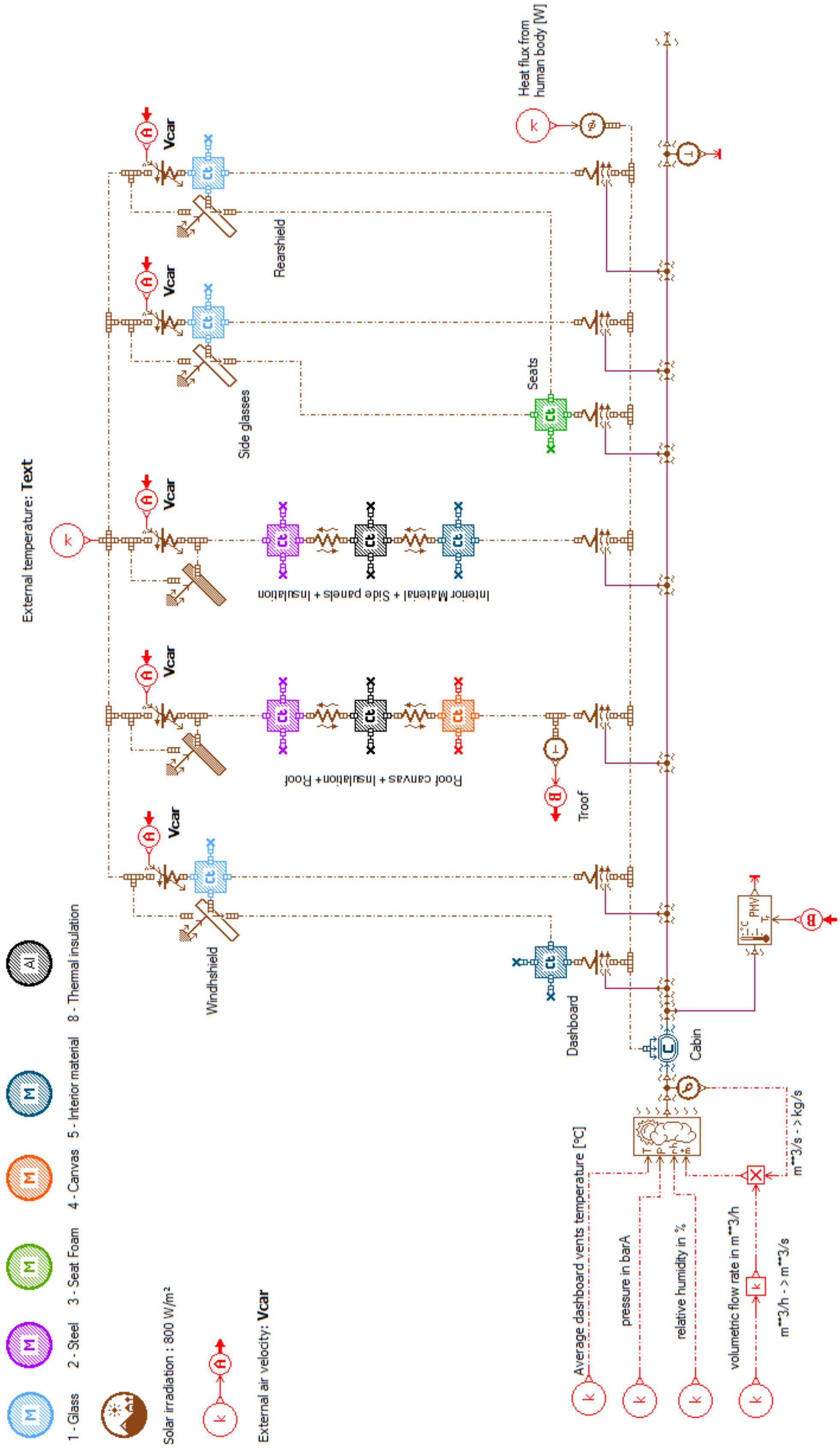

Figure 92. Improved car cabin for soaking simulation.

Similarly to the previous model, the global parameters overview is reported also for the improved one, highlighting the coefficients variation:

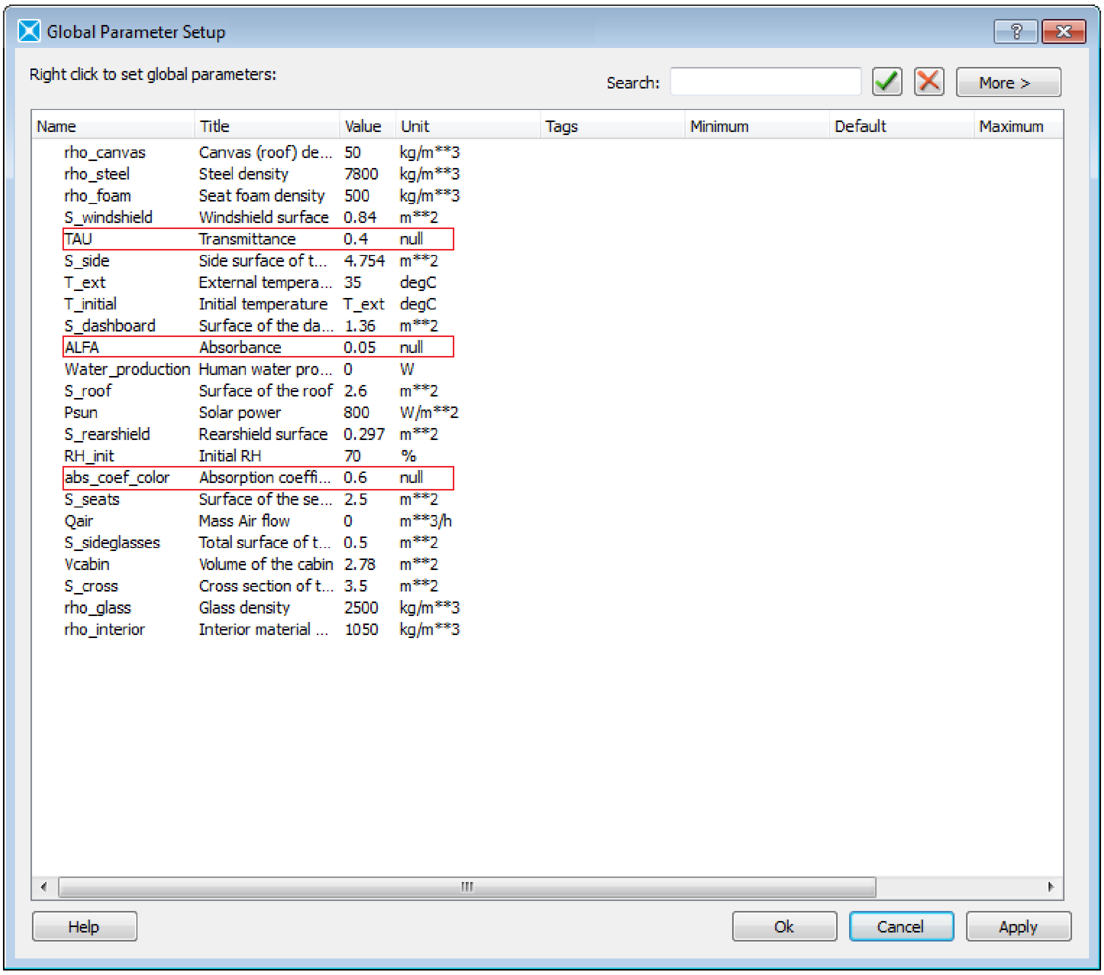

Figure 93. Improved car cabin global parameters.

The results of the improvements introduced in the car cabin are shown in the figure below:

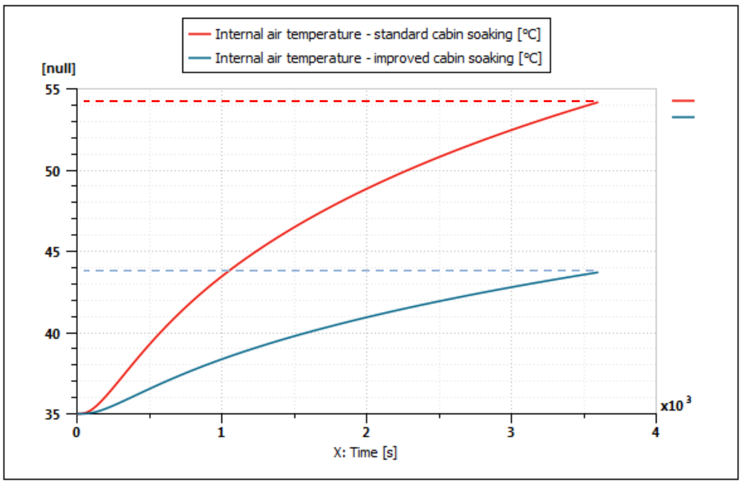

Figure 94. End-soak temperature comparison for standard and improved applications.

In particular the end-soaking temperatures obtained with the soaking simulations have been approximated to values reported in the following table and then employed for the cooldown cycle simulations:

End-soaking temperature	
Standard car cabin	Improved car cabin
54 °C	44 °C

Table 22. End-soaking temperatures obtained by the soaking simulations.

The results are coherent with respect to the PGG Industries studies which have estimate an air temperature decrease of around 12 °C [31].

5.3 Cooldown cycles

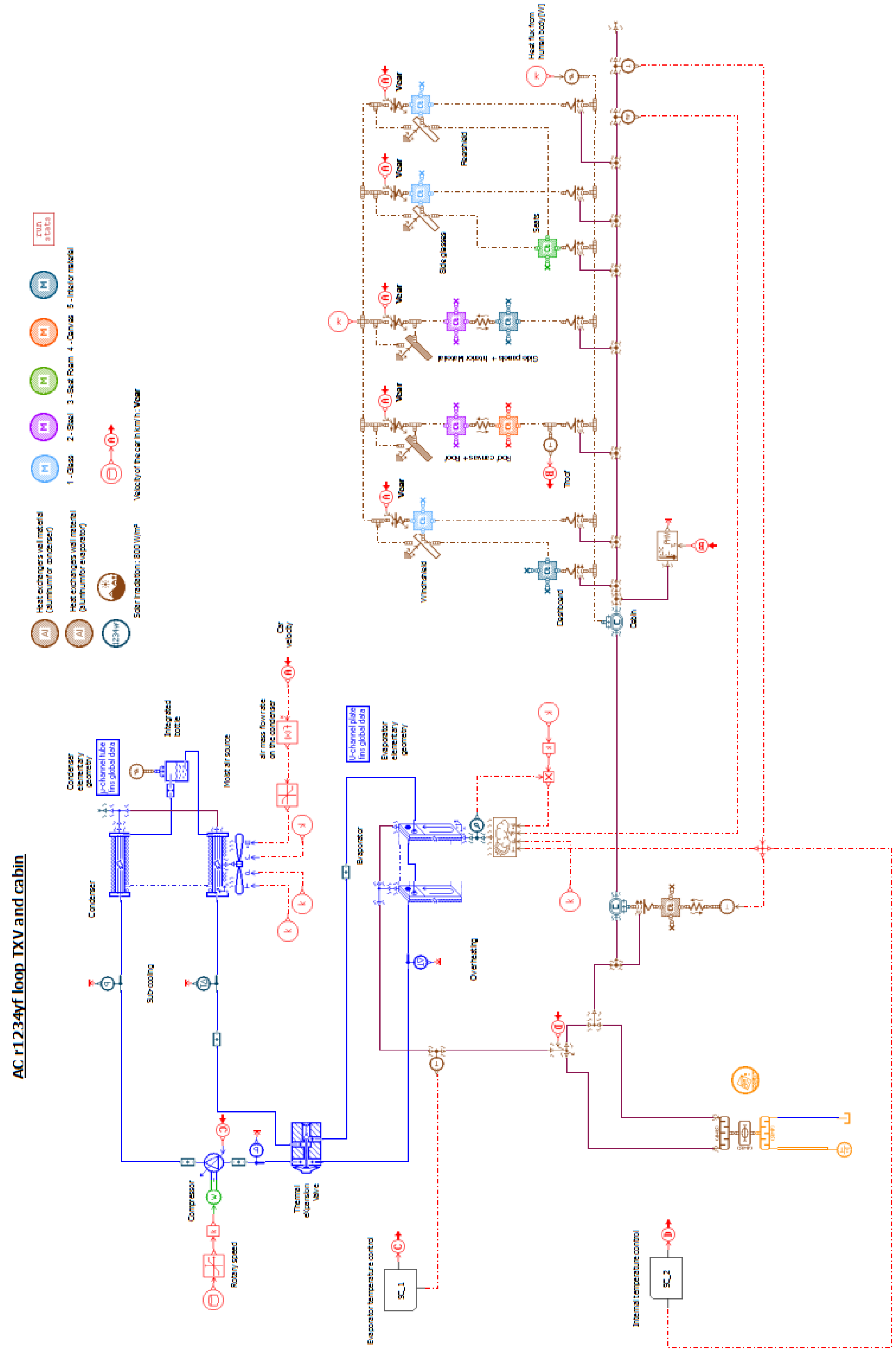

Figure 95. Standard sketch model for the actual operation of an AC system.

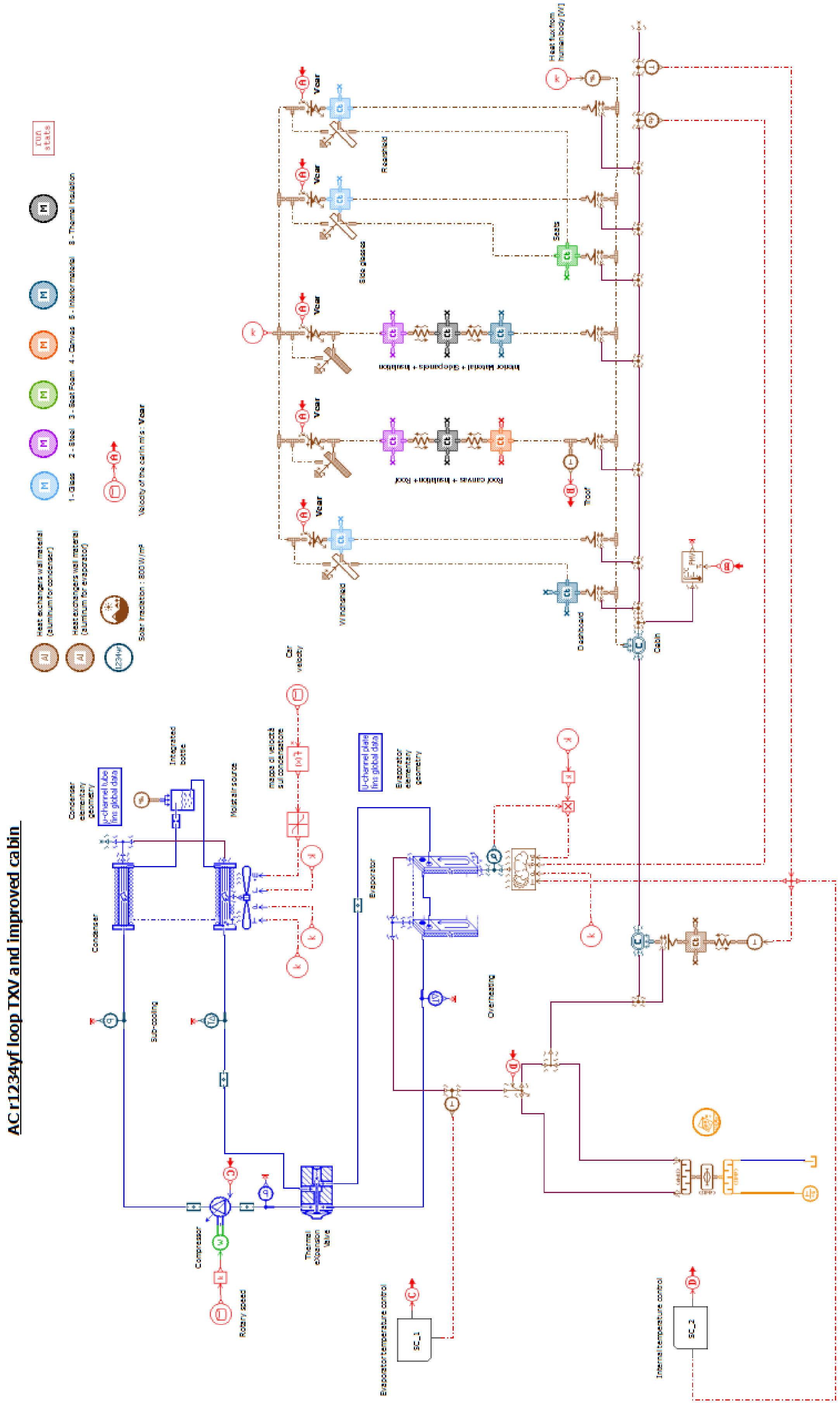

Figure 96. Modified sketch model for the actual operation of an AC system.

The models shown above have been enhanced with respect to the validations' cases thanks to the introduction of two sub-models which make the simulation more near to the actual air conditioning system operation and to the evolution of the air temperature during its cycle. The former represents a heater fed by the engine cooling system water which is aimed to post-heat the air mass flow rate coming from the evaporator; the latter is the ducts' sub-model which represents the mass of tubes which lead the air towards the cabin vents. Ducts modeled here can already be considered as part of the cabin model because they are located under the dashboard after the evaporator and then they are surrounded by air with a temperature near to the internal cabin air temperature. The mass flow rate flowing into the ducts is therefore heated because of this heat coming from to the external air.

In the following figure the heater modelling is drawn, listing the main components and describing the car cabin temperature regulation performed by a second control system:

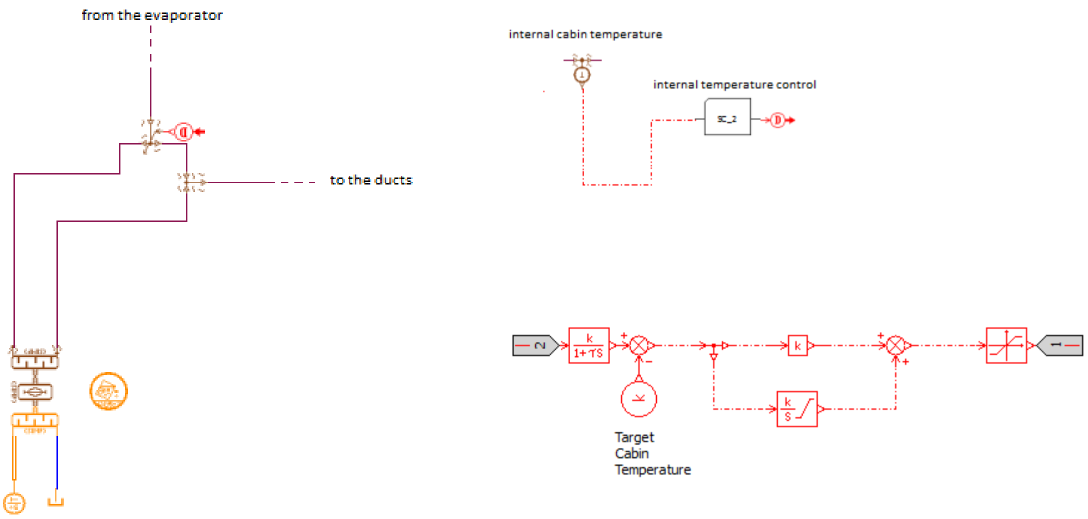

Figure 97. Heater and car cabin temperature control system.

In particular the heater is largely used for the post-heating of the air mass flow rate coming from the dehumidification occurring in the evaporator but it can also be exploited for the regulation of the cabin temperature. In fact, according to a signal communicating the air temperature into the cabin to the control system, the regulation occurs varying the slope of a deflector (modeled in Amesim with a flow splitter). This slope variation splits the air flowing in the central duct in two contributes: the former passes through a heat exchanger and it is heated by the engine cooling water system, the latter by-passes the deflection and then it mixes again with the other flow reaching a moderate temperature before of being introduced in the cabin by vents. Similarly to the compressor control system, also the car cabin temperature control system has been modeled using only a PI (Proportional Integrative) regulation and saturating the outcome signal in the interval [0, 100]. The set temperature imposed for the regulation is equal to the comfort temperature adopted in automotive applications for the average cabin temperature: $T_{set} = 23\,°C$.

In particular the components have been realized as shown below:

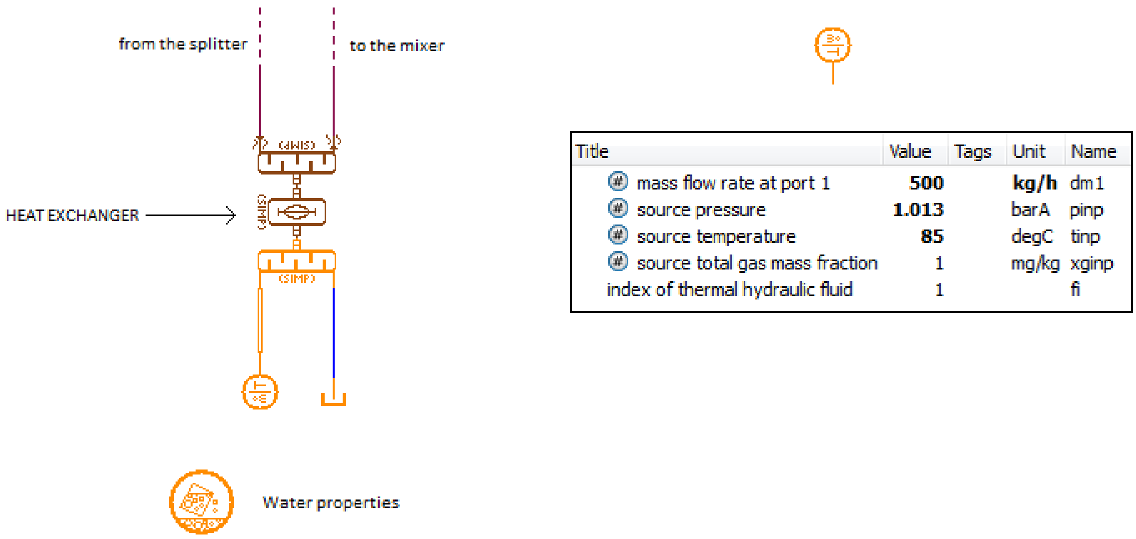

Title	Value	Tags	Unit	Name
mass flow rate at port 1	**500**		**kg/h**	dm1
source pressure	**1.013**		barA	pinp
source temperature	**85**		degC	tinp
source total gas mass fraction	1		mg/kg	xginp
index of thermal hydraulic fluid	1			fi

Figure 98. Heater modelling in Amesim.

With respect to the ducts, they have been modeled in Amesim as shown below:

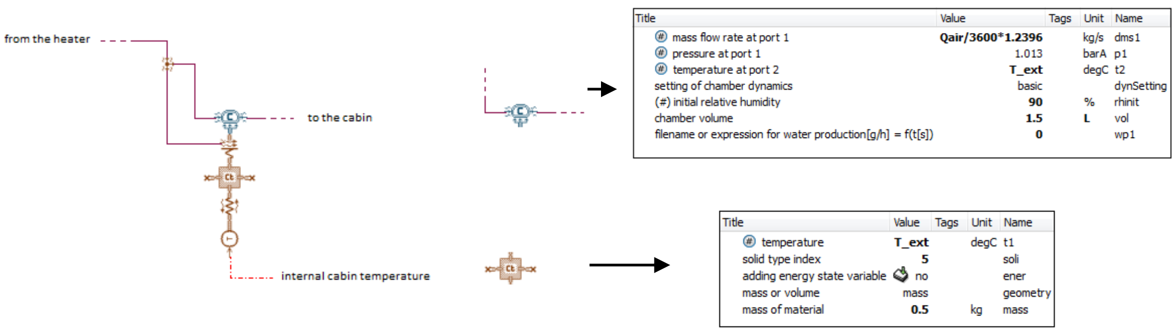

Title	Value	Tags	Unit	Name
mass flow rate at port 1	**Qair/3600*1.2396**		kg/s	dms1
pressure at port 1	1.013		barA	p1
temperature at port 2	**T_ext**		degC	t2
setting of chamber dynamics	basic			dynSetting
(#) initial relative humidity	**90**		%	rhinit
chamber volume	**1.5**		**L**	vol
filename or expression for water production[g/h] = f(t[s])	**0**			wp1

Title	Value	Tags	Unit	Name
temperature	**T_ext**		degC	t1
solid type index	**5**			soli
adding energy state variable	no			ener
mass or volume	mass			geometry
mass of material	**0.5**		kg	mass

Figure 99. Ducts modelling in Amesim.

In particular the blue component represents the ducts' volume crossed by the air flow rate, the brown mass represents the ducts' surfaces thickness: the external side can be

assumed at internal cabin conditions, the internal side is crossed by the air mass flow rate coming from the evaporator which is therefore heated by the external air conditions.
The operation of the air conditioning system has been modeled considering the blower as always working at the maximum power and then the air mass flow rate carried is always the maximum.

5.3.1 Introduction to the driving cycles employed

The driving cycles employed for the evaluation of the energy consumption reduction related to the air conditioning system have already been mentioned in previous paragraph. Nevertheless, it is mandatory to describe them making considerations on the environment conditions which the vehicle is subjected to.

New European Driving Cycle

The New European Driving Cycle (NEDC) is the driving cycle employed in the European Union to assess consumption and emissions of light passenger vehicles. It is realized repeating four ECE-15 urban driving cycles (UDC) and one Extra-Urban Driving cycle (EUDC). In particular the car velocity and the engine rotary speed of the considered vehicle are reported in the figures below:

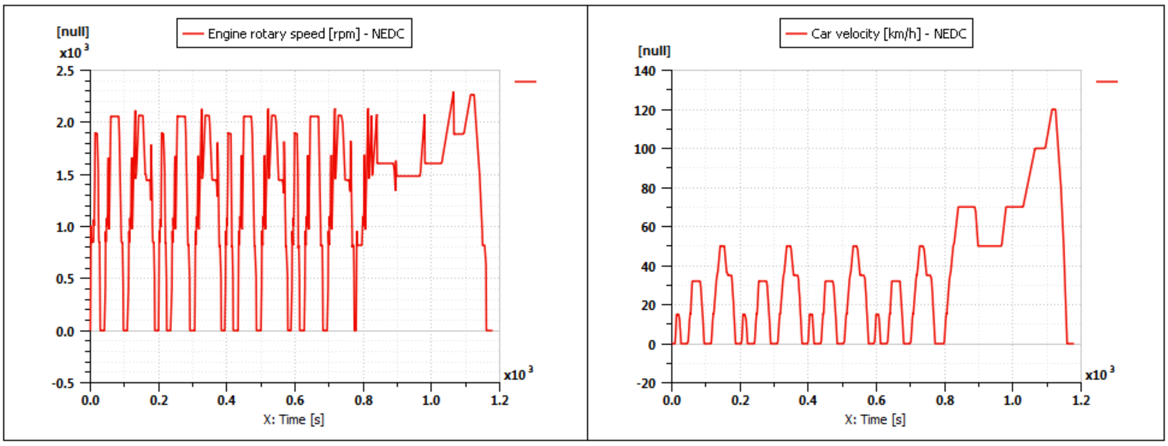

Figure 100. NEDC characteristics.

The environmental conditions are listed in the table below:

Environment conditions		
Solar irradiation	[W]	800
Temperature	[°C]	35
Relative humidity	[%]	70

Table 23. Environment conditions - NEDC.

The New European Driving Cycle is the most employed for the characterization of consumption and emissions of vehicles but it does not provide the impact assessment of the use of the accessory systems such as the air conditioning system. One of the goal of this work is the hence the estimation of the actual consumption of a vehicle in order to compare it with a better application realized with retrofits aimed to save energy.
In particular during the NEDC there are time steps in which the vehicle is switched off and then the engine rotary speed decreases under the minimum. Since the application considered in this project work concerns the evaluation of a cooldown cycle until the comfort temperature is reached, the NEDC data input has been modified to obtain a trend which warrants the air conditioning system operation:

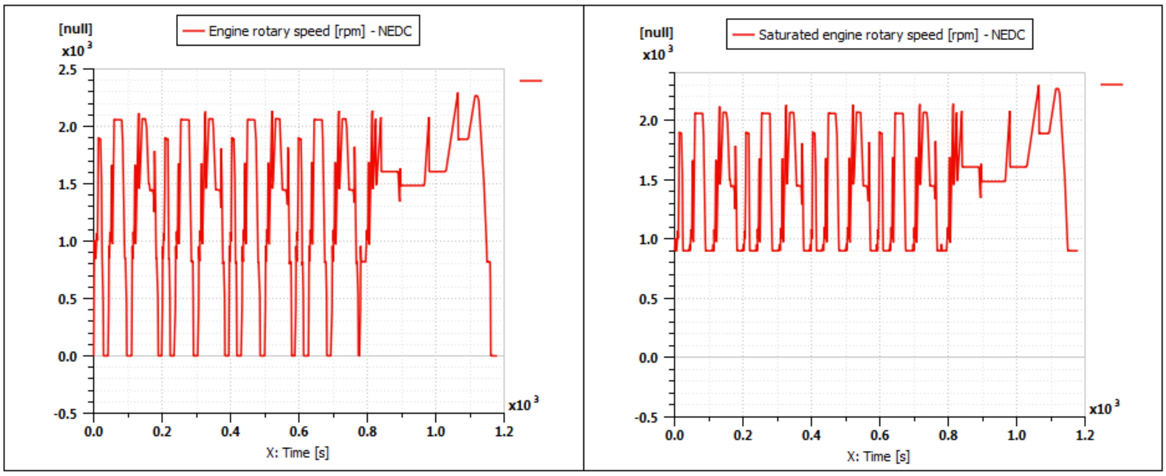

Figure 101. Saturation of the rotary speed trend in the NEDC.

Following the same analytical correlation employed in the cooldown test validation, the air velocity on the condenser has been evaluated and reported in the following figure with the external air velocity:

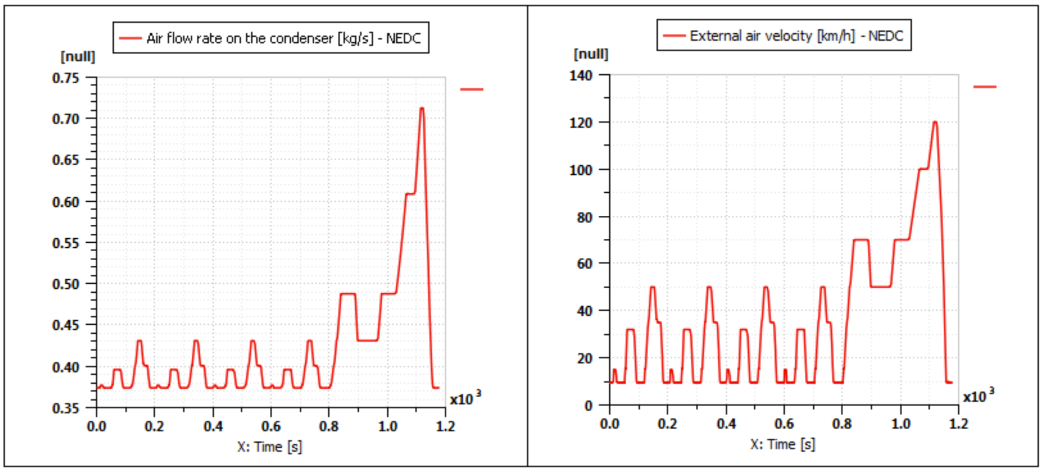

Figure 102. Air mass flow rate on the condenser and environment air velocity - NEDC.

Worldwide harmonized Light vehicles Test Procedure

The Worldwide harmonized Light vehicle Test Procedure (WLTP) was introduced after having noticed the low compatibility with the reality of the NEDC; in fact the NEDC is provided by cycles with very low accelerations and then very far from real drive mission.

This test procedure provides now a better combination between road load, total car weight, fuel quality and environment. The WLTP is constituted by three different WLT cycles realized according to the power-weight ratio of the vehicle; the WLTC adopted for this project work is the WLTC Class 3 employed for vehicle with power-weight ratio equal to $40 \div 100\ \left[\frac{kW}{tonn}\right]$ [35].

In particular in the following figure the engine rotary speed and the car velocity are reported:

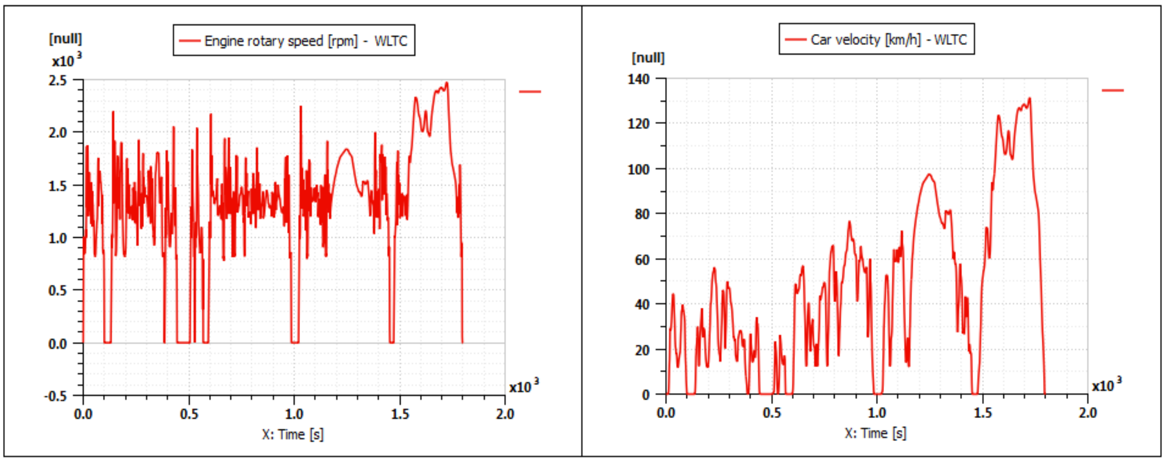

Figure 103. WLTC characteristics.

The environment conditions are equal to the conditions employed for the cooldown test based on the NEDC test listed in *Table 23. Environment conditions – NEDC*. Furthermore, the considerations on the engine rotary speed of the NEDC have been repeated also in the WLTC, saturating the rotary speed with a lower threshold equal to the minimum:

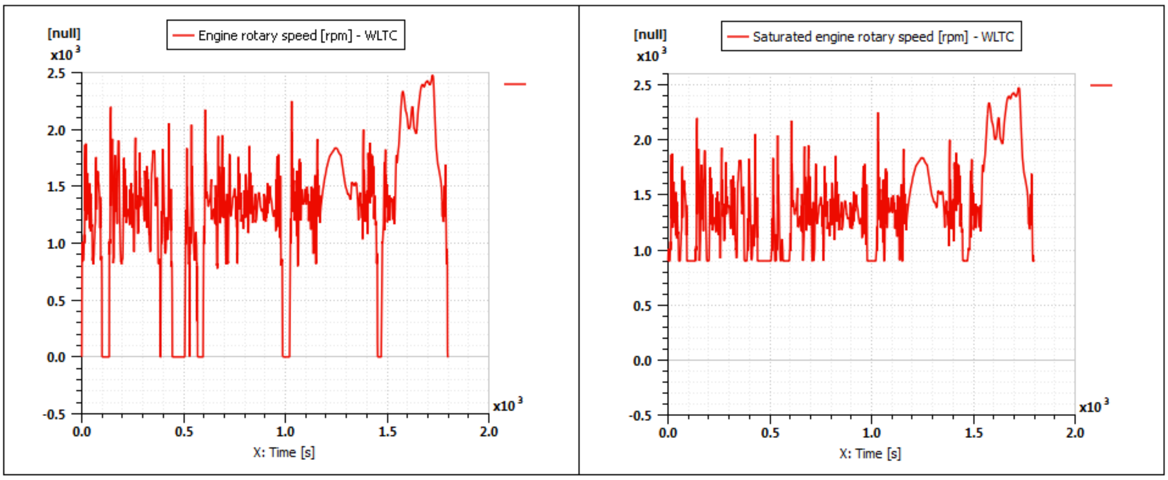

Figure 104. Saturation of the rotary speed trend in the WLTC.

Furthermore, the air velocity on the condenser and the external air velocity trends are shown below:

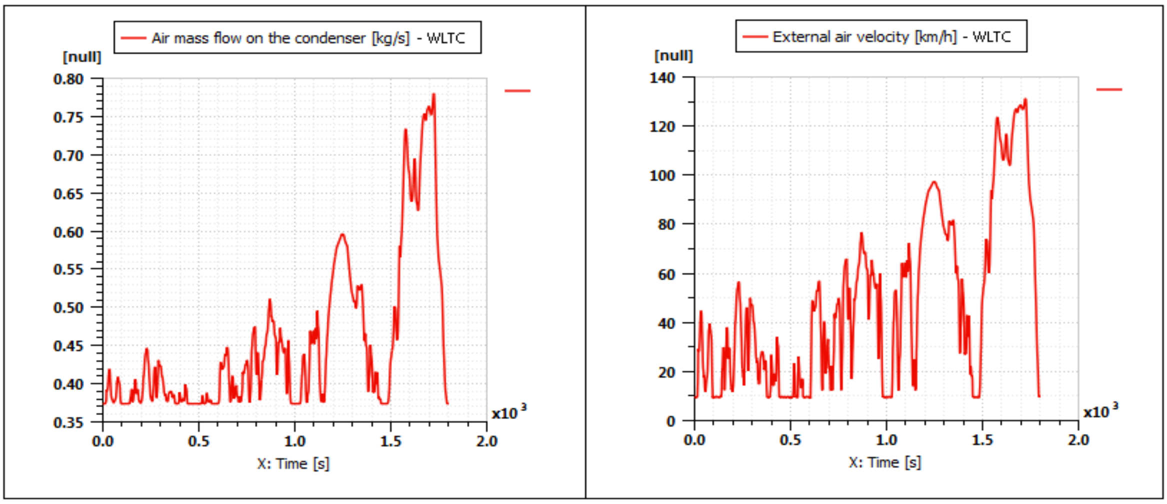

Figure 105. Air mass flow rate on the condenser and environment air velocity - WLTC.

Supplemental Federal Test Procedure – SC03

The Supplemental Federal Test Procedure (SFTP) is an U.S. group of driving cycles introduced by the U.S. Environmental Protection Agency (U.S. EPA) in 2007 in addiction to EPA Federal Test Procedure FPT-75, a test procedure adopted for light vehicles, light trucks and heavy-duty vehicles. The SFTP - SC03 has been introduced to evaluate the engine consumption and related emission considering the operation of the air conditioning system. The cycle has duration of 600 seconds and it is characterized by the following engine rotary speed and car velocity:

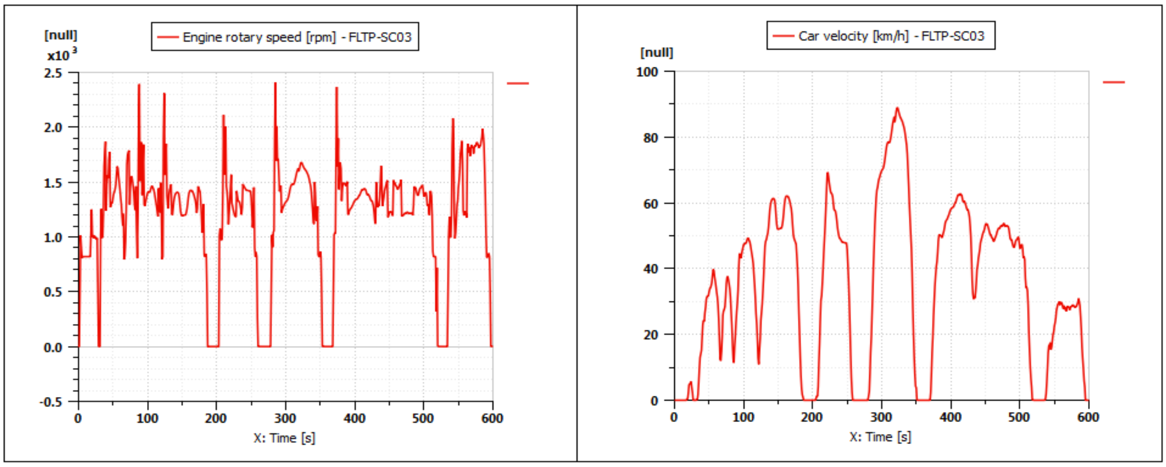

Figure 106. SFTP – SC03 characteristics.

The external conditions are different compared to the conditions related to NEDC and WLTP and they are listed below:

Environment conditions		
Solar irradiation	[W]	850
Temperature	[°C]	35
Relative humidity	[%]	40

Table 24. Environment conditions – SFTP-SC03.

With regards to the saturation of the engine rotary speed, air velocity on the condenser and external air velocity the considerations are equal to the other considered cycles. In particular the figures shown below include all the significant trends.

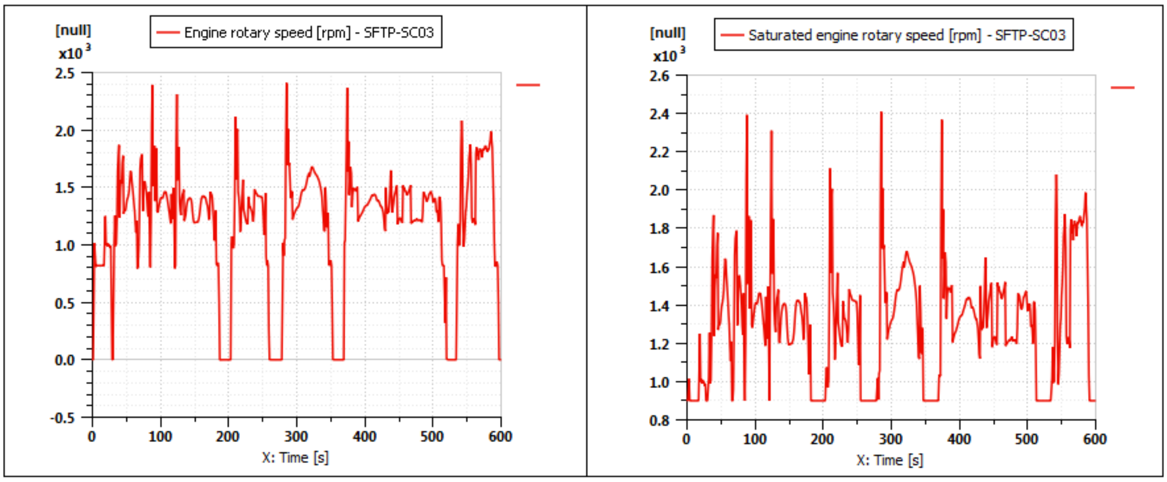

Figure 107. Saturation of the rotary speed trend in the SFTP-SC03.

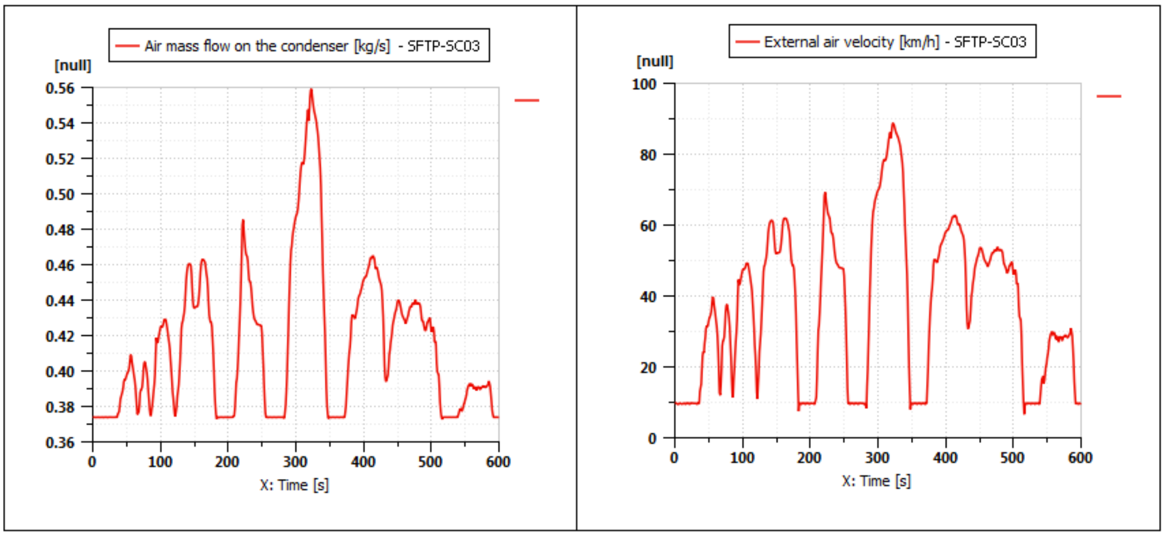

Figure 108. Air mass flow rate on the condenser and environmental air velocity – SFTP-SC03.

5.4 Assessment of thermal results

According to the data input to the model, results are significant: first of all, retrofits have reduced the end-soak temperature allowing the air conditioning system to reach the comfort temperature in a lower time-step. Consequently, the power requested by the air conditioning system is lower thanks to both the end-soaking temperature and the greater thermal capacity of the cabin.

5.4.1 New European Driving Cycle - NEDC

The NEDC has duration equal to 1180 seconds and comparing the internal air temperature in the standard and improved cases, results are already significant as shown below:

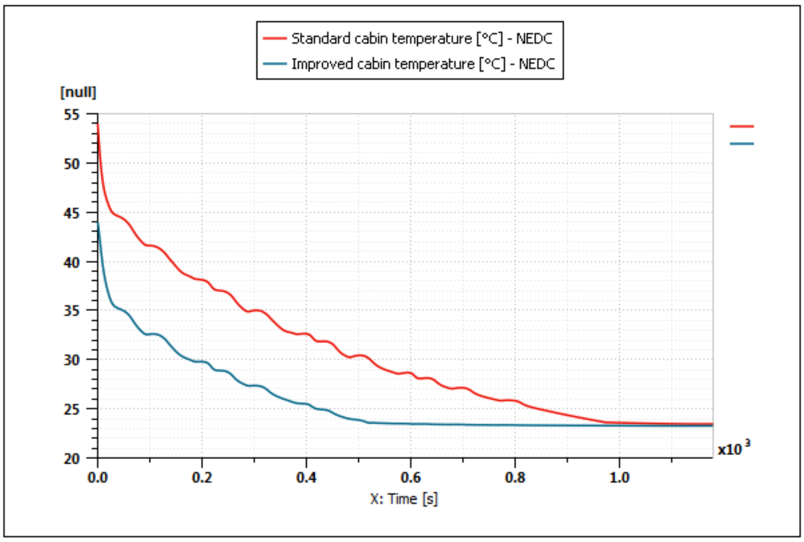

Figure 109. Simulated car cabin temperature in standard and improved applications - NEDC.

Thanks to the lower end-soak temperature and the presence of retrofits in the car cabin, the temperature trends are different and in the improved application the set average cabin temperature is reached before than the standard one. In particular:

Set temperature reaching time	
Standard cabin	Improved cabin
975 seconds	520 seconds

Table 25. Set temperature reaching time – NEDC.

The car cabin achieves hence the requested temperature after 975 seconds in the standard application and in 520 seconds in the improved application, reaching the requested conditions with a Δt = 455 seconds. The simulations show therefore how improvements introduced in the cabin allow to reach the set conditions in a lower time. The cabin temperature trends warrant therefore a different operation by the compressor; in fact, the displacement variation due to the control system is different and then the torque trend requested is also different.

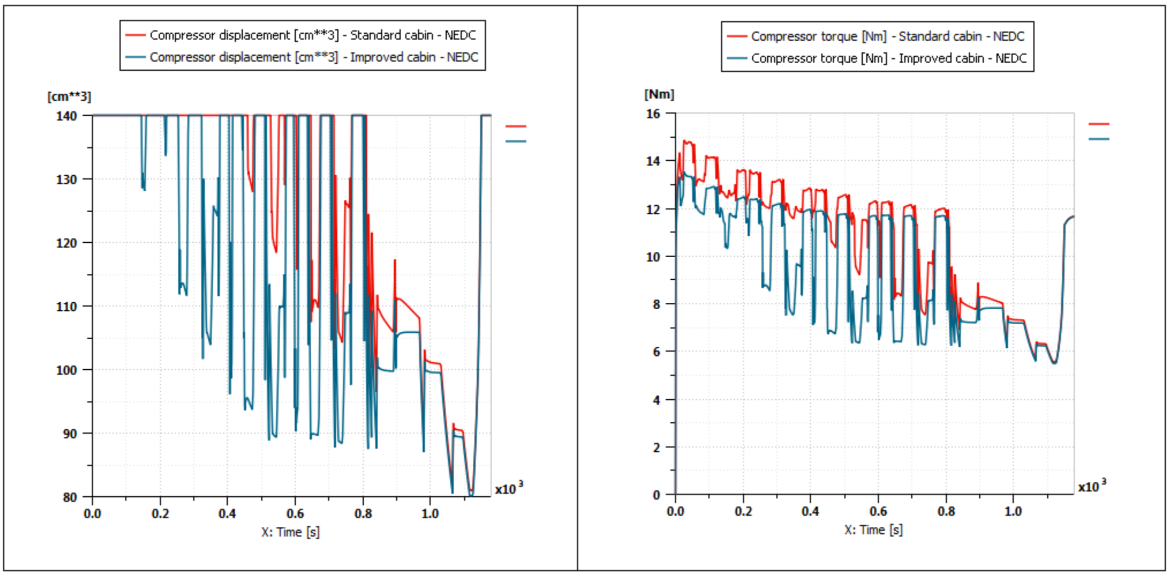

Figure 110. Compressor displacement and torque in standard and improved applications - NEDC.

5.4.2 Worldwide harmonized Light vehicles Test Procedure - WLTC

The new world driving cycle has been introduced to try to make the cycle more coherent with a typical driving mission. For this reason the duration has been increased to 1800 seconds and the velocity and engine rotary speed trends have been modified enhancing them with stronger accelerations. The results concerning the cabin air temperature are reported below:

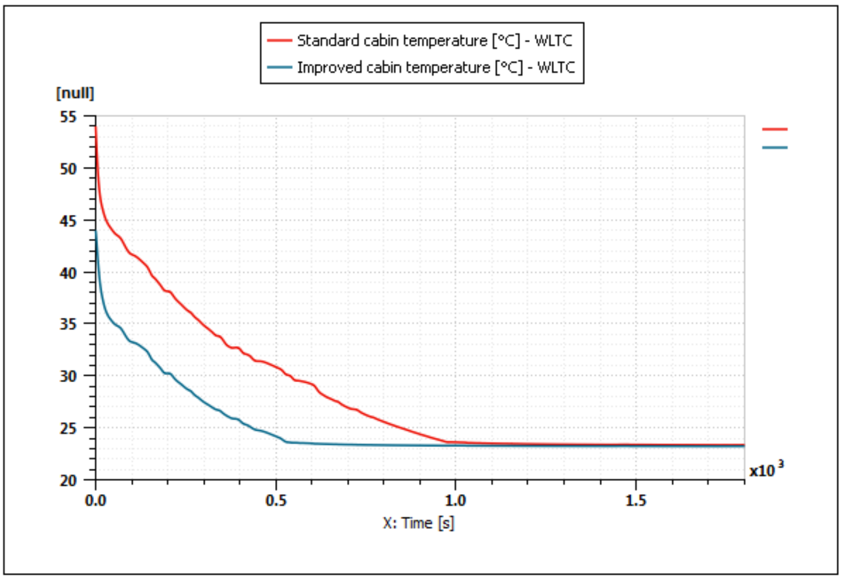

Figure 111. Simulated car cabin temperature in standard and improved applications - WLTC.

Thanks to the improvements introduced the results on the air conditioning system are significant also in the worldwide driving cycle, reaching the set temperature in 570 seconds instead of 980 seconds.

Comfort temperature reaching time	
Standard cabin	Improved cabin
980 seconds	570 seconds

Table 26. Set temperature reaching time – WLTC.

The reaching of the requested conditions occurs with a Δt = 410 seconds.

The gains can also be noticed in the displacement variation and torque of the compressor, as shown below:

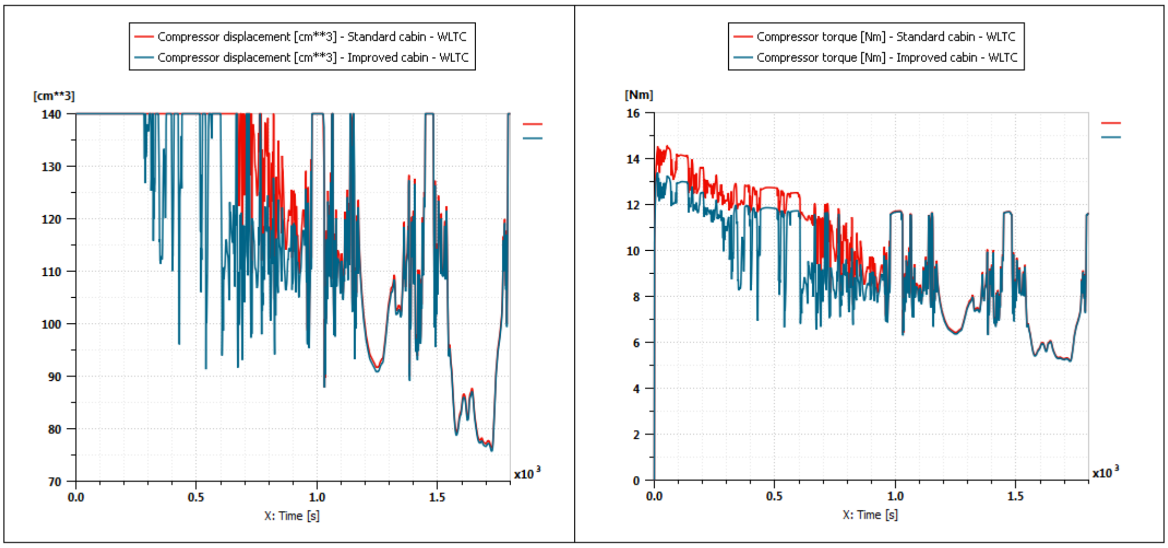

Figure 112. Compressor displacement and torque in standard and improved applications - WLTC.

5.4.3 Supplement Federal Test Procedure SFTP-SC03

The U.S. test procedure for the evaluation of consumption and emission is realized with the air conditioning system switched on. The duration is of 600 seconds and it is possible that the thermal comfort is not reached. The results of retrofits are shown below:

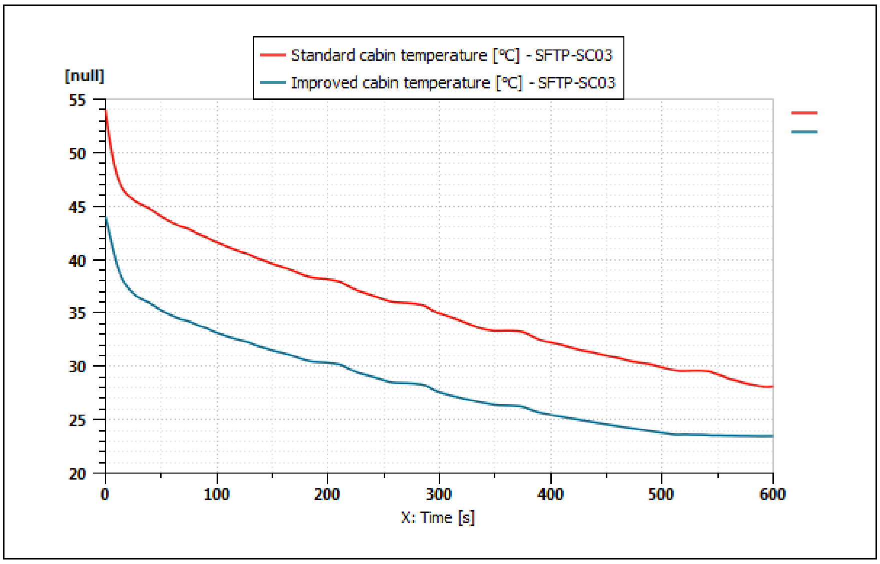

Figure 113. Simulated car cabin temperature in standard and improved applications – SFTP-SC03.

In this case, since the duration of the test is lower than the other test driving cycles, it is not possible to highlight the comfort cabin temperature reaching time for the standard cabin application. The improved cabin instead is able to reach the comfort temperature during the test duration:

Comfort temperature reaching time	
Standard cabin	Improved cabin
-	510 seconds

Table 27. Set temperature reaching time – SFTP-SC03.

In this case the evaluation of a Δt about the reaching of the requested conditions is not possible because of the short duration of the test driving cycle. Nevertheless, it is possible to notice how in the improved cabin application the set temperature is reached within the end of the test; otherwise in the standard cabin application the requested conditions achievement does not occur during the cycle duration.

The air conditioning system reacts reducing its energy consumption; in fact, the improvements of the displacement variation and requested torque warrant a lower power absorbed by the compressor:

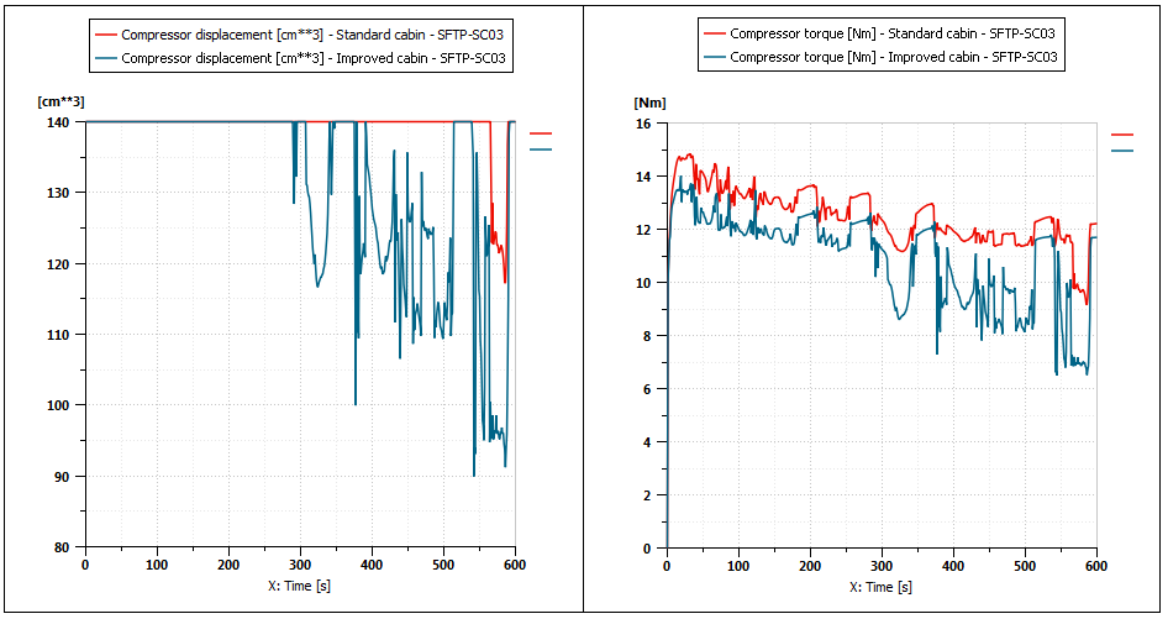

Figure 114. Compressor displacement and torque in standard and improved applications – SFTP-SC03.

5.5 Fuel consumption and CO_2 emission

According to the torque profiles obtained by the simulations of cooldown missions during NEDC, WLTC and SC03 in both standard and improved applications, it has been employed an FCA Italy internal tool to estimate the fuel consumption and the CO_2 emission. Basically, the analysis has been focused on the vehicle consumption in case of AC system switched off, in order to evaluate the consumption difference with respect to the case with AC system switched on. An important clarification is mandatory: since the driving cycles have been suitably modified to obtain a continuous cooldown mission, vehicle consumption and emission with AC system switched off are higher than data reported in *Table 28. Performance of the engine Multi-jet 2.0 l [23]*. Nevertheless, this modification does not influence the solidity of results because the difference with respect to the real homologation driving cycles is a communal aspect and for the application with AC system switched off and for the applications with AC system switched on.

In the following pages all results are shown, reporting fuel consumption and CO_2 emission trend. Furthermore, an analysis of the difference between standard and improved cabin applications is edited. For privacy reason, only quantitative results will be reported omitting profiles which could be linked to the vehicle application chosen for the present document.

5.5.1 NEDC results

Data will be reported listing at first results concerning the AC OFF application and then standard and improved cabin application:

Air conditioning system: OFF		
Properties	**Unit**	
Distance travelled	*[km]*	11.01
Fuel consumption [mass]	*[g/km]*	51.89
Fuel consumption [volume]	*[l/100km]*	6.2
CO_2 emission	*[g/km]*	163.7

Table 28. Fuel consumption and CO2 emission with AC OFF - NEDC

Air conditioning system: ON Standard cabin application		
Properties	**Unit**	
Distance travelled	*[km]*	11.01
Fuel consumption [mass]	*[g/km]*	59.39
Fuel consumption [volume]	*[l/100km]*	7.09
CO_2 emission	*[g/km]*	187.3

Table 29. Fuel consumption and CO_2 emission with AC ON in standard cabin application - NEDC

Air conditioning system: ON Improved cabin application		
Properties	**Unit**	
Distance travelled	*[km]*	11.01
Fuel consumption [mass]	*[g/km]*	58.41
Fuel consumption [volume]	*[l/100km]*	6.98
CO_2 emission	*[g/km]*	184.2

Table 30. Fuel consumption and CO_2 emission with AC ON in improved cabin application - NEDC

In particular, the fuel saved passing from standard to improved application is estimated below, combined with the CO_2 emission reduction:

$$FC_{standard,TOT} = 11.01 * 59.39 = 653.884\ g$$

$$FC_{improved,TOT} = 11.01 * 58.41 = 643.094\ g$$

$$\Delta FC = -0.11 \left[\frac{l}{100\ km}\right] \qquad \Delta FC_{TOT} = -11\ [g]$$

$$\Delta CO_2 = 184.2 - 187.3 = -3.1\ \left[\frac{g}{km}\right]$$

Furthermore, assessing consumption and emission for the same standard cabin application with and without the AC system switched on, simulations show the impact of the auxiliary system on the vehicle consumption:

$$FC_{standard,AC\ OFF} = 11.01 * 51.89 = 571.309\ g$$

$$FC_{standard,AC\ ON} = 11.01 * 59.39 = 653.884\ g$$

$$\Delta FC = +0.89 \left[\frac{l}{100\ km}\right] \qquad \Delta FC_{TOT} = +82.27\ [g]$$

$$\Delta CO_2 = 187.3 - 163.7 = +23.6\ \left[\frac{g}{km}\right]$$

Considering an average distance travelled in one year by a vehicle (around 11000 km) and supposing around 90 days of A/C system operation (20 June – 10 September), a linear correlation between days and kilometres can permit to assess an approximate impact of retrofits on the A/C system consumption:

$$km_{summer} = 11200 * \frac{365}{90} = \sim 2700\ km$$

Assessment with respect to one year - NEDC		
Comparison		
A/C On – A/C Off	*Fuel consumption reduction [l]*	24
	CO_2 emission reduction [kg]	63,7
Standard cabin – Improved cabin – A/C On	*Fuel consumption reduction [l]*	2,97
	CO_2 emission reduction [kg]	8,37

Table 31. Impact of A/C system and technologies with respect to one year - NEDC

5.5.2 WLTC results

At the same time, the results obtained by the simulation on WLTC are reported below:

Air conditioning system: OFF		
Properties	**Unit**	
Distance travelled	*[km]*	23.268
Fuel consumption [mass]	*[g/km]*	50.44
Fuel consumption [volume]	*[l/100km]*	6.02
CO_2 emission	*[g/km]*	159.1

Table 32. Fuel consumption and CO_2 emission with AC OFF - WLTC

Air conditioning system: ON Standard cabin application		
Properties	**Unit**	
Distance travelled	*[km]*	23.268
Fuel consumption [mass]	*[g/km]*	55.32
Fuel consumption [volume]	*[l/100km]*	6.61
CO_2 emission	*[g/km]*	174.5

Table 33. Fuel consumption and CO_2 emission with AC ON in standard cabin application – WLTC

Air conditioning system: ON Improved cabin application		
Properties	**Unit**	
Distance travelled	*[km]*	23.268
Fuel consumption [mass]	*[g/km]*	54.95
Fuel consumption [volume]	*[l/100km]*	6.56
CO_2 emission	*[g/km]*	173.3

Table 34. Fuel consumption and CO_2 emission with AC ON in improved cabin application - WLTC

The estimation of the fuel consumption reduction and the CO2 emission reduction is shown below:

$$FC_{standard,TOT} = 23.268 * 55.32 = 1287.186\ g$$

$$FC_{improved,TOT} = 11.01 * 58.41 = 1278.577\ g$$

$$\Delta FC = -0.05 \left[\frac{l}{100\ km}\right] \qquad \Delta FC_{TOT} = -8.61\ [g]$$

$$\Delta CO_2 = 173.3 - 174.5 = -1.2 \left[\frac{g}{km}\right]$$

Furthermore, in the same way than NEDC, simulations show increasing fuel consumption in the cabin application with the AC system switched on, as shown below:

$$FC_{standard,AC\ OFF} = 23.268 * 50.44 = 1173.638\ g$$

$$FC_{standard,AC\ ON} = 23.268 * 55.32 = 1287.186\ g$$

$$\Delta FC = +0.59 \left[\frac{l}{100\ km}\right] \qquad \Delta FC_{TOT} = +113.548\ [g]$$

$$\Delta CO_2 = 174.5 - 159.1 = +15.4 \left[\frac{g}{km}\right]$$

Similarly to NEDC, the assessment of an approximate impact of retrofits on the A/C system consumption with respect to one year has been produced:

$$km_{summer} = 11200 * \frac{365}{90} = \sim 2700\ km$$

Assessment with respect to one year - WLTC		
Comparison		
A/C On – A/C Off	*Fuel consumption reduction [l]*	15,93
	CO_2 emission reduction [kg]	41,58
Standard cabin – Improved cabin – A/C On	*Fuel consumption reduction [l]*	1,35
	CO_2 emission reduction [kg]	3,24

Table 35. Impact of A/C system and technologies with respect to one year - WLTC

5.5.3 SFTP-SC03 results

Finally, results extrapolated by the simulation on the SFTP-SC03 driving cycle are shown in the following tables:

Air conditioning system: OFF		
Properties	**Unit**	
Distance travelled	*[km]*	5.767
Fuel consumption [mass]	*[g/km]*	48.45
Fuel consumption [volume]	*[l/100km]*	5.79
CO_2 emission	*[g/km]*	152.8

Table 36. Fuel consumption and CO_2 emission with AC OFF - SFTP-SC03

Air conditioning system: ON Standard cabin application		
Properties	**Unit**	
Distance travelled	*[km]*	5.767
Fuel consumption [mass]	*[g/km]*	56.12
Fuel consumption [volume]	*[l/100km]*	6.7
CO_2 emission	*[g/km]*	177

Table 37. Fuel consumption and CO_2 emission with AC ON in standard cabin application - SFTP-SC03

Air conditioning system: ON Improved cabin application		
Properties	**Unit**	
Distance travelled	*[km]*	5.767
Fuel consumption [mass]	*[g/km]*	55.07
Fuel consumption [volume]	*[l/100km]*	6.58
CO_2 emission	*[g/km]*	173.7

Table 38. Fuel consumption and CO_2 emission with AC ON in improved cabin application - SFTP-SC03

At the same time the estimation of the fuel consumption reduction and the CO2 emission reduction for SFTP-SC03 is shown below:

$$FC_{standard,TOT} = 5.767 * 56.12 = 323.644\ g$$

$$FC_{improved,TOT} = 5.767 * 55.07 = 317.589\ g$$

$$\Delta FC = -0.12 \left[\frac{l}{100\ km}\right] \qquad \Delta FC_{TOT} = -6.05\ [g]$$

$$\Delta CO_2 = 173.3 - 174.5 = -3.3\ \left[\frac{g}{km}\right]$$

The difference between standard cabin applications with and without AC system switched on is evaluated below:

$$FC_{standard,AC\ OFF} = 5.767 * 48.45 = 279.41\ g$$

$$FC_{standard,AC\ ON} = 5.767 * 56.12 = 323.644\ g$$

$$\Delta FC = +0.91 \left[\frac{l}{100\ km}\right] \qquad \Delta FC_{TOT} = +44.234\ [g]$$

$$\Delta CO_2 = 177 - 152.8 = +24.2\ \left[\frac{g}{km}\right]$$

Similarly to the other cases, the assessment of an approximate impact of retrofits on the A/C system consumption with respect to one year has been produced:

$$km_{summer} = 11200 * \frac{365}{90} = \sim 2700\ km$$

Assessment with respect to one year – SFTP-SC03		
Comparison		
A/C On – A/C Off	*Fuel consumption reduction [l]*	24,57
	CO_2 emission reduction [kg]	65.3
Standard cabin – Improved cabin – A/C On	*Fuel consumption reduction [l]*	3,24
	CO_2 emission reduction [kg]	8.9

Table 39. Impact of A/C system and technologies with respect to one year - SFTP-SC03

CONCLUSIONS

According to the results obtained with the study described in the present document, it is possible to make some considerations about the evolution of the carmakers companies' overview and about the related worldwide users' reaction.

Although the environmental consequences involve every country, the solutions to the most dangerous phenomena the World is dealing with are not largely considered significant. The demonstration is represented by the switch by U.S.A to the intensive coal exploitation and especially by the failure of the Kyoto Protocol. Nevertheless, the Paris Agreement signed on December 2015 has established strong limits about the uncontrolled fossil fuel utilization, declaring to the World the intention to reduce the greenhouse gases emissions to 40 gigatons, limiting the global warming to 1.5 ÷ 2 °C per year. All sectors are involved: energy production, agriculture, buildings and transportation. The last one is the focus of the project and, although the larger part of companies are switching to EVs, the World (especially the EU) seems not be sufficiently reactive to this change. BEV are for now playing a slight contribute because of problems related to battery operation time, charging duration and battery charging stations (quite sufficiently distributed only in China) while PHEVs are having more success thanks to the exclusion of the problems of BEVs listed above. First among everyone is Hyundai.

Nevertheless, greenhouse gases must be reduced and Paris Agreement has imposed strong fines for every gram of CO_2 for kilometre emitted over the average limit of 95 $\left[\frac{g_{CO_2}}{km}\right]$. Hence, during the transition towards a World travelled by clean energy vehicles, it is useful to assess other retrofits to try to reduce the environmental impact of present vehicles, combining two powerful tools: clean energy and energy saving.

The project concentrates in particular to one of the most underestimated auxiliary system in passenger cars. In a World characterized by fussy users the thermal comfort is not neglected anymore and therefore driving cycles for homologation should take it into account. The results show an increasing vehicle fuel consumption with respect to the European homologation cycle and above all an increasing of CO_2 emission. Furthermore, the power consumption of the compressor of the air conditioning system is clearly lower in the improved cabin application compared to the standard one, demonstrating how retrofits concerning the solar irradiation and thermal insulation can increase the energy efficiency of the AC system of a vehicle.

The strong point of this project is its versatility. In fact, every consideration made on an internal combustion vehicle about the retrofits assessment can perfectly be re-adapted to an EV application, varying boundary conditions like the typology of compressor, regulation and the different operation possibility.

Finally, it is appropriate to consider this work as a starting point on which in future someone may base on, examining in depth internal material coatings and its role in the heat exchange or switching the focus to the vehicle behaviour during winter. Furthermore the involvement of electrical components such as vents and blower may improve the project work, analysing the impact of the inefficient electrical components on the vehicle consumption.

REFERENCES

[1] World Energy Outlook 2017 – International Energy Agency – IEA

[2] International Energy Outlook 2017 – Energy Information Administration – EIA

[3] U.S. Central Intelligence Agency – The World Factbook. First semester 2017

[4] https://www.conserve-energy-future.com/ozone-layer-and-causes-of-ozone-depletion.php

[5] Booklet notes – Tecnica del freddo e criogenia – C. Silvi

[6] United Nations Framework Convention On Climate Change – UNFCCC

[7] CO2 emissions from fuel combustion 2017: highlights – International Energy Agency - IEA

[8] Intergovernmental Panel on Climate Change – IPCC – Climate change 2014

[9] Global Transportation Energy Consumption: Examination of Scenarios to 2040 using ITEDD - Energy Information Administration – EIA – 2017

[10] PA CO2 Emission Report 2017 Final – PA consulting

[11] Global EV Outlook 2017. Two million and counting – International Energy Agency - IEA

[12] Booklet – Thermal Comfort – Energy savings and comfort in buildings – G. V. Fracastoro. - 2015

[13] ASHRAE Standard 55 – ANSI/ASHRAE 55 – 2010 – Thermal Environmental Condition for Human Occupancy, 2010.

[14] LMS Amehelp – LMS Imagine.Lab Amesim 15.0.1

[15] http://comfort.cbe.bekerley.edu/

[16] http://denso-ts.com

[17] http://mahle.com

[18] C&R Technologies site web

[19] https:// technicalguru4u.wordpress.com/2017/05/09/throttling-process

[20] Booklet – Joule Thompson expansion – Tecnica del freddo e criogenia – C. Silvi – 2016

[21] Filp Nielsen – Automotive Climate Systems – Investigation of current energy use and future energy savings measures – Thesis for the degree of doctor in philosophy – Sweden 2016

[22] http://www.hanonsystem.com/En/technology/Climate#tab1-2

[23] Commission Regulation (EC) No 692/2008 of 18 July 2008 implementing and amending Regulation (EC) No 715/2007 of the European Parliament and of the Council on type-approval of motor vehicles with respect to emissions from light passenger and commercial vehicles (Euro 5 and Euro 6) and on access to vehicle repair and maintenance information – 2008

[24] www.greenstart.it/ecco-come-fatto-il-ciclo-nedc-9365

[25] https://www.nissan.it/wltp.html

[26] Regulation (EU) No 517/2014 of the European Parliament and of the Council of 16 April 2014 on fluorinated greenhouse gases and repealing Regulation (EC) No 842/2006

[27] Ing. Antonio Metallo – Analisi sperimentale delle prestazioni energetiche dei fluidi frigoriferi tipo HFO candidate alla sostituzione dell'R134a – Tesi Dottorato di Ricerca – 2015

[28] Handbook ASHRAE – Refrigeration – 1998

[29] https://www.nissanglobal.com/EN/TECHNOLOGY/OVERVIEW/ thermal_insulation_roof.html

[30] http://www.ips-innovations.com/solar_reflective_coatings.html

[31] http://www.ips-innovations.com/automotive_applications.html

[32] NREL/CP – 540 – 40986. Reduction in Vehicle temperatures and fuel use from cabin ventilation, solar – reflective paint, and a new solar – reflective glazing.

[33] https://www.pcimag.com/articles/102920-ir-reflective-pigments-a-black-rainbow-of-options

[34] IR-reflective pigment contained in non-coated plastic for automotive – Eric Walker, ウォーカー エリック - Honda Motor Co Ltd – 2008

[35] https://www.smart.com/it/it/index/WLTP.html